Enhancing Flowability of Fine Cohesive Active Pharmaceutical Ingredients

A dissertation submitted in
partial fulfillment of
requirements for the award
of degree of

Master of Engineering

in

Thermal Engineering

by

Rahul Sharma
Registration Number: 801683020

Under the Supervision of

Dr. Gautam Setia
Assistant Professor
Department of Mechanical Engineering

DEPARTMENT OF MECHANICAL ENGINEERING
THAPAR INSTITUE OF ENGINEERING AND TECHNOLOGY,
PATIALA
JULY-2018

CERTIFICATE

I hereby declare that the dissertation entitled "**Enhancing Flowability of Fine Cohesive Active Pharmaceutical Ingredients**" is an authentic record of my work carried out as requirement for the award of the degree of **Master of Engineering** in **Thermal Engineering** at **Thapar Institute of Engineering and Technology, Patiala** under the supervision of **Dr. Gautam Setia** (Assistant Professor, Department of Mechanical Engineering, Thapar Institute of Engineering and Technology, Patiala). No part of the matter embodied in this report has been submitted to any other university or institute for the award of any degree.

Rahul Sharma
ME Thermal
801683020

Dated: 13 July 2018

It is certified that the above statement made by the student is correct to the best of my knowledge and belief.

Dr. Gautam Setia
Assistant Professor
Department of Mechanical Engineering
Thapar Institute of Engineering and Technology, Patiala.

ACKNOWLEDGEMENT

There is always a sense of gratitude, which is expressed for others for their help and assistance that they render during all phases of life, I too would like to do so, as I really wish to express my gratitude towards all those who have been helpful to me, directly or indirectly, during the course of my master's degree.

I would like to sincerely thank my mentor **Dr. Gautam Setia** for his guidance, constant encouragement and motivation throughout the tenure of my thesis. His advice and guidance were priceless and had a deep impact on my thinking and research work as well.

I would also like to express my gratitude towards Thapar Institute of Engineering and Technology, Patiala and especially Department of Mechanical Engineering for providing me with a conducive environment for my studies and appropriate funding for my research work.

I am deeply grateful and thankful towards Mr. Harjinder Singh for his support and help in fabrication of the dry coating machine.

I would like to thank all my friends on and off campus which made my stay in Patiala a fruitful one and for being with me in my good and tough times.

Lastly, I thank my parents and brother for their constant encouragement and support throughout my life and during the duration of this degree without which this dissertation would not have been possible.

Table of Contents

Certificate I

Acknowledgement II

List of Figures VI

List of Tables XII

List of Symbols and Abbreviations XV

Abstract 1

Chapter 1: Introduction and Objectives 2

1.1 Introduction 2

1.2 Objectives 4

Chapter 2: Literature Review 5

2.1 Uniaxial compression test 5

2.2 Mohr stress circle representation of stresses 6

2.3 Introduction to Powder Flow Tester (PFT) 8

2.4 Previous work on powder flow properties and testing 9

Chapter 3: Materials and Methods 16

3.1 Materials 16

3.2 Methodology 17

3.3 Testing methodology 18

Chapter 4: Results and Discussions 22

Hand blending results 22

4.1 SEM images 22

4.2 EDS results 23

4.3 Paracetamol blended with Avicel PH-101 24

4.4 Paracetamol blended with Avicel PH-102 29

4.5 Paracetamol blended with nano silica (Aerosil R972 Pharma) 34

4.6 Ibuprofen blended with Avicel PH-101 40

4.7 Ibuprofen blended with Avicel PH-102 45

4.8 Ibuprofen blended with nano silica (Aerosil R972 Pharma) 50

Chapter 5: Dry Coating 56

5.1 Introduction 56

5.2 Background/theory of dry coating 58

5.3 Reduction in cohesive force by introduction of roughness 60

5.4 Techniques/machines used for dry coating 66

5.4.1 Co-Mill 67

5.4.2 Fluid Energy Mill 70

5.4.3 Magnetic Assisted Impact Coater 73

5.4.4 Mehanofusion 75

5.4.5 LabRAM 78

5.4.6 Hybridizer and Cyclomix 80

5.4.7 Random techniques 81

5.5 Novel dry coating technique 82

5.6 Dry coating results with paracetamol 87

Chapter 6: Conclusions and Future Scope of Work 106

Conclusions 106

Future scope of work 108

References 109

Appendix: A 114

Publication 119

List of Figures

Figure 2.1.	Uniaxial compression test	5
Figure 2.2.	Measurement of the unconfined yield strength in a σ,τ diagram	6
Figure 2.3.	Instantaneous flow function and lines of constant flowability	7
Figure 2.4.	(a) Powder Flow Tester, (b) Vane lid, (c) Wall friction lid, (d) Trough, (e) Shaping blade with curve profile, (f) Shaping blade with flat profile.	8
Figure 3.1.	Blends of ibuprofen and paracetamol with different glidants	18
Figure 3.2.	Failure locus construction by shear stress and normal stress data	19
Figure 3.3.	Flow characterization data derived from the shear flow tester (PFT)	19
Figure 3.4.	Wall failure locus construction by shear stress and normal stress data	20
Figure 3.5.	Bulk density test PFT raw data	21
Figure 4.1.	SEM images of (a) Paracetamol at magnification of 150x & 250x respectively, (b) Ibuprofen at magnification of 60x & 100x respectively, (c) Paracetamol at magnification of 1000x, (d) Ibuprofen at magnification of 700x, (e) Avicel PH-101 at magnification of 250x & 1000x respectively, (f) Avicel PH-102 at magnification of 200x & 700x respectively	22
Figure 4.2.	Flow function curve of paracetamol blended with Avicel PH-101	24
Figure 4.3.	Internal friction curve of paracetamol blended with Avicel PH-101	24
Figure 4.4.	Wall friction curve of paracetamol blended with Avicel PH-101	25

Figure 4.5.	Bulk density curve of paracetamol blended with Avicel PH-101	25
Figure 4.6.	Flow function curve of paracetamol blended with Avicel PH-102	29
Figure 4.7.	Internal friction curve of paracetamol blended with Avicel PH-102	29
Figure 4.8.	Wall friction curve of paracetamol blended with Avicel PH-102	30
Figure 4.9.	Bulk density curve of paracetamol blended with Avicel PH-102	30
Figure 4.10.	Flow function curve of paracetamol blended with Aerosil R972 Pharma	34
Figure 4.11.	Internal friction curve of paracetamol blended with Aerosil R972 Pharma	34
Figure 4.12.	Wall friction curve of paracetamol blended with Aerosil R972 Pharma	35
Figure 4.13.	Bulk density curve of paracetamol blended with Aerosil R972 Pharma	35
Figure 4.14.	SEM images of (a) Paracetamol at magnification of 250x, (b) Paracetamol at magnification of 1000x, (c) Paracetamol 80%SAC at magnification of 550x, (d) Paracetamol 80%SAC at magnification of 2000x, (e) Paracetamol 80%SAC at magnification of 7000x.	37
Figure 4.15.	Flow function curve of ibuprofen blended with Avicel PH-101	40
Figure 4.16.	Internal friction curve of ibuprofen blended with Avicel PH-101	40
Figure 4.17.	Wall friction curve of ibuprofen blended with Avicel PH-101	41
Figure 4.18.	Bulk density curve of ibuprofen blended with Avicel PH-101	41

Figure 4.19.	Flow function curve of ibuprofen blended with Avicel PH-102	45
Figure 4.20.	Internal friction curve of ibuprofen blended with Avicel PH-102	45
Figure 4.21.	Wall friction curve of ibuprofen blended with Avicel PH-102	46
Figure 4.22.	Bulk density curve of ibuprofen blended with Avicel PH-102	46
Figure 4.23.	Flow function curve of ibuprofen blended with Aerosil R972 Pharma	50
Figure 4.24.	Internal friction curve of ibuprofen blended with Aerosil R972 Pharma	50
Figure 4.25.	Wall friction curve of ibuprofen blended with Aerosil R972 Pharma	51
Figure 4.26.	Bulk density curve of ibuprofen blended with Aerosil R972 Pharma	51
Figure 4.27.	SEM images of (a) Ibuprofen at magnification of 100x, (b) Ibuprofen at magnification of 700x, (c) Ibuprofen 80%SAC at magnification of 270x, (d) Ibuprofen 80%SAC at magnification of 500x, (e) Ibuprofen 80%SAC at magnification of 1000x.	52
Figure 5.1.	Adhesive forces due to various mechanisms of adhesion as a function of the distance *a* between the surfaces of a sphere and a plate: 1, liquid bridges; 2, electrostatic forces for conductors; 3, electrostatic forces for insulators; 4, van der Waals forces	58
Figure 5.2.	Comparison of the adhesion force and gravity for very smooth and rough spheres of different diameters	59
Figure 5.3.	Adhesive forces of various mechanisms of adhesion for the sphere plate model (on contact) as a function of the diameter of the sphere: 1, liquid bridges; 2, electrostatic forces for conductors; 3, electrostatic forces for insulators; 4, van der Waals forces	60

Figure 5.4.	Influence of the radius *r* of an asperity on the adhesive forces due to various mechanisms of adhesion for the sphere-plate model (contact gap *a* = ao, ao = 4 x 10^{-4} μm). Adhesive forces of various mechanisms of adhesion for the sphere plate model (on contact) as a function of the diameter of the sphere: 1, liquid bridges; 2, electrostatic forces for conductors; 3, electrostatic forces for insulators; 4, van der Waals forces	61
Figure 5.5.	(a) Contact of two-coated cohesive particles and (b) Location of guest particles	64
Figure 5.6.	Co-Mill	67
Figure 5.7.	Sturtevant Qualification FEM	70
Figure 5.8.	Magnetic Assisted Impact Coater	73
Figure 5.9.	Mechanofusion	75
Figure 5.10.	Laboratory scale Resonant Acoustic Mixer	78
Figure 5.11.	Draft of the dry coating machine without supports	84
Figure 5.12.	Draft of the dry coating machine with supports	84
Figure 5.13.	(a) Dry coating machine working with bend, (b) Connection from the air receiver to the suction line	85
Figure 5.14.	Pressure in pressure regulator set as 4 kg/cm^2	85
Figure 5.15.	(a) Non return valve & pressure regulator, (b) Air receiver, (c) Air dryer (d) Compressor	86
Figure 5.16.	Flow function curve of paracetamol dry coated with 20%SAC (0.49 wt./wt.% Aerosil R972 Pharma) at different pressures and processing times	87

Figure 5.17.	Internal friction curve of paracetamol dry coated with 20%SAC (0.49 wt./wt.% Aerosil R972 Pharma) at different pressures and processing times	88
Figure 5.18.	Wall friction curve of paracetamol dry coated with 20%SAC (0.49 wt./wt.% Aerosil R972 Pharma) at different pressures and processing times	88
Figure 5.19.	Bulk density curve of paracetamol dry coated with 20%SAC (0.49 wt./wt.% Aerosil R972 Pharma) at different pressures and processing times	89
Figure 5.20.	Flow function curve of paracetamol dry coated with 20%SAC (0.49 wt./wt.% Aerosil R972 Pharma) at 3 kg/cm^2 pressure and 10 and 20 min processing times	89
Figure 5.21.	Internal friction curve of paracetamol dry coated with 20%SAC (0.49 wt./wt.% Aerosil R972 Pharma) at 3 kg/cm^2 pressure and 10 and 20 min processing times	90
Figure 5.22.	Wall friction curve of paracetamol dry coated with 20%SAC (0.49 wt./wt.% Aerosil R972 Pharma) at 3 kg/cm^2 pressure and 10 and 20 min processing times	90
Figure 5.23.	Bulk density curve of paracetamol dry coated with 20%SAC (0.49 wt./wt.% Aerosil R972 Pharma) at 3 kg/cm^2 pressure and 10 and 20 min processing times	91
Figure 5.24.	Flow function curve of paracetamol dry coated with 20%SAC (0.49 wt./wt.% Aerosil R972 Pharma) at 4 kg/cm^2 pressure and 10,20 and 30 min processing times	94
Figure 5.25.	Internal friction curve of paracetamol dry coated with 20%SAC (0.49 wt./wt.% Aerosil R972 Pharma) at 4 kg/cm^2 pressure and 10,20 and 30 min processing times	94
Figure 5.26.	Wall friction curve of paracetamol dry coated with 20%SAC (0.49 wt./wt.% Aerosil R972 Pharma) at 4 kg/cm^2 pressure and 10,20 and 30 min processing times	95
Figure 5.27.	Bulk density curve of paracetamol dry coated with 20%SAC (0.49 wt./wt.% Aerosil R972 Pharma) at 4 kg/cm^2 pressure and 10,20 and 30 min processing times	95
Figure 5.28.	Flow function curve of paracetamol dry coated with 20%SAC (0.49 wt./wt.% Aerosil R972 Pharma) at 5 kg/cm^2 pressure and 10 and 20 min processing times	99

Figure 5.29.	Internal friction curve of paracetamol dry coated with 20%SAC (0.49 wt./wt.% Aerosil R972 Pharma) at 5 kg/cm^2 pressure and 10 and 20 min processing times	99
Figure 5.30.	Wall friction curve of paracetamol dry coated with 20%SAC (0.49 wt./wt.% Aerosil R972 Pharma) at 5 kg/cm^2 pressure and 10 and 20 min processing times	100
Figure 5.31.	Bulk density curve of paracetamol dry coated with 20%SAC (0.49 wt./wt.% Aerosil R972 Pharma) at 5 kg/cm^2 pressure and 10 and 20 min processing times	100
Figure 5.32.	Flow function curve of paracetamol dry coated with 80%SAC (1.97 wt./wt.% Aerosil R972 Pharma) at 4 kg/cm^2 and 6 kg/cm^2 pressure and 10 min processing time	104
Figure 5.33.	Internal friction curve of paracetamol dry coated with 80%SAC (1.97 wt./wt.% Aerosil R972 Pharma) at 4 kg/cm^2 and 6 kg/cm^2 pressure and 10 min processing time	104
Figure 6.1.	Dry coating machine functioning with the maximum conveying length of 8 sections and a bend connecting the upper and lower sections together with the hopper assembly and bag filter connected to the upper hopper	108
Figure A1.	SEM images of (a) Chilli at magnification of 100x, (b) Chilli at magnification of 150x, (c) Turmeric at magnification of 150x, (d) Turmeric at magnification of 250x	114
Figure A2.	Flow function and time consolidated flow function curve of chilli and turmeric powder	115
Figure A3.	Internal friction curves of chilli and turmeric powder under flow function and time consolidated flow function curves	116
Figure A4.	Wall friction curves of chilli and turmeric powder	116
Figure A5.	Bulk density curves of chilli and turmeric powder	117

List of Tables

Table 3.1	d_{10}, d_{50}, d_{90}, d_{32} diameters of different materials	16
Table 3.2	wt./wt.% of nano-silica required to achieve the mentioned surface area coverage on paracetamol	17
Table 3.3	wt./wt.% of nano-silica required to achieve the mentioned surface area coverage on ibuprofen	17
Table 4.1.	EDS results of mean of three spectrums of paracetamol 80%SAC (all results in weight%)	23
Table 4.2.	EDS results of mean of three spectrums of ibuprofen 80%SAC (all results in weight%)	23
Table 4.3.	Major principal consolidating stress, unconfined failure strength, effective angle of internal friction and cohesion values of paracetamol and Avicel PH-101 blends	26
Table 4.4.	Wall friction and bulk densities values of paracetamol and Avicel PH-101 blends	27
Table 4.5.	Major principal consolidating stress, unconfined failure strength, effective angle of internal friction and cohesion values of paracetamol and Avicel PH-102 blends	31
Table 4.6.	Wall friction and bulk densities values of paracetamol and Avicel PH-102 blends	32
Table 4.7.	Major principal consolidating stress, unconfined failure strength, effective angle of internal friction and cohesion values of paracetamol nano-silica blends	38
Table 4.8.	Wall friction and bulk densities values of paracetamol nano-silica blends	38
Table 4.9.	Major principal consolidating stress, unconfined failure strength, effective angle of internal friction and cohesion values of ibuprofen and Avicel PH-101 blends	42
Table 4.10.	Wall friction and bulk densities values of ibuprofen and Avicel PH-101 blends	43
Table 4.11.	Major principal consolidating stress, unconfined failure strength, effective angle of internal friction and cohesion values of ibuprofen and Avicel PH-102 blends	47

Table 4.12.	Wall friction and bulk densities values of ibuprofen and Avicel PH-102 blends	48
Table 4.13.	Major principal consolidating stress, unconfined failure strength, effective angle of internal friction and cohesion values of ibuprofen nano-silica blends	53
Table 4.14.	Wall friction and bulk densities values of ibuprofen nano-silica blends	54
Table 5.1..	Major principal consolidating stress, unconfined failure strength, effective angle of internal friction and cohesion values of paracetamol 20% SAC dry coated samples at 3 kg/cm^2 operating pressure and 10 and 20 minutes processing time	92
Table 5.2..	Wall friction and bulk densities values of paracetamol 20% SAC dry coated samples at 3 kg/cm^2 operating pressure and 10 and 20 minutes processing time	92
Table 5.3.	Major principal consolidating stress, unconfined failure strength, effective angle of internal friction and cohesion values of paracetamol 20% SAC dry coated samples at 4 kg/cm^2 operating pressure and 10, 20 and 30 minutes processing time	97
Table 5.4.	Wall friction and bulk densities values of paracetamol 20% SAC dry coated samples at 4 kg/cm^2 operating pressure and 10, 20 and 30 minutes processing time	97
Table 5.5.	Major principal consolidating stress, unconfined failure strength, effective angle of internal friction and cohesion values of paracetamol 20% SAC dry coated samples at 5 kg/cm^2 operating pressure and 10 and 20 minutes processing time	102
Table 5.6.	Wall friction and bulk densities values of paracetamol 20% SAC dry coated samples at 5 kg/cm^2 operating pressure and 10 and 20 minutes processing time	102
Table 5.7.	Major principal consolidating stress, unconfined failure strength, effective angle of internal friction and cohesion values of paracetamol 80% SAC dry coated samples at 4 kg/cm^2 & 6 kg/cm^2 operating pressure and 10 minutes processing time	105
Table A1.	d_{10}, d_{50}, d_{90} and d_{32} diameters of chilli and turmeric	114
Table A2.	Chilli EDS results of mean of three spectrums (all results in weight%)	115
Table A3.	Turmeric EDS results of mean of three spectrums (all results in weight%)	115

Table A4. Major principal consolidating stress, unconfined failure strength, effective angle of internal friction and cohesion values of chilli and turmeric powder under flow function and time consolidation flow function tests 117

Table A5. Wall friction and bulk densities values of chilli and turmeric 118

List of Symbols

σ_1	Consolidation stress or major principal stress, kPa
σ_c	Unconfined yield strength, kPa
σ_2	Horizontal stress or minor principal stress, kPa
τ	Shear stress, kPa
ffc	Flowability
σ_E	Consolidation normal stress, kPa
σ_N	Normal stress, kPa
τ_E	Peak shear stress, kPa
τ_{SS}	Steady state shear stress, kPa
H	van der Waals attraction force, dyne
a	Gap between the surface of the sphere and the plate, μm
R	Radius of the sphere, μm
h	Lifshitz-van der Waals constant, eV
$\bar{\omega}$	Depends on the dielectric constants of the two bodies
r	Radius of curvature of asperity, nm
Fad	Adhesion force between adhering particle and a nanoscale roughness surface, N
rms	Root mean square roughness, nm

λ	Peak to peak distance between hemispherical asperity, nm
A	Hamaker constant, J
R	Radius of adhering particle, μm
Ho	Distance of closest approach between surfaces, nm
H_1	Distance between two coated host particles, nm
ρ_d	Particle density of guest particles, kg/m^3
ρ_D	Particle density of host particles, kg/m^3
D	Diameter of host particles, μm
d	Diameter of guest particle, nm
z_0	Default distance between two surfaces in contact, μm
S	Area of the contact circle, μm^2
R_1	Radius of the contact circle, μm
N	Number of guest particles coated on the surface of each host particle
d_{10}	Diameter at which 10% of a sample's mass is comprised of smaller particles, μm
d_{50}	Diameter at which 50% of a sample's mass is comprised of smaller particles, μm
d_{90}	Diameter at which 90% of a sample's mass is comprised of smaller particles, μm
d_{32}	Sauter mean diameter, μm
^	Exponentiation

Abbreviations

PFT	Powder Flow Tester
SEM	Scanning electron microscope
EDS	Energy-dispersive X-ray spectroscopy
PSD	Particle-size distribution
SAC	Surface area coverage
FEM	Fluid Energy Mill
MAIC	Magnetic Assisted Impact Coater
LabRAM	Laboratory Resonant Acoustic Mixer
CAB	Cohesive adhesive balance
MCC	Microcrystalline cellulose
CS	Consolidation stress
NB	Nominal bore
SS	Stainless steel
TC	Tri clover
rpm	Revolutions per minute

min	Minute
wt./wt.%	Weight / weight %
Para20%	20 wt. /wt. % paracetamol in a blend
Para40%	40 wt. /wt. % paracetamol in a blend
Para60%	60 wt. /wt. % paracetamol in a blend
Para80%	80 wt. /wt. % paracetamol in a blend
Para20% SAC	Aerosil R972 pharma added to paracetamol to achieve 20% theoretical SAC
Para40% SAC	Aerosil R972 pharma added to paracetamol to achieve 40% theoretical SAC
Para60% SAC	Aerosil R972 pharma added to paracetamol to achieve 60% theoretical SAC
Para80% SAC	Aerosil R972 pharma added to paracetamol to achieve 80% theoretical SAC
Ibu20%	20 wt. /wt. % ibuprofen in a blend
Ibu40%	40 wt. /wt. % ibuprofen in a blend
Ibu60%	60 wt. /wt. % ibuprofen in a blend
Ibu80%	80 wt. /wt. % ibuprofen in a blend
Ibu20% SAC	Aerosil R972 pharma added to ibuprofen to achieve 20% theoretical SAC
Ibu40% SAC	Aerosil R972 pharma added to ibuprofen to achieve 40% theoretical SAC
Ibu60% SAC	Aerosil R972 pharma added to ibuprofen to achieve 60% theoretical SAC
Ibu80% SAC	Aerosil R972 pharma added to ibuprofen to achieve 80% theoretical SAC

Abstract

The effectiveness of pharmaceutical excipients and hydrophobic nano silica as flow regulator has been studied and two active pharmaceutical ingredients (API's) i.e. paracetamol and ibuprofen are used to gauge the effectiveness. Avicel PH-101 and Avicel PH-102 are chosen as pharmaceutical excipients and Aerosil R972 pharma is used as hydrophobic nano silica, the API's and the excipients are micro sized. Flow function, wall friction and bulk density tests to gauge the said effect are conducted on Brookfield Powder Flow Tester (PFT). The samples for testing are prepared by hand blending/manual mixing to ascertain the capability of simple inexpensive mixing in comparison to expensive blenders and machines. Ibuprofen and paracetamol are mixed with Avicel PH-101, Avicel PH-102 and Aerosil R972 pharma in different blend percentages and SAC% respectively. Scanning electron microscope images are taken to analyze the silica surface coverage and energy-dispersive X-ray spectroscopy technique is used to ascertain the presence of silica in API's. The blended samples of paracetamol with Avicel PH-101 and Avicel PH-102 have shown great improvement in flowability in comparison to the blended samples of ibuprofen with Avicel PH-101 and Avicel PH-102. Mixing with nano-silica has drastically improved the flowability of ibuprofen coupled with significant improvement in paracetamol's flowability. Wall friction characteristics of ibuprofen and paracetamol when blended with Avicel PH-101 and Avicel PH-102 have shown no significant change, however significant change is witnessed in nano blended samples. Compressibility of all blended samples generally decreased. Bulk densities of the samples blended with Avicel PH-101 and Avicel PH-102 decreased and of samples blended with nano silica it increased. The study conducted underlined the efficacy of the hand blending process by showing that significant improvement in flow properties can be brought about by it. PFT has confirmed the anticipated results of the powder blends indicative of its reliability, moreover repeatable results are obtained which established the repeatability of the instrument. A need for developing a low cost dry coating machine is felt and is thus fabricated and tests are carried on it to test its efficacy. Initial testing has shown encouraging results and further extensive testing needs to follow.

Keywords: Powder Flow Tester; Flow function; Fine cohesive powders; Surface area coverage; Blending percentage; Novel dry coating technique.

Chapter 1

Introduction and Objectives

1.1 Introduction

Powders are one of the most important and most widely used industrial material form in various industries like pharmaceutical, food, agricultural, automotive etc. (Schulze, 2008). The current research is mainly focused on the pharmaceutical industries where the wide use of various pharmaceutical powders has many operational difficulties. For example, fine powder (below 100 micrometer) have problems such as agglomeration (formation of lumps), segregation, high compressibility and reaction to moisture and as a result low flowability (Teunou and Fitzpatrick, 2000; Iqbal and Fitzpatrick, 2006; Deng *et al.*, 2010; Ittershagen *et al.*, 2013)**.** Moreover, powders were seen to have reduced flowability with increase in consolidation time (Teunou and Fitzpatrick, 2000)**.** Also, Hann and Stražišar (2007) concluded that moisture content had great importance in determining the bulk flow with increasing moisture impeding the flow. Schwedes (1996) discussed the idea of flow aid to improve the flow of powders and suggested that the flowability can be described by the flow function. Cannavacciuolo *et al.* (2009) devised limiting aeration conditions for collapsing established arches in silos to ensure arch free flow. For powders, it has been well established that as the particle size decreases, the cohesive forces and mainly the van der Waals forces increase in comparison to gravity forces. The adhesion force between two particles depends on van der Waals force, capillary force and surface tension. At low moisture levels the capillary force action can be ignored in comparison to van der Waals forces. For fine particles, between van der Waals and surface tension, more importance is given to van der Waals forces where, the van der Waals forces depend mainly on the particle sizes and the surface morphology (Schulze, 2008; Tomas and Kleinschmidt, 2009; Deng *et al.*, 2010; Huang, Zhang and Zhu, 2010; Zhou *et al*., 2010 a). As the van der Waals forces exceed the gravity forces, the powders show cohesive nature and poor flowability as they can no longer easily flow under their own gravity (Pingali *et al.*, 2009)**.** The reason for the small particles to have a large cohesive and adhesive force with the other particles and walls respectively can be attributed to their greater surface area than the bigger particles. The bigger particles tend to roll over each other and have low cohesive forces because of the dominating gravity forces (Mullarney *et al.*, 2011).

To tackle the problem of poor flowability of fine powders for further processing various methodology/techniques were developed in recent years. One specific way of improving the flowability is by using glidants or flow aids in the powder. The glidants or flow aids are also powders in which particles can be of same size as the primary powder or are smaller. Simple mixing of the fine cohesive micro range powder with powders having similar or bigger sized particles having good flowability, improves the flowability of the resulting powder mixture.

However, in case of use of nanometer size range powder particles as flow aids, the primary powder particles can be termed as host particles and the nano powders are regarded as guest particles as they tend to cover the surface of host particles (Meyer and Zimmermann, 2004; Mullarney *et al.*, 2011; Zhou *et al.*, 2011). Nano powders (guest particles) mixing with the host particles does not guarantee improved flowability. The flowability can be improved if the guest particles adhere on the surface of the host particles (Zhou *et al.*, 2010 a). Also, the improvement in the flow of powders can depend on plenty of factors like orientation of atoms in the surface, shape and size of particle, charge acquired, surface roughness and chemistry, hydrophobicity or hydrophilicity and other factors (Meyer and Zimmermann, 2004; Chen *et al.*, 2010; Jallo *et al.*, 2010, 2012; Han *et al.*, 2011; Zhou *et al.*, 2011)**.**

In literature there have been numerous instances like (Meyer and Zimmermann, 2004; Yang *et al.*, 2005; Chaudhuri *et al.*, 2006; Pingali *et al.*, 2009; Mullarney *et al.*, 2011; Zhou *et al.*, 2010 a, 2010 b, 2013) where blending is used for improving the flowability and other related properties of powders. The powder samples which are mixed/ blended with similar scale (micrometer) flow aids are not treated further and tested for its effect. After blending the samples with nanoparticles, the blend is further sent to various dry coating machines to further enhance the properties. The technique of ensuring the guest particles stick or adhere to the host particles is called coating. When this coating is done on dry powders and in absence of liquid it is called dry coating (Zhou *et al.*, 2010 a, 2010 b; Qu et al., 2017). The basic idea behind nano-coating is that the guest particles act as roughness on the host particle surfaces and thus increasing the distance between two host particles, hence decreasing the van der Waals forces and in turn cohesivity. Uniform coating of nanoparticles on the host particle surface can cause reduction in cohesiveness as the coating changes the surface properties of the host particle and its interaction or contact nature with other coated particles (Meyer and Zimmermann, 2004; Schulze, 2008; Tomas and Kleinschmidt, 2009)**.**

In recent times, to evaluate the flowability of fine powders various equipment based on classical Jenike shear cell test methodology (Jenike, 1964) have been introduced, such as FT4 Powder Rheometer from Freeman Technology, Powder Flow Tester from Brookfield and Powder Rheometer by Anton Paar etc. FT4 Powder Rheometer has been widely and reliably used to analyze flowability of powders and has been extensively used for pharmaceutical research. FT4 Powder Rheometer measures the powder's resistance to flow while in motion and includes a shear cell to calculate the powder shear strength. Wall friction kit helps in conducting wall friction test and allows quantifying powder shear with the process equipment surface and bulk properties such as bulk density. Powder rheometer by Anton Paar enables testing of powders under the fluidization and consolidation states. Cohesion strength and wall friction of the powders can be calculated. Recently Brookfield came up with a low cost and more reliable (claimed) Powder Flow Tester (PFT) (Berry, Bradley and McGregor, 2015)**.** However, it seems that limited investigation has been done on pharmaceutical powders with PFT. Moreover, effect of various flow aids on pharmaceutical powders is still an ongoing area of research. Hence there is a need of an investigation of flow behavior of various API's and effect of flow aids on the flow properties which should be evaluated with the help of PFT. Also, there is a need to gauge the impact of simple hand

blending of micrometer and nanometer scale flow aids with the host powder with the use of recently introduced PFT (comparatively less expensive equipment) on the powder properties.

In the light of above needs, the current research will primarily focus on repeatable testing with Brookfield PFT where the flow properties of powders (typical cohesive API's) and their blends with different flows aids are measured to analyze/compare their efficacy. This work also has the potential to examine the reliability and repeatability of the newly introduced shear cell tester i.e. PFT. Various flow tests can be designed to confirm the anticipated results with PFT. Various dry coating machines are being used worldwide to improve the flow properties of cohesive API powders, so a need for fabricating a novel and affordable dry coating machine based on the principles of present dry coating machines was felt and therefore a machine was fabricated and tests performed on it for testing its efficacy.

1.2 Objectives

The current research will primarily focus on testing the flow properties of powders on PFT and hence trying to improve the properties by, blending with similar sized powder particles (micrometer sized particles blended with micrometer sized particles), blending with nanoparticles (micrometer sized particles blended with nanometer sized particles), dry coating with nanoparticles (micrometer sized particles surface coated with nanometer sized particles).

Accordingly the objectives of this dissertation include:

1. To investigate the flow properties of paracetamol and ibuprofen API's on as received basis.

2. To investigate the flow properties of blends of above mentioned API's in different wt./wt.% with two different excipients namely Avicel PH-101 and Avicel PH-102 used as micrometer sized glidant.

3. To investigate the flow properties of blends of above mentioned API's at different SAC% with Aerosil R972 Pharma used as nanometer sized glidant.

4. To develop a novel dry coating machine and testing it for its efficacy.

Chapter 2

Literature Review

To understand powder flow behavior the basics of powder flow testing were studied leading to the need of using Brookfield Powder Flow Tester (PFT).

2.1. Uniaxial compression test

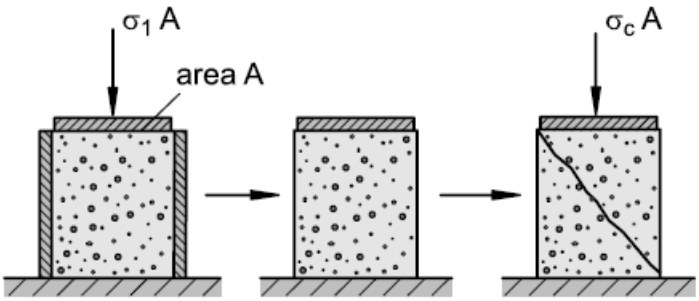

Figure 2.1. Uniaxial compression test (Schulze, 2008)

In the uniaxial compression test as described in Figure 2.1, fine grained bulk solid is filled in a hollow cylinder with cross sectional area A, internal walls of the cylinder are assumed to be frictionless. The bulk solid is loaded with a vertical stress σ_1 known as the consolidation stress or major principal stress and is thus compressed. After consolidation the bulk solid specimen is relieved of the consolidation stress and the hollow cylinder is removed. If the consolidated cylindrical specimen is loaded with increasing vertical stress, the specimen breaks or fails at a particular stress. This failure causing stress σ_c is called unconfined yield strength, compressive strength or cohesive strength. The bulk solid specimen fails or yields at a particular stress σ_c, but it is dependent on the prior stress history of the powder. At different σ_1 different σ_c values are obtained. The stress history or prior consolidation affects the bulk density of the material or the packing of particles in the specimen due to which σ_c is affected. Usually greater consolidation stress σ_1 leads to greater unconfined yield strength σ_c. Uniaxial compression tests conducted at different consolidation stress gives different unconfined yield strengths and we obtain various pairs of (σ_1, σ_c) values. Plotting these points on a plot where σ_c is ordinate and σ_1 abscissa and passing through these points a curve gives a flow function or instantaneous flow function. The uniaxial compression test is one of the most basic tests to obtain a flow function curve.

2.2 Mohr stress circle representation of stresses

The uniaxial compression test is represented by the Mohr circles in the Figure 2.2. Circle A represents the consolidation with stress σ_1 acting vertically on the bulk solid specimen. Horizontal stress acts in perpendicular direction to the vertical stress and is a result of the vertical stress σ_1. As the walls of the hollow cylinder are assumed to be frictionless, there is no shear stress on the walls and on the top and bottom of the specimen. Thus the circle A ably represents the consolidation stage as shear stress $\tau = 0$ and the circle cuts the σ axis at σ_1 and σ_2 which are the principal stresses.

After the consolidation stress has been relieved and the hollow cylinder removed, the sample is loaded with increasing vertical stresses. The increasing stresses are represented by circles B_1, B_2 and B_3. The minor principal stress is zero in all cases as lateral surface of the specimen is unrestrained and unloaded. At failure of the specimen, B_3 represents the stresses in the sample. Load corresponding to B_3 causes incipient flow of the specimen, the yield limit of the specimen must have been attained. Incipient flow is defined as the failure of the bulk solid i.e. when the bulk solid starts to flow and plastic deformation takes place. The flow only starts when the circle B_3 and A cut the yield limit tangentially. So when the circles cut the yield limit tangentially we get the major principal stresses of circles B_3 & A as the unconfined yield strength and principal consolidation stress respectively. Yield limit gives a value of shear stress τ, for every normal stress σ to initiate the flow. Mohr circles B_1 & B_2 cause only the elastic deformation of the bulk solid specimen as the stresses associated with these circles are not enough to cause plastic deformation or failure. If for inducing failure, stress on the consolidated sample is applied in the horizontal direction together with vertical stress, Mohr circle C represents that case.

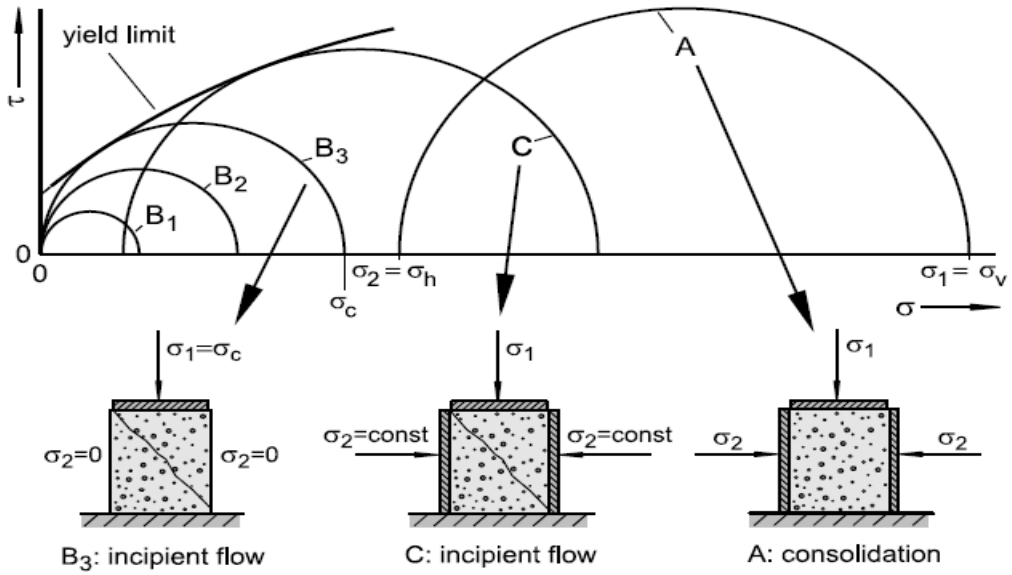

Figure 2.2. Measurement of the unconfined yield strength in a σ,τ diagram (Schulze, 2008)

Flowability of the bulk solid specimen can be defined numerically as the ratio of consolidation stress σ_1 to the unconfined yield strength σ_c (Schulze, 2008).

$$ffc = \sigma_1 / \sigma_c$$

Flow regions can be defined to characterize the flow of the bulk solid as follows:

- *ffc < 1 not flowing*
- *1 < ffc < 2 very cohesive*
- *2 < ffc < 4 cohesive*
- *4 < ffc < 10 easy-flowing*
- *10 < ffc free-flowing*

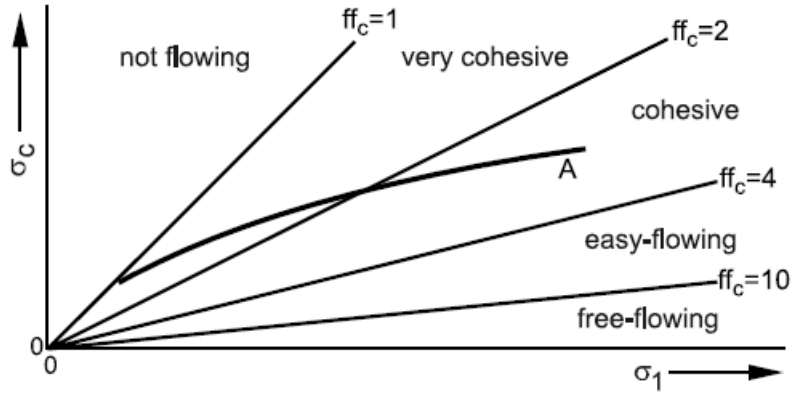

Figure 2.3. Instantaneous flow function and lines of constant flowability (Schulze, 2008; Jenike, 1964).

A is the instantaneous flow function or flow function curve plotted by various points of (σ_1, σ_c).

The use of uniaxial compression tester for fine grained, cohesive bulk solids is problematic as very low unconfined yield strength values are obtained and preparing frictionless walls is very time consuming if not entirely impossible. Also important parameters like wall friction cannot be ascertained by this test, so shear testers are preferred in advanced bulk solids technology. The shear testers work in two steps analogous to the uniaxial test i.e. consolidation of the bulk specimen called as pre shear and subsequently measuring a point on the yield limit by shear or shear to failure. Brookfield PFT which is an annular shear tester is used in the present research work.

2.3 Introduction to Powder Flow Tester (PFT)

Powder Flow Tester or PFT's functioning is based on Jenike's methodology (Jenike, 1964). PFT is an annular shear tester in which the sample is loaded in an annular shear cell. An annular lid helps in applying axial and torsional loads on the powder samples and the loads applied are controlled by the axial or the rotary motion of the lid. The lid is connected to the compression plate of the PFT. Annular shaped aluminium trough is used for filling the samples for testing. The trough has a perforated screen in the bottom which holds the powder in place and prevents the powder particles on the bottom from sliding on the smooth metal surface when the trough rotates. Shaping blade with curved profile is attached to the inner catch tray and is inserted in the annular opening of the trough to prepare samples for flow function tests, flat profile shaping blade is used for wall friction and bulk density tests. The powder is sieved through a fine sieve and falls on the trough, the sample is prepared by rotating the shaping blade clockwise and anticlockwise, thus generating a curved profile for flow function tests and flat profile for wall friction and bulk density tests. Annular vane lid is used for the flow function tests and wall friction lid is used for the wall friction and bulk density tests. Vane lid is made of SS304 and has small compartments which trap the particles and cause them to shear against the powder particles in the trough. The wall friction lid is also made of SS304 and has a smooth bottom surface with 2B finish which slides over the powder particles in the trough and helps measure the friction of powder against the surface of lid. All the experiments are conducted at room temperature ranging from 22-27 °C and powders are tested on as received basis. PFT is operated through Powder Flow Pro software which analyses and accumulates the raw data during flow function, wall friction and bulk density tests and provides a plethora of information to analyze the powder behavior.

(a)

(b)

(c)

(d) 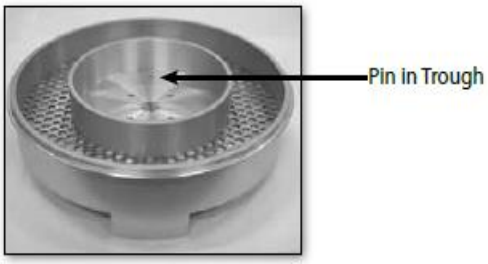

(e) 

(f) 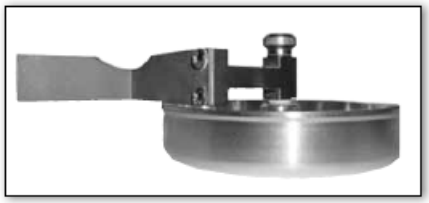

Figure 2.4. (a) Powder Flow Tester, (b) Vane lid, (c) Wall friction lid, (d) Trough, (e) Shaping blade with curve profile, (f) Shaping blade with flat profile.

2.4 Previous work on powder flow properties and testing

Ramlakhan *et al.* (2000) listed magnetic particle size, mass ratio of magnetic to powder particles as key system parameters and frequency, processing time and current as key operating parameters. Poly (methyl methacrylate) was chosen as host material for the study due to its smooth and spherical particles. The magnetic particles are agitated by an external magnetic field and hence impart energy to the host and guest particles and assisting in coating. Increase in magnetic to powder mass ratio leads to increase in collision frequency and thus shorter processing times to obtain similar coating results. Increasing the processing time beyond a specific limit led to reduction on flowability and caused particle attrition. It was discussed that even discrete guest particles on the host surface were sufficient in reducing cohesivity. Continuous impaction of magnet particles after optimum processing conditions leads to destruction in coating integrity and also change in shape of particles. A mechano-chemical reaction proposed as the reasoning of increased hydrophilicity of cellulose due to the surface reaction between cellulose and silica particles. Surface coverage increased with increasing current and processing time, frequency gave periodic fluctuations in the surface coverage results. Increasing the magnet to powder ratio and magnet particle size improved surface coverage. The spinning motion of the guest particles promoted breakage of agglomerates and spreading of guest particles, the translation motion aided in particle collisions.

Jonat *et al.* (2004) used microcrystalline cellulose (MCC) to study the effect of hydrophilic and hydrophobic colloidal silicon dioxide as flow regulators. MCC and silica were mixed in a Turbula mixer and the effect of silica as flow regulator was seen by comparing the angle of repose, bulk and tapped densities. Silica distribution on MCC surface was better for

hydrophobic silica, thus hydrophobic silica improved the flow properties better than the hydrophobic silica. Both the hydrophobic and hydrophilic silica were tested under various mixing conditions, the hydrophobic silica's effect as flow regulator was seen independent of the mixing conditions whereas the hydrophilic silica improved as a flow regulator under stronger mixing conditions. A linear correlation was seen between angle of repose and adhesion force measured by atomic force microscopy indicating that the angle of repose was a sufficient method to test the effectiveness of silica as flow regulator for routine measurements.

Kaerger, Edge and Price (2004) studied the effect of size and shape of paracetamol particles on the flow behavior of blends with microcrystalline cellulose. The effect of paracetamol particle shape was gauged by preparing samples using two techniques i.e. (a) Novel engineered Solution Atomization and Xstallization by Sonication (SAXS) and (b) Micronization by milling. SAXS is a process in which solution of particles with ethanol is sprayed with pressure atomizer and after ethanol evaporates, particles are sonicated and later dried for use. The results of micronization and SAXS was compared with untreated blend and angle of repose and tapped and bulk densities were calculated to gauge the efficacy of the micronization and SAXS process. The blends were mixed in a Turbula mixer and then magnesium stearate was added to them and was again mixed. SAXS paracetamol blends showed properties of larger sized untreated paracetamol particle blends. SAXS paracetamol blends performed better than the micronized paracetamol blends and showed comparable flow and improved tabletability in comparison to sized untreated paracetamol particle blends.

Mujumdar *et al.* (2004) used MAIC, mechanofusion and hybridizer together with varying wt./wt.% of guest particles to determine best combination for improving magnesium shelf life. Coating magnesium with hydrophobic guest particles will delay formation of magnesium hydroxide and hence increase shelf life. Wax coating was found to be covering a larger surface of magnesium particles in comparison to silica particles due to which wax showed less water absorption. Surface coverage was better in mechanofusion and hybridizer because of higher local temperatures assisting in wax softening and better spreading. The coated samples showed reduced moisture adsorption and the study showed that dry coating can be used to improve shelf life of magnesium and other particles. Extended time duration tests showed that different techniques would produce different results and no one machine can be labelled to be as always outperforming the other.

Meyer and Zimmermann (2004) studied effects of mixing time on surface coverage and its effect on flowability. Particles are cohesive if the adhesive forces outweigh the particle weight. Studies by varying the nanoparticles and by varying the blending time was conducted to study its effect on flowability. The reduction in tensile strength of the sample related poorly with the size of the nanoparticles. Hydrophobic nanoparticles performed better in reducing tensile strength than their hydrophilic competitors. Reasoning for this behavior seen in this study was as follows, hydrophilic nanoparticles have greater hydrogen bond formation and van der Waals forces due to which they form agglomerates and disperse poorly. All nanoparticle coated powders showed improved flowability. Hydrophobic nanoparticles show better surface coverage in comparison to hydrophilic nanoparticles as the breakage of

agglomerates is easier in the former. After increasing the mixing time beyond a certain limit the cohesivity increased as entire surface of host particle is covered.

Müller *et al.* (2008) used corn starch as host or pharmaceutical excipient and various types of fumed and precipitated and fumed nano silica powders. Binary powder mixtures of host powder and the flow regulator were prepared in a Turbula mixer. Tensile strength tester was used to test the tensile strength of the samples and gauge the effectiveness of flow regulators. Mechanism of the flow enhancement was attributed to the increase in surface roughness of the host particles by the adsorption of the flow regulating particles. Flow regulating potency of the silica powders was dependent on the de-agglomeration of the silica particles. Different combinations of varying silica particle size and cornstarch were tested and it was found that best flow regulating effect was achieved at roughly a silica surface area coverage of 20% on the host particles, silica powders with greater specific surface area had more stable agglomerates and thus inferior flow enhancement.

Ouabbas *et al.* (2009) conducted a study in which MgSt was coated on silica gel in hybridizer and cyclo-mix in wt./wt.% of 5 and 15 and then compared with the results of mixing in turbula mixer. Stability and quality of coated powders changes with change in storage conditions, particularly relative humidity plays a major role in pharmaceutical and food powder handling and storage. Hybridizer performs coating by high impaction forces and friction heat, high impaction is caused by interaction of powder with blades and wall. Hybridizer improved the flow of coated silica but the Cyclomix reduced the flowability attributed mainly to breaking of silica particles (fine particles have larger cohesive force). Turbula mixer did not improve flow. Processing silica with MgSt increased the hydrophobicity in all the three machines. Interestingly, after storage for a specific time under specific humidity conditions, the MgSt layer disappeared once again exposing the silica surface.

Zhang *et al.* (2009) studied the effect of coating silica, alumina and titania nano powders on micro sized potassium chloride. Study showed that the silica nano particles have better surface coverage than alumina and titania powders because in the titania and alumina powders, cohesive forces between particles dominate the cohesive forces between nano particles and host particles causing agglomeration of nano particles and improper spreading on host particles. Emphasis was laid on the fact that fluid energy milling promotes simultaneous micronization and coating, if micronization and coating were to be done in separate steps, the micronized powder would form agglomerates and thus providing hindrance in proper coating of guest particles. The best flow improvement was found in the case of silica coating as the particles had better surface coverage.

Zhou et al. (2010 b) compared the effects of simple blending and mechanofusion on powder properties. As in earlier studies, it was again confirmed that mechanofusion does not alter particle size and the improvement in flow was because of coating and its characteristics. Mechanofused samples showed better surface coverage and reduction in sharp edges, latter can be due to attrition or the guest particles coating the edges. Poured and tapped densities of the mechanofused samples were higher than untreated or simply mixed samples. Cohesion

values decreased for all the mechanofused powders tested. One interesting parameter proposed in this study was particle size. It is well known that greater the particle size greater the gravity forces and lesser the cohesive force, it was proposed that a particle size should be determined for pharmaceutical applications which maximizes coating efficiency. In this study, particle range of 7-20 micrometer was ascertained to have the best effect of coating.

Jallo *et al.* (2010) compared silane and dry coating methods for flow improvement and linked it further to combustion and reactivity. Coating takes place by the high energy impacts of the guest particles on the hosts, the guest particles stay attached or adhere to the surface as the van der Waals force between guest and host particles is greater than the weight of the guest particle. Large surface roughness or extremely smooth surfaces can be a source of increasing cohesivity as more contact area is available for interactions. Silane treatment improved flow by reducing surface energy and dry coating improved flow due to reduction in surface roughness. Easy dispersion and uniform aerosol formation of powders aid in combustion but the inertness of coatings such as silica and titania can decrease the combustion enthalpies. Improved flowability resulted in higher pressure value during constant volume explosion when powders were modified without using oxide coatings.

Jallo *et al.* (2012) emphasized that impact of coating on flow and other properties should not come at a cost of changed particle size and shape. Surface coverage of 10-20% and discrete coverage of guest particle can be enough to improve the flowability. Elasticity and hardness of particles were major factors influencing particle attrition as a magnet to powder mass ratio of 2:1 or 3:1 caused high particle attrition. Dry coating improved the flowability of all the powders tested. The coating reduces the direct contacts between host particles and increases there inter particle distance causing reduction in van der Waals forces. The operating parameters of MAIC for surface coverage and minimum particle attrition vary for different powders.

Kojima and Elliott (2013) used a polymer powder, poly (styrene-co-di vinyl benzene) (PS-DVB) as the primary micrometer size powder to investigate the improvement in bulk flowability by addition of hydrophilic and hydrophobic silica nanoparticles as flow regulators. Powder mixture was obtained by using a mixer with stainless steel rotating blades. Cohesion and internal friction of PS-DVB powders was used to gauge the effect of flow regulators and Ring Shear tester was used to conduct the tests. It was found that the effectiveness of flow regulators in reducing the cohesion depended on its ability to disrupt/reduce direct contact between PS-DVB particles. An increase in amount of silica particles beyond a certain limit saw an increase in cohesion because the silica nanoparticles started agglomerating on the PS-DVB particle surface and formed a flat film structure on it, this film increases the effective surface area. Nano sized flow regulators generally work best when the particles form asperities on the host surface and not a regular film. The nanoparticles which had smaller sized agglomerates reduced cohesion more and internal friction was higher at greater surface coverage of nanoparticles as the silica-silica contacts grew. The performance of the hydrophobic and hydrophilic flow regulators could be attributed to the ease of breaking their agglomerates during mixing.

Ghoroi, Gurumurthy, *et al.* (2013) used MAIC and found that coated nanoparticles imparted nano scale roughness on the guest particles and that reduces host-host particle contact, hence reducing cohesivity and agglomeration tendency thus increasing the dispersibility. Attrition of the particles was minimum. Surface coated API's and excipients generally showed improvement in flowability in comparison to uncoated ones. Powders which have good flow generally pack better because of the low cohesion forces due to which the structure collapses during settling of particles. The author plotted conditioned bulk density and flow function coefficient and defined two regions i.e. "probable" and "definite" for direct compaction and barring one API used in this study, all other dry coated API's fell in one of the two regions indicating that dry coating can aid in direct compaction.

Zhou *et al.* (2013) investigated the flowability enhancement of a powder blend of mainly ibuprofen and microcrystalline cellulose by coating it with silica nanoparticles. The samples were blended in a v-blender and then sent for further processing in co-mill. Flow factor of the uncoated and coated powder blends was determined to gauge the impact of coating. Silica nanoparticles significantly improved flowability and co-milling cycles and the silica wt./wt.% loading were the two most important parameters affecting the improvement. It was found that simple blending was very effective in improving the flow of ibuprofen blend containing silica nanoparticles and the use of coating device could be avoided. Silica coated ibuprofen blends showed improved compactability and tabletability without impacting compressibility. Overall silica coated ibuprofen blends showed improved properties and this could be achieved by simple blending.

Ghoroi, Han, *et al.* (2013) linked dispersibility with dry coating and dispersion effects on flowability. Small particles are generally more cohesive than larger particles and have poor dispersibility. Micronized acetaminophen without coating showed agglomeration whereas Leucine coated showed rough surface on SEM analysis and little agglomeration. The micronized dry coated powders showed improved dispersibility and required much lesser energy to achieve fully dispersed state in comparison to uncoated micronized powders indicating that the dry coating reduced cohesive forces and hence made it easier to disperse the powder. All coated powders showed improved flow, fluidization and bulk densities indicating better packing which can be linked to better dispersibility caused by reduction in cohesion.

Huang *et al.* (2015) coated micronized acetaminophen (API) blends containing Avicel 105 and Pharamatose 450M (excipients) with nano silica in resonant acoustic mixer or LabRAM. The efficacy of nano silica in improving flow was seen by determining flow function and bulk density. It was seen that the improvement was substantial in blends which had coated acetaminophen and this was seen across blends with different acetaminophen loading. Compactability improved regardless of the fine excipients. The study showed that the coating technique could be used to improve the flow of fine API blends with fine excipients and at the same time achieving improved tablet compactability. It was seen that at high API loading regardless of the excipient size the properties improved substantially of the coated API blends and such improvement was not seen in simple blended samples.

Capece *et al.* (2015) used Bond number which is the ratio of the inter-particle cohesion force to particle weight as an investigative tool to determine relation between cohesive inter particle forces and flow function coefficient. In this study, acetaminophen was used as API and microcrystalline cellulose and starch as excipients, these were mixed in LabRAM in different mass proportions to form various blends. Surface modification by coating acetaminophen with nano silica was also carried out in LabRAM and blends were formed again with the excipients. Multi component granular Bond number was defined and used to successfully predict the flow of binary, ternary and quinary mixtures. The surface modified acetaminophen blends showed great enhancement in flowability as compared to the untreated acetaminophen blends. The granular Bond number was found to be most applicable to fine cohesive powders where van der Waals forces dominate.

Karde, Panda and Ghoroi (2015) investigated the effect of humidity on the powder flow. At high humidity capillary forces assume significance and the adsorbed moisture strengthens van der Waals forces by increasing apparent diameter and decreasing inter particle distance. The uncoated powders showed increased aggregation tendencies with increasing relative humidity levels because of capillary bridge formation between particles. The coated powder samples showed no aggregation tendencies on increasing RH levels because of the hydrophobic nature of the coating and also the increased surface roughness which prevented capillary bridge formation. The coated samples showed no real change in bulk density, pour bulk density and compressibility on increasing the RH level whereas the uncoated powder properties were very sensitive to change in RH levels. Some earlier studies showed that an excessive reduction in RH levels increases the friction effect between particles due to reduction in lubrication between particles and ultimately leading to poor flow. The study conducted showed that the powders can be made immune to changing RH conditions by dry coating with respect to flow and packing properties.

Zhu *et al.* (2017) used cubic SAPO-34 zeolite particles as host and spherical silica nanoparticles as guest particles or flow regulators. Cubic host particles were chosen to study the effectiveness of silica nanoparticles on the flow of irregularly shaped particles as an extreme case. The SAPO-34 powder was first dispersed into deionized water and then silica particles were added under magnetic stirring. This suspension was then sonicated and then filtered and dried to obtain the coated samples. To test the flowability both static and dynamic characteristic of the powder namely angle of repose and fluidization was tested. The coated SAPO-34 saw reduction in the angle of repose and complete fluidization at particular nanoparticle size and surface area coverage on the host surface. Thus, nanoparticles helped to improve the flowability characteristics in the extreme case of cubic shaped particles but it was felt that the problem of nanoparticle agglomeration should be looked into for practical applications of coating.

Ruzaidi, Mandal and Chatterjee (2017) studied the glidant effect of hydrophobic and hydrophilic nano-silica on poorly flowing API ibuprofen. Flow characterization techniques like angle of repose and Carr index were used together with flow factor, effective angle of

internal friction and cohesion obtained from tests conducted on Powder Flow Tester to study the glidant effect. Ibuprofen and silica samples were mixed in a V-Blender. It was found that angle of repose and Carr index were broadly able to classify the silica-API powders in terms of flowability but to assess the actual flowability, powder flow during bulk flow or consolidation should be studied. Both hydrophobic and hydrophilic silica improved the flowability almost to an equal extent and 0.5-1.0 wt./wt.% silica was found to be the most effective in improving the flow properties.

The following text discusses the work on powder flow properties conducted at Thapar Institute of Engineering and Technology, Patiala with the help of PFT. Rohilla (2016) conducted a study on impact of physical properties of powders on their flow properties and subsequently followed up it with (Rohilla *et al.*, 2018)**.** Fly ash samples from different electro static precipitator hoppers were collected and tested. It was found that the flow properties varied with the median particle size. Further, hoppers for mass flow discharge were designed by using this data and models were developed to predict the hopper dimensions. Garg (2017) conducted a study on various pharmaceutical powders and also a detergent powder to gauge the powder flow properties and subsequently designed hoppers using this data. In both the studies arching flow factor was not calculated which is a vital parameter to add in the Powder Flow Pro software for designing hoppers. Arching flow factor varies for each powder and thus should be calculated separately and entered into Powder Flow Pro to obtain accurate dimensions of hoppers.

Chapter 3

Materials and Methods

3.1 Materials

Ibuprofen and paracetamol were selected as active pharmaceutical ingredient's or API's for gauging the effect of blending on flow properties due to their widespread use and known poor flow properties (Pingali *et al.*, 2009; Ghoroi, Gurumurthy, *et al.*, 2013; Ghoroi, Han, *et al.*, 2013; Zhou *et al.*, 2013; Qu *et al.*, 2017). Ibuprofen was purchased from IOL Pharma Limited, Ludhiana and paracetamol from EG Pharmaceutical, Baddi.

Avicel PH-101 and Avicel PH-102 were used as pharmaceutical excipients to improve the flowability of the cohesive API powders. Aerosil R972 pharma (average particle size of 16nm, Karde, Panda and Ghoroi, 2015) which is a silane treated silicon dioxide nano-powder was also used to study the effect on flowability of the cohesive API's. Avicel PH-101 and Avicel PH-102 were purchased from All Well Pharma, Chandigarh and Aerosil R972 Pharma from Kanchan Rasayan, Mumbai.

Table 3.1: d_{10}, d_{50}, d_{90} and d_{32} diameters of different materials

Material	***d_{10}(µm)***	***d_{50}(µm)***	***d_{90}(µm)***	***d_{32}(µm)***
Ibuprofen	3.657	21.948	72.506	7.666
Paracetamol	2.838	14.267	72.297	5.978
Avicel PH-101	21.894	62.153	129.853	36.794
Avicel PH-102	34.051	127.676	267.585	70.879

Note: d_{10}, d_{50}, d_{90} means 10%, 50% and 90% below this size; d_{32} = volume/surface mean

3.2 Methodology

Blends of paracetamol with Avicel PH-101 and Avicel PH-102 were prepared in the wt. / wt. ratios of 20, 40, 60 and 80%. Similarly ibuprofen blends with Avicel PH-101 and Avicel PH-102 were prepared in the wt. / wt. ratios of 20, 40, 60 and 80%. Blends of paracetamol and ibuprofen with nano-silica were prepared in order to cover 20, 40, 60 and 80% of the surface area of paracetamol and ibuprofen.

Amount of nano-silica needed for covering the surface area was calculated by using the formula provided in Yang *et al.* (2005)**.**

$$\mathrm{Gwt\%} = \frac{(\mathrm{Nd^3\rho_d})}{(\mathrm{D^3\rho_D}) + (\mathrm{Nd^3\rho_d})} \times 100 \qquad (3.1)$$

$$N = \frac{4(\mathrm{D} + \mathrm{d})^2}{\mathrm{d}^2} \qquad (3.2)$$

ρ_d= Particle density of guest particles, ρ_D= Particle density of host particles
D= Diameter of host particles, d= Diameter of guest particles

Size of R972 Pharma: 16nm
d_{32} of paracetamol: 5.978 µm
d_{32} of ibuprofen: 7.666 µm

True density of R972 Pharma: 2650 kg/m^3
True density of paracetamol: 1250 kg/m^3
True density of ibuprofen: 1075 kg/m^3

The following are the wt. / wt.% of nano-silica required to achieve the mentioned surface area coverage. The wt. / wt.% was kept under 2%.

Table 3.2.Paracetamol

wt./wt.%	SAC(%)
0.49453316	20
0.98906633	40
1.48359949	60
1.97813267	80

Table 3.3.Ibuprofen

wt./wt.%	SAC(%)
0.40495413	20
0.80990826	40
1.21486238	60
1.61981651	80

The blends were prepared by sieving the API's and excipients independently through a sieve and then mixing the powders in a plastic container. Mixing was done by rapid shaking for 10 minutes for each sample.

Overall a total of 24 blended samples were prepared.

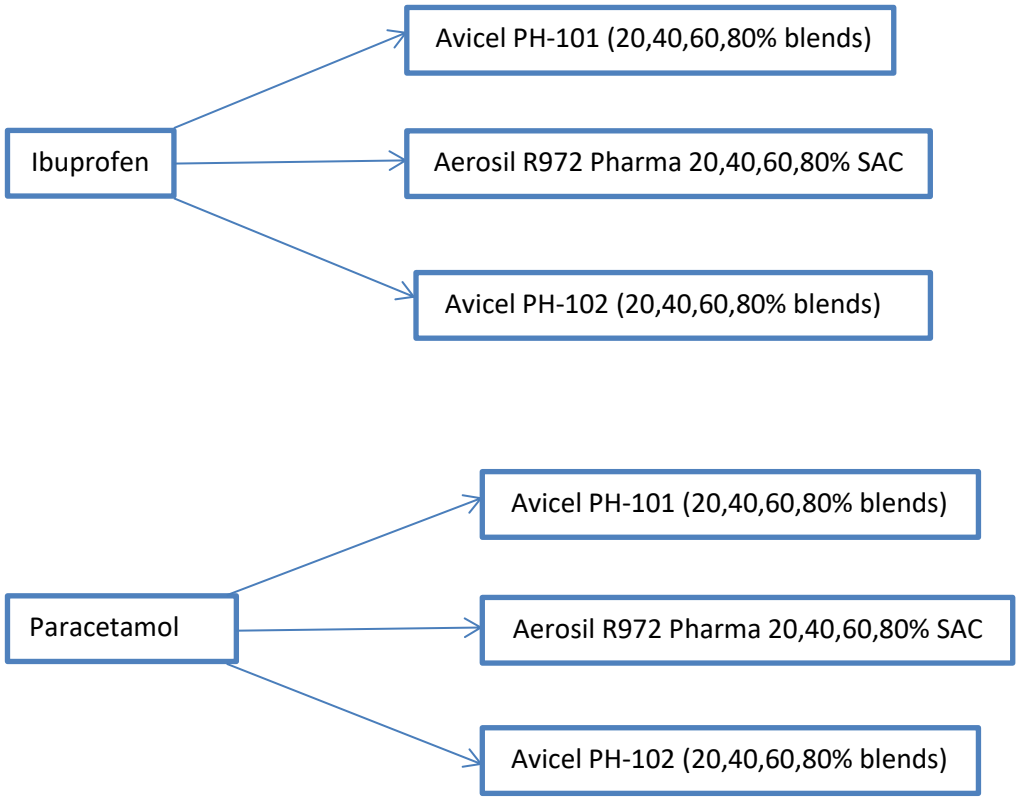

Figure 3.1. Blends of ibuprofen and paracetamol with different glidants.

3.3 Testing Methodology

Testing was done on Brookfield PFT. On each sample mentioned in the above section the following tests were conducted and repeated five times.

The following three tests were conducted on PFT.

(a) Standard flow function test

The flow function test is used to characterize the relative cohesive strengths of powders which can be used to assess their gravity flow behavior through hoppers and bins. In this test, the sample is consolidated at different normal stresses and then sheared till steady state. At each consolidation stress level, failure locus is constructed to determine the unconfined yield strength at that consolidation stress level. Each failure locus is constructed after shearing the sample at the consolidation stress (CS), CS*(1/3) and CS*(2/3) and calculating peak shear stress for that CS. One more point is obtained by shearing the sample again at the consolidation stress and calculating the peak shear stress. Failure locus is the best fit curve of

these four points. Two Mohr circles are constructed with the help of the failure locus namely unconfined failure Mohr circle and consolidation Mohr circle which gives the values of unconfined yield strength and consolidation stress to plot the flow function. In the standard flow function test, the sample is tested at five consolidation stresses meaning construction of five failure locus and obtaining unconfined failure strength and consolidation strength from each locus.

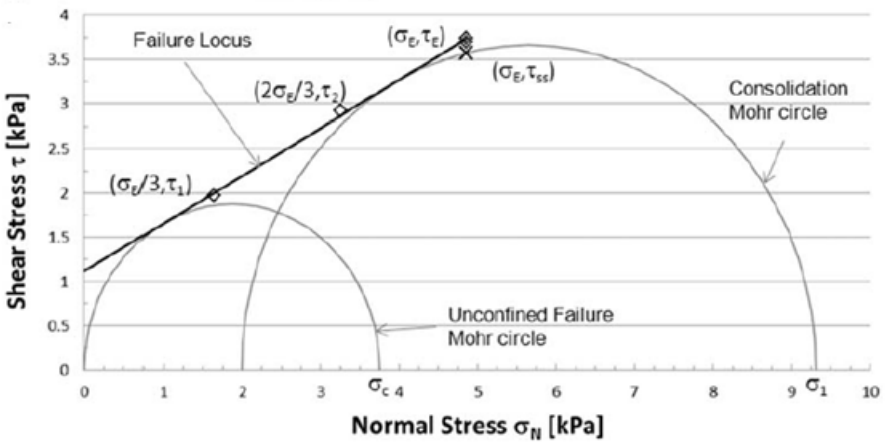

Figure 3.2. Failure locus construction by shear stress and normal stress data (Berry, Bradley and McGregor, 2015)
σ_c = unconfined failure strength (kPa)
σ_E = consolidation normal stress (kPa), σ_N= normal stress (kPa)
τ_E= peak shear stress (kPa), τ_{SS}= steady state shear stress (kPa)

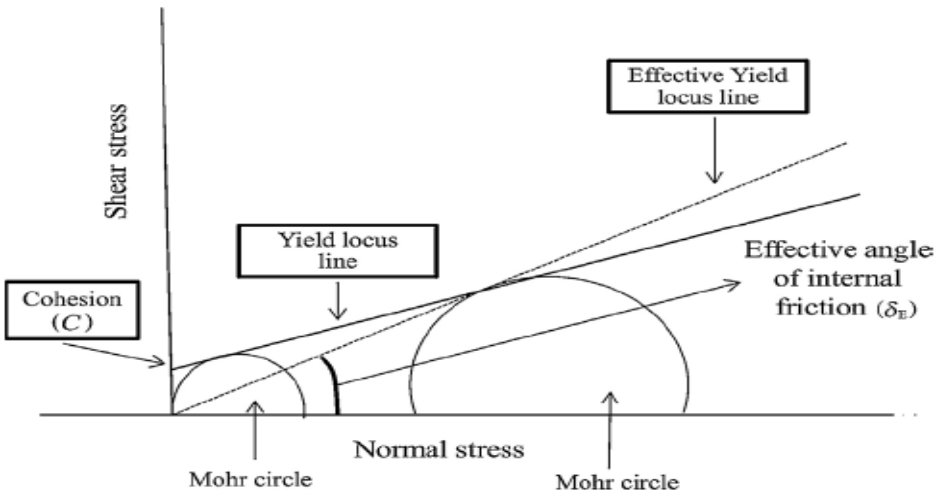

Figure 3.3. Flow characterization data derived from the shear flow tester (PFT) (Ruzaidi, Mandal and Chatterjee, 2017)

The yield locus line helps to ascertain two other major parameters related to powder flow namely effective angle of internal friction and cohesion.

Effective angle of internal friction is defined as the angle between the normal stress axis and a line that starts at the origin and is tangent to the consolidation Mohr circle. This angle is a measure of the inter particle friction and indicates the friction two sliding layers of powders face at a particular normal stress. A lower effective angle of internal friction generally indicates better flowability.

Cohesion is the value of shear stress where the yield locus cuts the shear stress axis. It is an indicator of the shear strength of the bulk solid at zero normal stress. Lower cohesion generally leads to better flowability of bulk solid specimen.

(b) Standard wall friction test

The wall friction test is used to measure the friction acting between the powder and a hopper or chute wall surface at the onset of flow. Wall friction angle is calculated for different normal/consolidation loads by constructing the wall yield locus. At each normal stress wall shear stress is applied to the sample to shear it. At each normal load, peak wall shear stress is calculated for wall displacement. The collection of points made by wall shear stress and normal load gives the wall yield locus. The wall friction angle is calculated by calculating the slope of a line through the origin to the wall yield locus cutting at the particular normal stress.

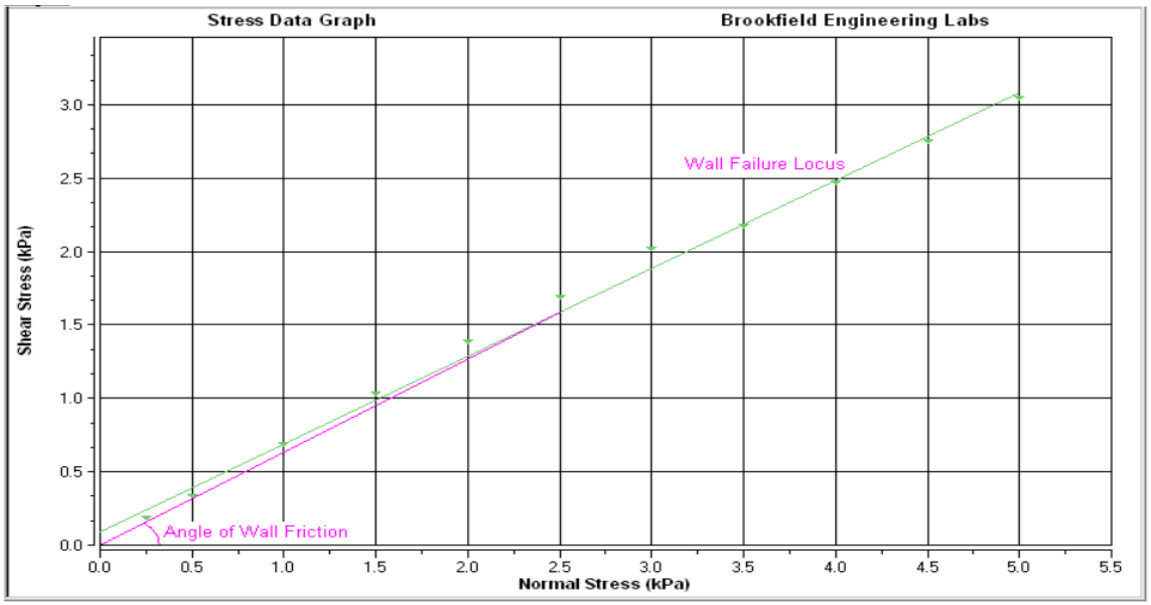

Figure 3.4. Wall failure locus construction by shear stress and normal stress data

(c) Standard bulk density test

This test measures the bulk density of a powder under various loads. The sample is loaded and increasing compaction loads are applied and bulk density is calculated at each load.

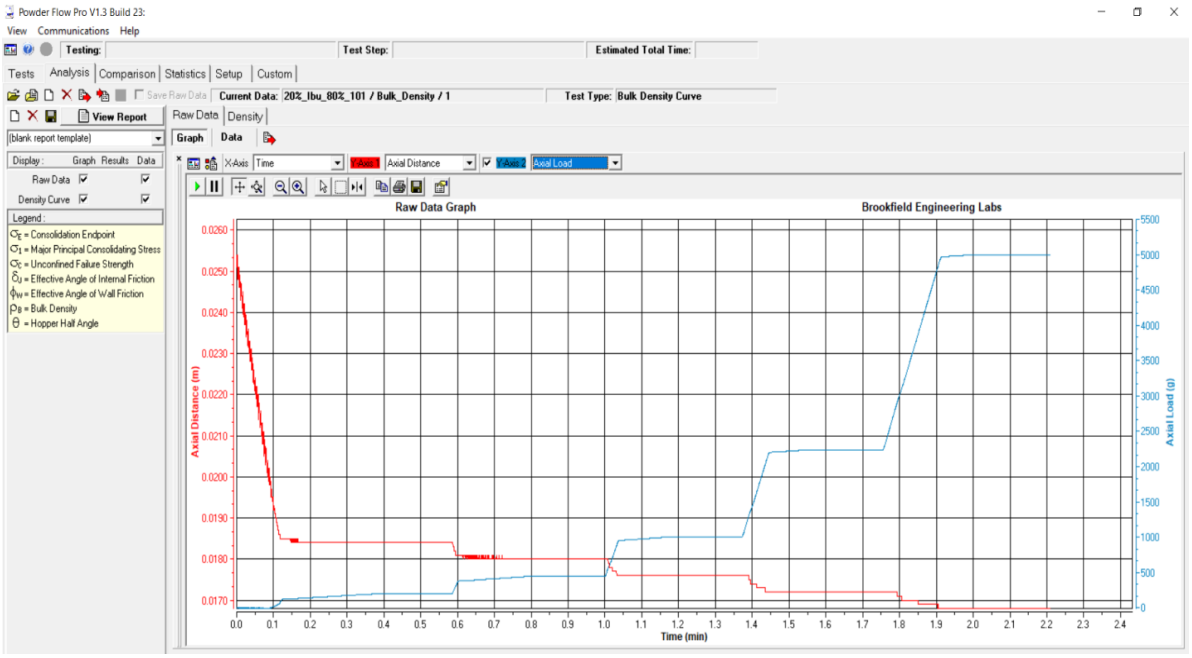

Figure 3.5. Bulk density test PFT raw data

PFT performs the bulk density test in the following manner. The user is asked the sample weight of the powder when the trough is loaded on PFT. A series of compaction loads are applied on the sample in increasing magnitude through the wall friction lid and the lid position or the axial distance travelled by the lid is calculated /noted. In doing so the volume of the compressed powder volume can be calculated by multiplying the axial distance travelled by lid and the annular cross sectional area of the trough and then subtracting it from the original trough volume. The mass of the powder specimen loaded is divided by this volume to obtain the bulk density. Bulk densities at each compaction load are thus calculated and each compaction load corresponds to a particular stress value. Thus bulk density curve between normal stress and bulk density of the sample is obtained by plotting the corresponding normal stress and bulk density values.

Chapter 4

Results and Discussions

4.1 Scanning electron microscope (SEM) images

A scanning electron microscope (JEOL JSM-5510LV) was used to assess the morphology of particles and EDS results were taken to confirm the presence of silica in the nano blended samples.

(a)

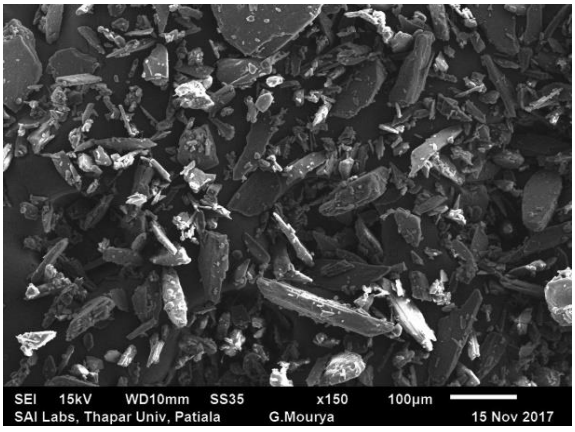

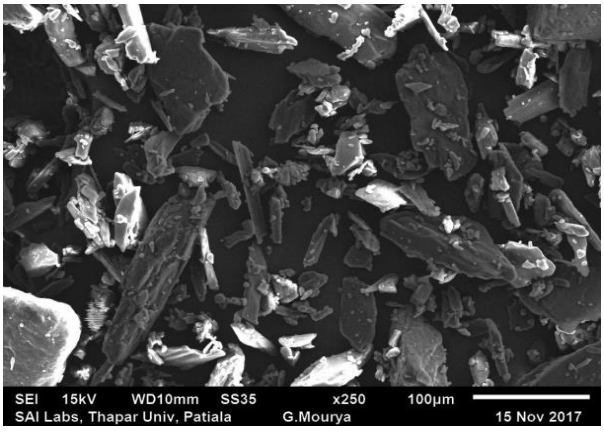

(b)

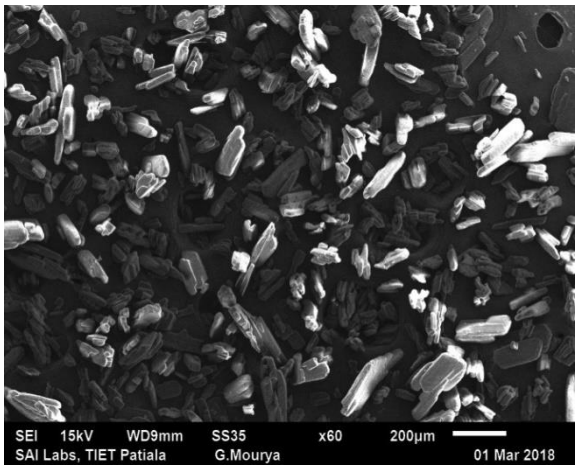

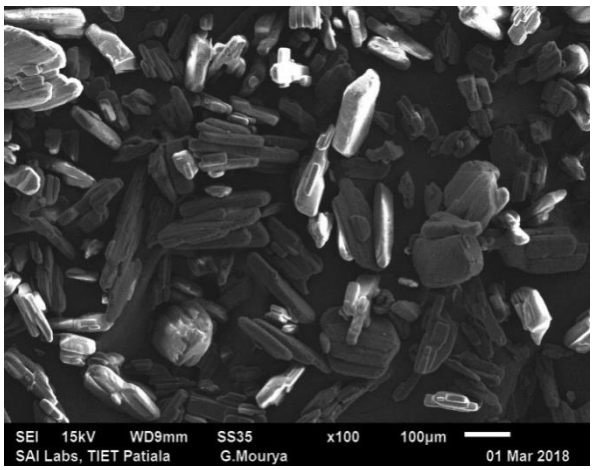

(c)

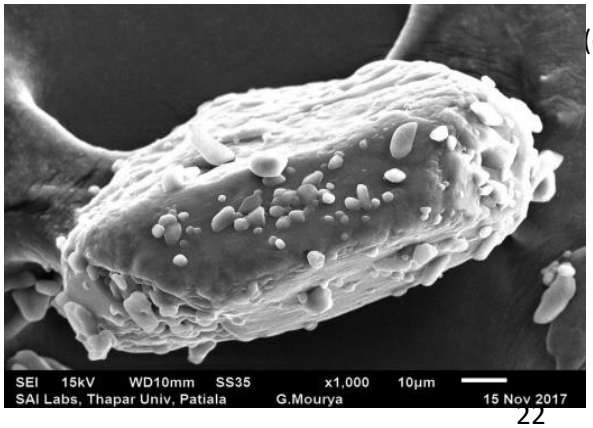

(d)

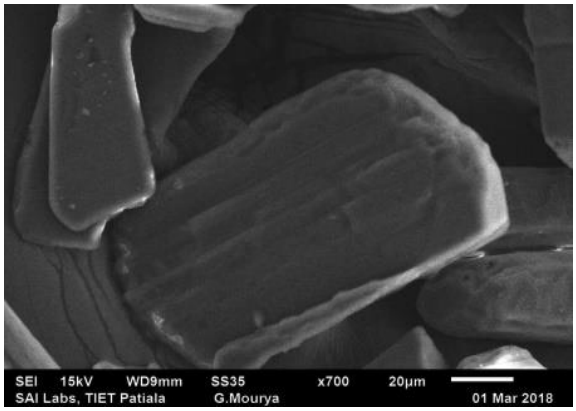

(e)

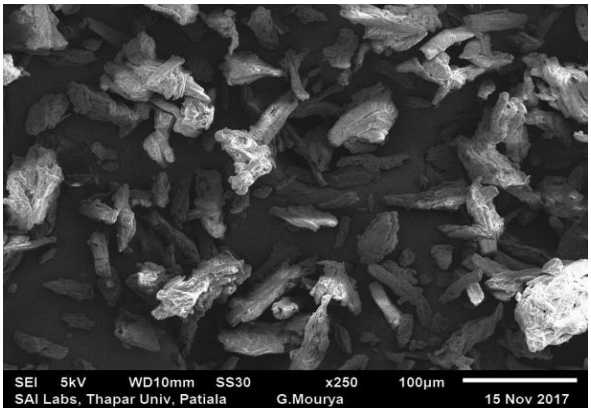

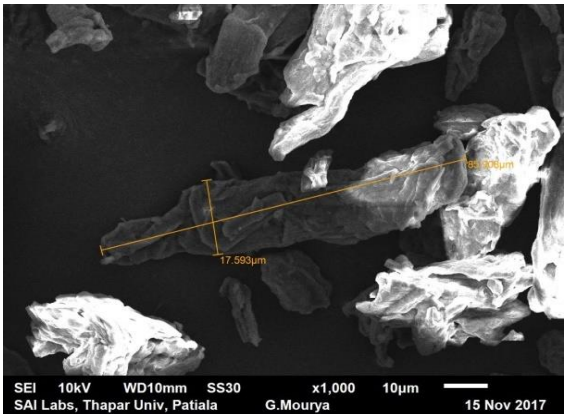

(f)

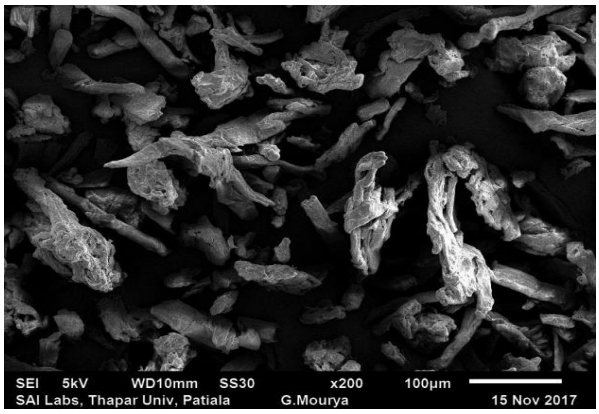

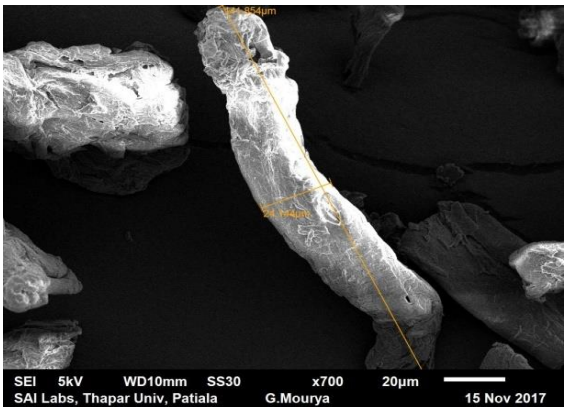

Figure 4.1. SEM images of (a) Paracetamol at magnification of 150x & 250x respectively, (b) Ibuprofen at magnification of 60x & 100x respectively, (c) Paracetamol at magnification of 1000x, (d) Ibuprofen at magnification of 700x (e) Avicel PH-101 at magnification of 250x & 1000x respectively, (f) Avicel PH-102 at magnification of 200x & 700x respectively.

4.2 Energy-dispersive X-ray spectroscopy (EDS) results of mean of three spectrums (all results in weight%)

Table 4.1. Paracetamol 80% SAC

Carbon	Nitrogen	Oxygen	Silicon
52.27	12.34	31.89	3.51

Table 4.2. Ibuprofen 80% SAC

Carbon	Oxygen	Silicon
71.78	24.90	3.33

4.3 Paracetamol blended with Avicel PH-101

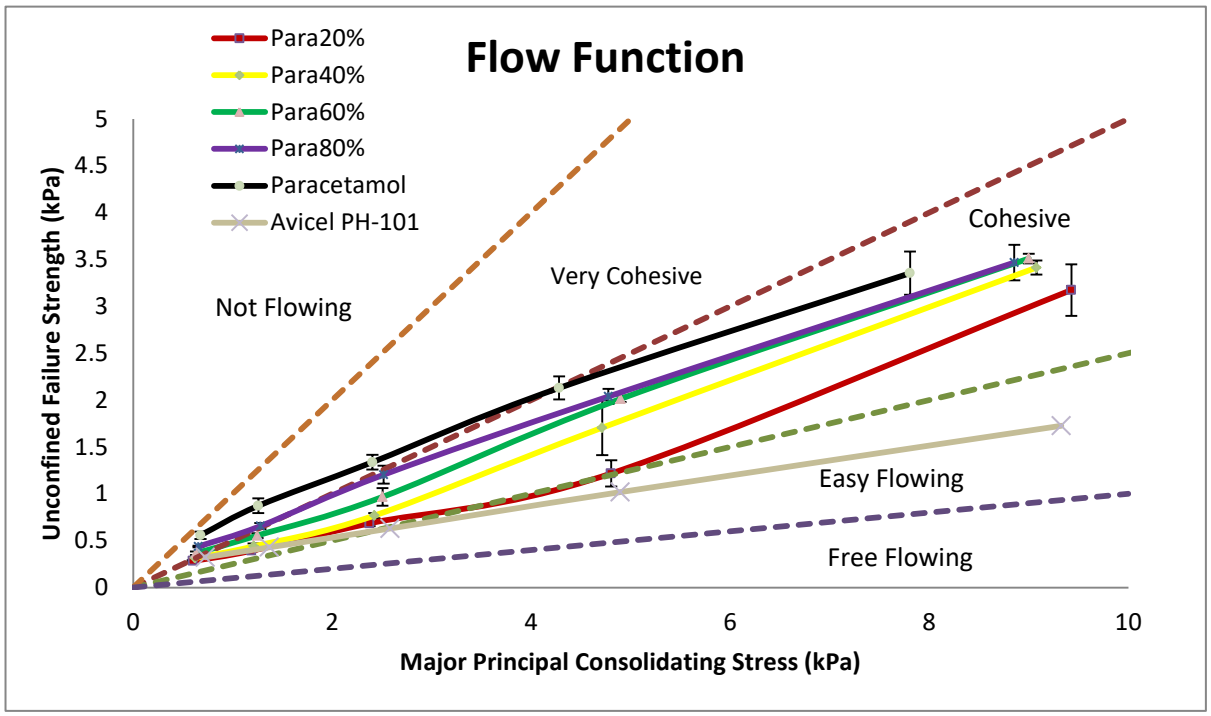

Figure 4.2. Flow function curve of paracetamol blended with Avicel PH-101

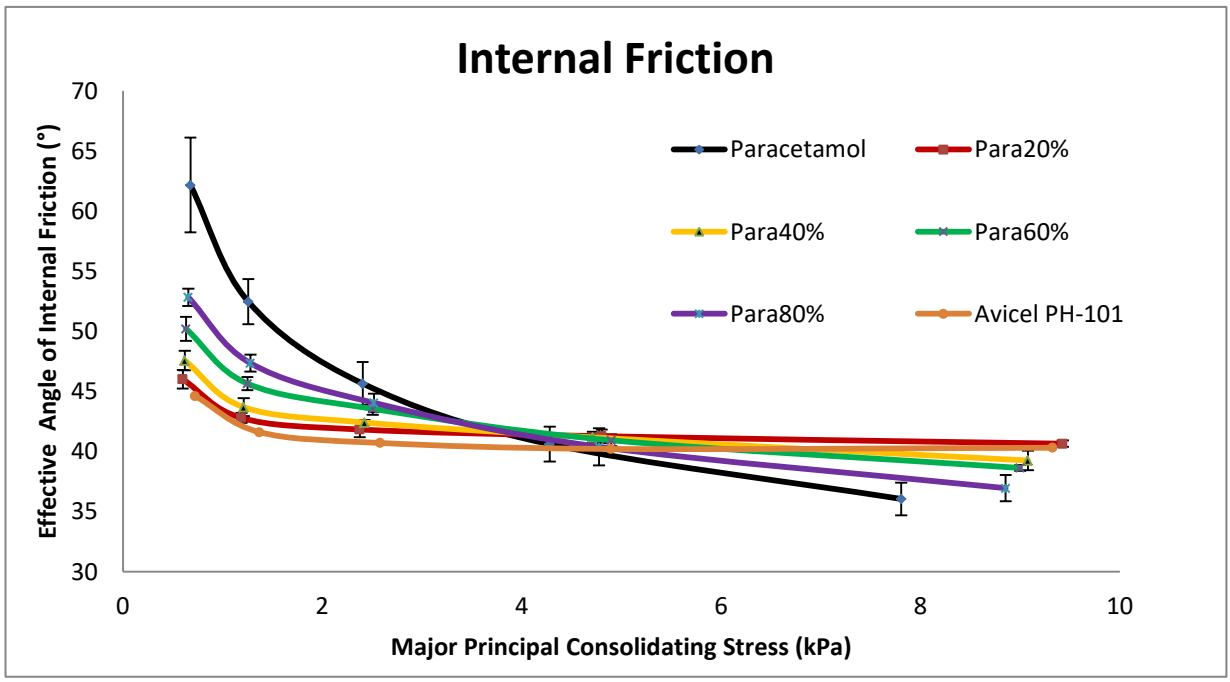

Figure 4.3. Internal friction curve of paracetamol blended with Avicel PH-101

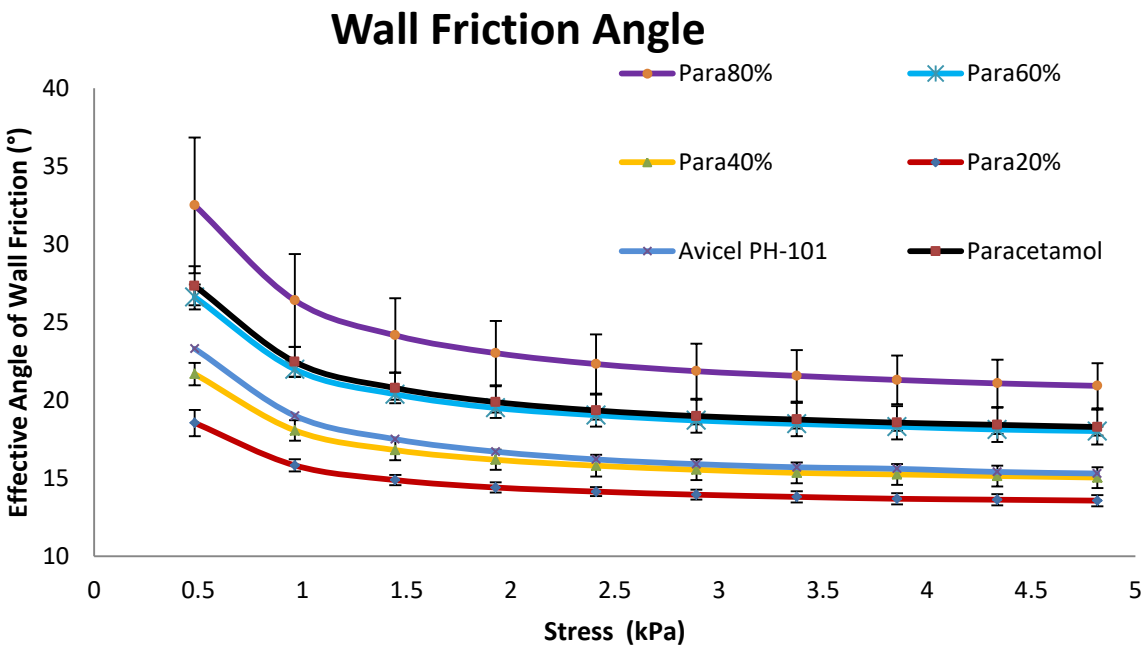

Figure 4.4. Wall friction curve of paracetamol blended with Avicel PH-101

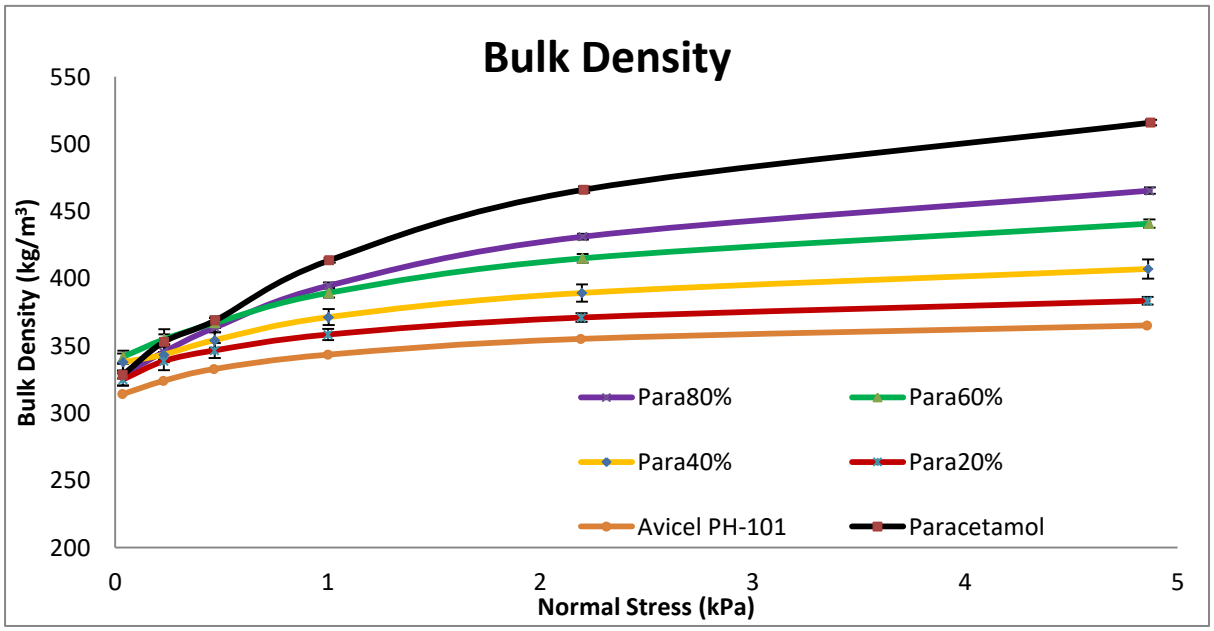

Figure 4.5 Bulk density curve of paracetamol blended with Avicel PH-101

Figure 4.2 reveals that the maximum flowability improvement was in the case of 80% blend (Para20%) whereas the 20% blend (Para80%) had minimum improvement in flowability. The reason behind this is that Avicel PH-101 has greater flowability than 100% paracetamol and therefore as the percentage of Avicel PH-101 in the blend increases, the flowability increases with it.

Wall friction was lowest in the case of 80% blend (Para20%) and highest for 20% blend (Para80%) as seen in Figure 4.4, even higher than the pure paracetamol. It means the particles

are facing higher friction in the 20% blend and would not flow easily. Particles with lower wall friction transfer their weight downwards rather than on the wall due to which the flow improves.

Bulk density of pure paracetamol was highest and increased with an increase of paracetamol in the blend as seen in Figure 4.5. This trend is easy to explain as the bulk density of pure paracetamol is greater than Avicel PH-101 and as a result, an increase in the paracetamol content in the blend leads to increase in the density. Pure paracetamol showed better compressibility than the blends as indicated by the bulk densities with increasing normal loads.

Flowability and bulk density results are well supported by the cohesion and effective angle of internal friction values tabulated in Table 4.3. Lower cohesion means greater flowability. It can be seen that the cohesion values for the blended samples were lesser than paracetamol, hence in agreement with the flowability results. The cohesion values increased with the increase in the paracetamol content in the blend. Internal friction angle gives the friction between the powder particles, a greater variation in internal friction angle means greater compressibility of the powder sample. It is because at increasing stresses, the powder particles are compacted and their interlocks are broken which are the primary source of friction. This is the reason the internal friction angle reduces with increasing stress. Range of internal friction angles of blended samples was less as compared to paracetamol indicating poor compressibility but improved flowability as the internal friction angles were lower than paracetamol at comparable stresses indicating reduced friction between particles.

Table 4.3. Major principal consolidating stress, unconfined failure strength, effective angle of internal friction and cohesion values of paracetamol and Avicel PH-101 blends

	Flow function			
Material	Major principal consolidating stress (kPa)	Unconfined failure strength (kPa)	Effective angle of internal friction (°)	Cohesion (kPa)
Paracetamol	0.6774	0.5578	62.15	0.1586
	1.2578	0.8718	52.45	0.2656
	2.4045	1.3372	45.64	0.415
	4.2808	2.1294	40.6	0.6986
	7.8068	3.3534	36.04	1.1332
20% Paracetamol + 80% Avicel PH-101	0.6	0.2822	46	0.0782
	1.1888	0.3914	42.78	0.1044
	2.3756	0.6846	41.82	0.1816
	4.8034	1.2168	41.26	0.3194
	9.4278	3.174	40.64	0.8986
40% Paracetamol + 60% Avicel PH-101	0.6204	0.3138	47.56	0.0868
	1.211	0.4392	43.68	0.1176
	2.424	0.7676	42.4	0.205
	4.7136	1.7054	41.16	0.492

	9.0776	3.4136	39.24	1.025
60% Paracetamol + 40% Avicel PH-101	0.6322	0.3656	50.2	0.1022
	1.2486	0.5548	45.64	0.1516
	2.5058	0.9666	43.54	0.2652
	4.8992	2.0126	40.92	0.5988
	9.0002	3.51	38.62	1.0818
80% Paracetamol + 20% Avicel PH-101	0.6554	0.4376	52.82	0.1276
	1.2786	0.6556	47.34	0.1834
	2.5174	1.2034	44.04	0.3556
	4.7758	2.0378	40.38	0.625
	8.8544	3.4672	36.94	1.1092
Avicel PH-101	0.7258	0.3216	44.6	0.073
	1.37	0.429	41.6	0.1005
	2.582	0.6296	40.7	0.154
	4.8958	1.0178	40.2	0.254
	9.3268	1.7256	40.3	0.457

Table 4.4. Wall friction and bulk densities values of paracetamol and Avicel PH-101 blends

	Wall friction		Bulk density	
Material	Stress (kPa)	Effective angle of wall friction (°)	Stress (kPa)	Density (kg/m³)
Paracetamol	0.482	27.34	0.0362	328.42
	0.963	22.46	0.2304	352.96
	1.4452	20.78	0.4716	368.9
	1.928	19.88	1.0088	413.5
	2.4102	19.34	2.2062	465.98
	2.892	18.98	4.8746	515.82
	3.374	18.76		
	3.8556	18.56		
	4.337	18.42		
	4.8172	18.28		
20% Paracetamol + 80% Avicel PH-101	0.4828	18.54	0.036	324.92
	0.9634	15.82	0.229	338.58
	1.4458	14.88	0.4676	346.52
	1.9282	14.4	1.0018	358.32
	2.4102	14.14	2.1942	370.96
	2.892	13.94	4.8592	383.42
	3.374	13.8		
	3.8556	13.68		
	4.3368	13.62		
	4.8174	13.56		
40% Paracetamol + 60% Avicel PH-101	0.4824	21.68	0.0374	337.82
	0.9638	18.06	0.2294	343.46
	1.4456	16.8	0.4684	354.18
	1.928	16.18	1.004	371.28

	2.4104 2.892 3.3738 3.8558 4.337 4.8178	15.8 15.54 15.34 15.24 15.14 15.04	2.1966 4.8612	389.24 407.06
60% Paracetamol + 40% Avicel PH-101	0.4826 0.9636 1.4458 1.9284 2.41 2.892 3.3738 3.8558 4.3372 4.8182	26.62 21.98 20.38 19.5 19.04 18.7 18.48 18.3 18.12 18.02	0.0378 0.2304 0.4698 1.0062 2.1998 4.8668	341.84 354.78 366.9 389.34 414.98 440.72
80% Paracetamol + 20% Avicel PH-101	0.4822 0.9636 1.4454 1.9284 2.4102 2.892 3.374 3.8558 4.3376 4.8182	32.5 26.4 24.16 23.02 22.32 21.86 21.56 21.3 21.08 20.92	0.0362 0.229 0.47 1.0056 2.2014 4.8696	328.42 345.38 363.56 394.7 431.06 465.28
Avicel PH-101	0.483 0.964 1.445 1.928 2.411 2.892 3.374 3.856 4.337 4.817	23.3 19 17.5 16.7 16.2 15.9 15.7 15.6 15.4 15.3	0.035 0.227 0.466 1.0025 2.192 4.857	314.05 323.9 332.7 343.375 355.1 365.1

4.4. Paracetamol blended with Avicel PH-102

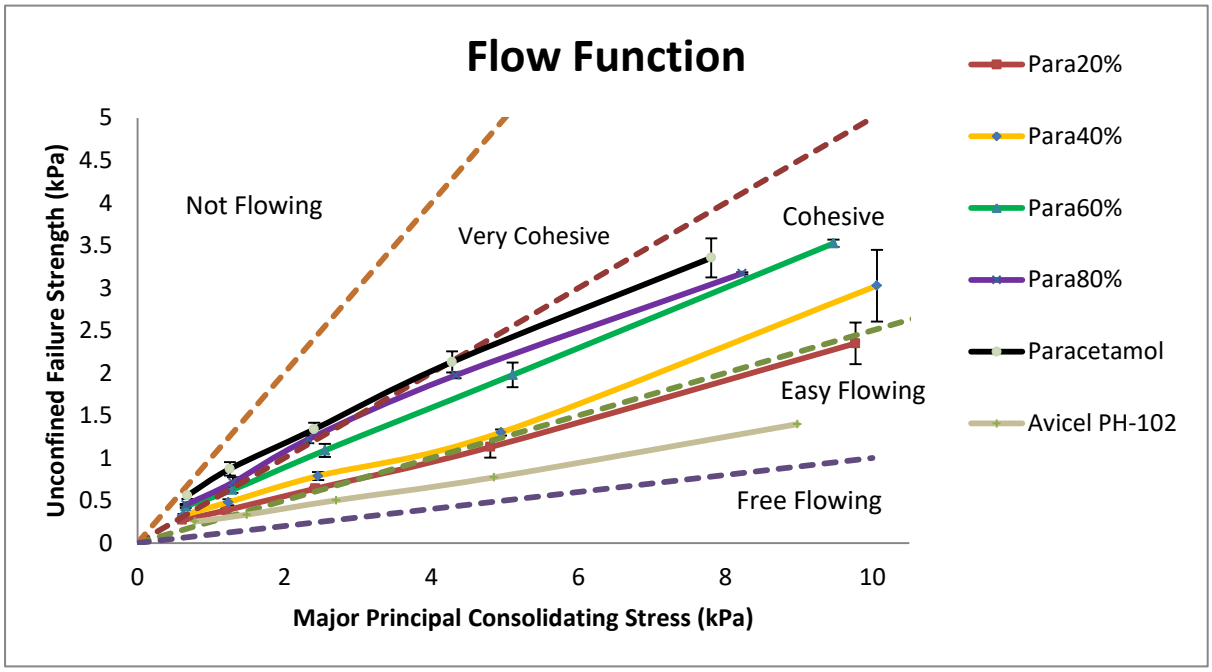

Figure 4.6. Flow function curve of paracetamol blended with Avicel PH-102

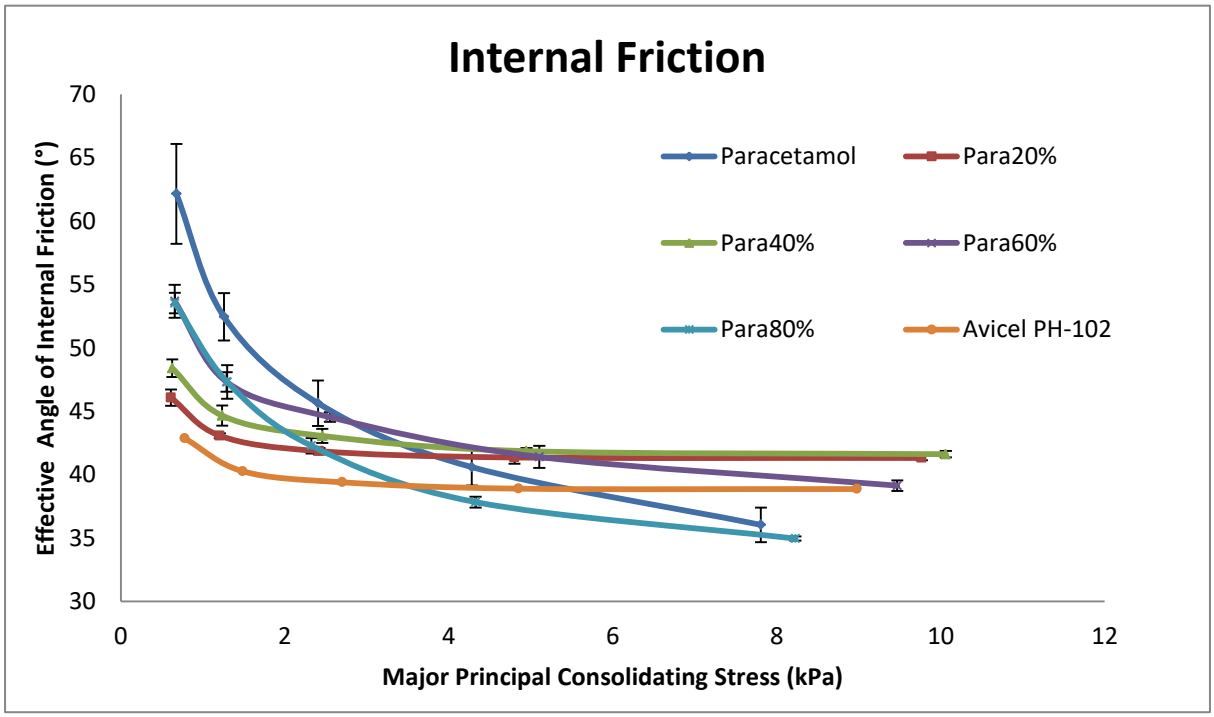

Figure 4.7. Internal friction curve of paracetamol blended with Avicel PH-102

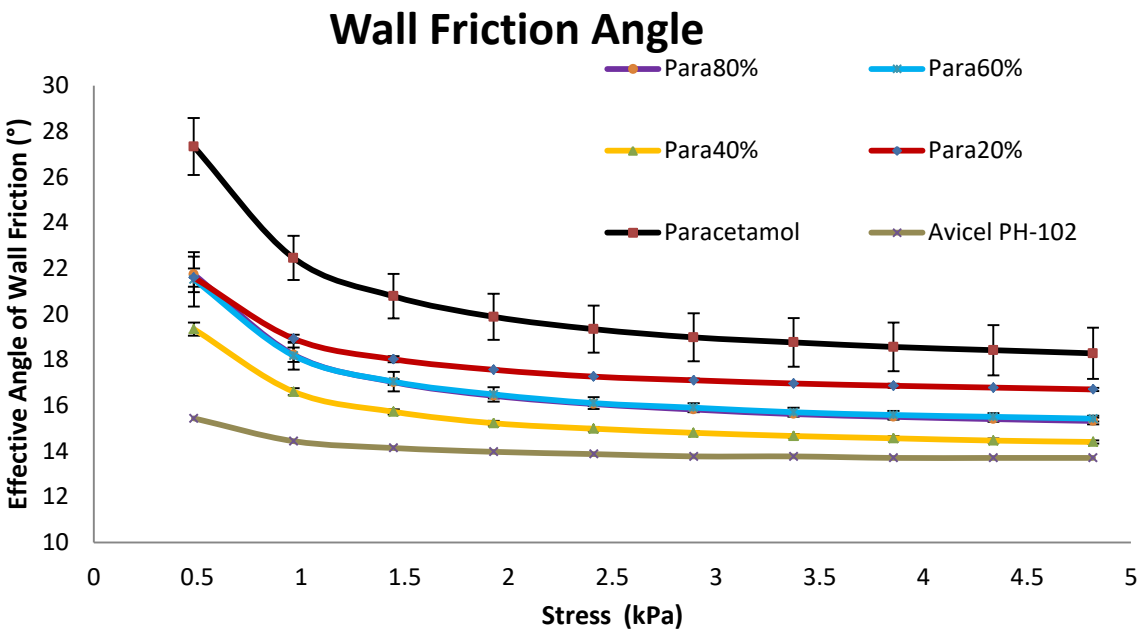

Figure 4.8. Wall friction curve of paracetamol blended with Avicel PH-102

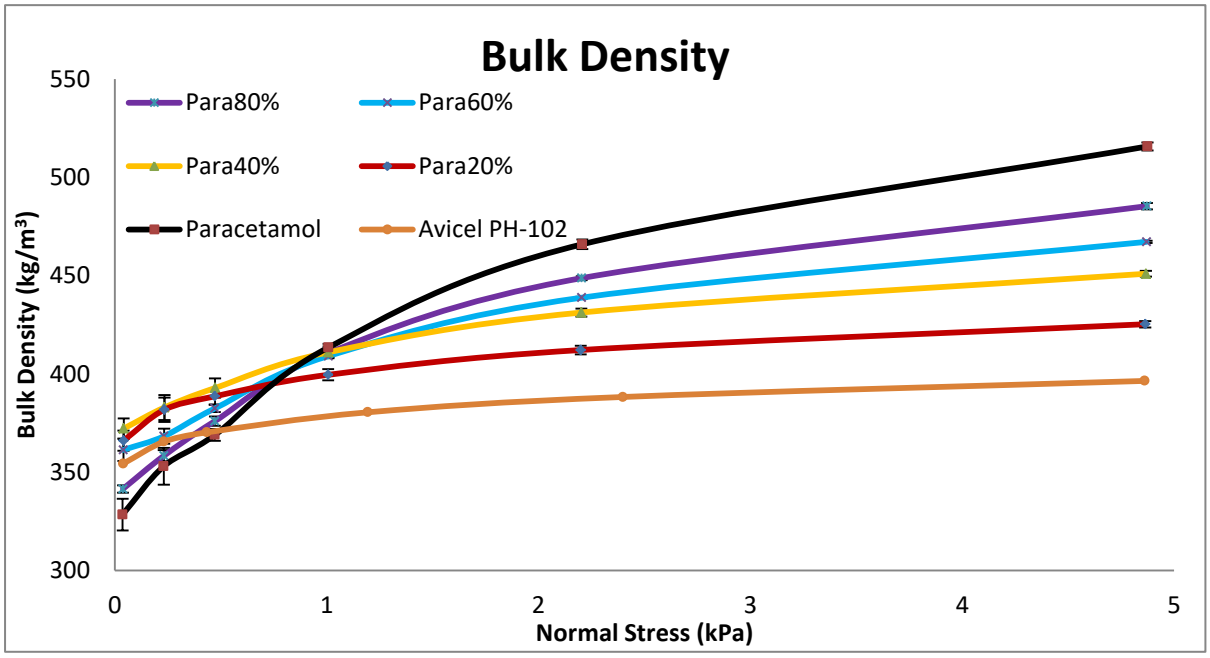

Figure 4.9. Bulk density curve of paracetamol blended with Avicel PH-102

80% blend of paracetamol (Para20%) with Avicel PH-102 has shown the most improvement in flowability and the least improvement was in 20% blend (Para80%) with the 40% (Para60%) and 60% (Para40%) blends between them as seen in Figure 4.6. As the percentage of relatively free flowing Avicel PH-102 increased in the blend the flowability improved.

In Figure 4.8, least reduction in wall friction angles was observed in the 80% blend (Para20%), greatest reduction was seen in the 60% blend (Para40%) with the 40% and 20%

blends sandwiched between these two. This was not in agreement with the improvement in flowability and can be attributed to the interaction between Avicel PH-102 and paracetamol particles.

Bulk density was largest for pure paracetamol and decreased with the increasing Avicel PH-102 content. The bulk density of pure paracetamol is greater than Avicel PH-102 and as a result, with increase in the paracetamol content in the blend, the density increases. Pure paracetamol showed better compressibility than the blends as indicated by the bulk densities with increasing normal loads as can be seen in Figure 4.9.

Flowability and bulk density results are well supported by the cohesion and effective angle of internal friction values tabulated in Table 4.5. Lower cohesion means greater flowability. It can be seen that the cohesion values for the blended samples were lesser than paracetamol, hence in agreement with the flowability results. As the paracetamol content in the blend increased, cohesion increased leading to reduction in flowability. Internal friction angle gives the friction between the powder particles, a greater variation in internal friction angle means greater compressibility of the powder sample. It is because at increasing stresses the powder particles are compacted and their interlocks are broken which are the primary source of friction. This is the reason the internal friction angle reduces with increasing stress. Range of internal friction angles of blended samples was less as compared to paracetamol indicating poor compressibility but improved flowability as the internal friction angles were lower than paracetamol at comparable stresses indicating reduced friction between particles.

Table 4.5. Major principal consolidating stress, unconfined failure strength, effective angle of internal friction and cohesion values of paracetamol and Avicel PH-102 blends

	Flow function			
Material	Major principal consolidating stress (kPa)	Unconfined failure strength (kPa)	Effective angle of internal friction (°)	Cohesion (kPa)
Paracetamol	0.6774	0.5578	62.15	0.1586
	1.2578	0.8718	52.45	0.2656
	2.4045	1.3372	45.64	0.415
	4.2808	2.1294	40.6	0.6986
	7.8068	3.3534	36.04	1.1332
20% Paracetamol + 80% Avicel PH-102	0.6108	0.2704	46.08	0.0734
	1.2066	0.3842	43.08	0.1008
	2.4206	0.6392	41.86	0.1664
	4.8014	1.1284	41.36	0.2916
	9.769	2.348	41.32	0.61
40% Paracetamol + 60% Avicel PH-102	0.627	0.328	48.4	0.09
	1.2362	0.4796	44.66	0.128
	2.4566	0.7884	43.06	0.2076
	4.9464	1.3006	41.86	0.3382
	10.061	3.0264	41.62	0.8154

60% Paracetamol + 40% Avicel PH-102	0.657	0.4338	53.68	0.1222
	1.2898	0.624	47.32	0.1698
	2.5498	1.0888	44.54	0.3014
	5.1038	1.9758	41.4	0.5714
	9.47	3.5242	39.14	1.0574
80% Paracetamol + 20% Avicel PH-102	0.6592	0.4492	53.54	0.1312
	1.2976	0.712	47.32	0.2086
	2.325	1.2196	42.28	0.3932
	4.327	1.9718	37.84	0.6544
	8.2278	3.1702	34.96	1.0536
Avicel PH-102	0.778	0.2512	42.87	0.0580
	1.4872	0.3334	40.27	0.0723
	2.702	0.502	39.40	0.1110
	4.8526	0.7722	38.90	0.1850
	8.98	1.398	38.87	0.3750

Table 4.6. Wall friction and bulk densities values of paracetamol and Avicel PH-102 blends

	Wall friction		Bulk density	
Material	Stress (kPa)	Effective angle of wall friction (°)	Stress (kPa)	Density (kg/m³)
Paracetamol	0.482	27.34	0.0362	328.42
	0.963	22.46	0.2304	352.96
	1.4452	20.78	0.4716	368.9
	1.928	19.88	1.0088	413.5
	2.4102	19.34	2.2062	465.98
	2.892	18.98	4.8746	515.82
	3.374	18.76		
	3.8556	18.56		
	4.337	18.42		
	4.8172	18.28		
20% Paracetamol + 80% Avicel PH-102	0.483	21.6	0.0404	366.04
	0.964	18.92	0.2334	381.76
	1.4456	18.02	0.4722	388.58
	1.9282	17.56	1.0064	399.52
	2.4104	17.26	2.1988	412.16
	2.8922	17.1	4.864	425.28
	3.374	16.96		
	3.856	16.86		
	4.3378	16.78		
	4.818	16.7		
40% Paracetamol + 60% Avicel PH-102	0.483	19.34	0.0412	372.16
	0.964	16.6	0.2336	382.9
	1.4462	15.72	0.4728	392.82
	1.9282	15.22	1.008	411
	2.41	14.98	2.2016	431.24

	2.892 3.374 3.8558 4.3368 4.818	14.8 14.66 14.56 14.46 14.4	4.8668	450.98
60% Paracetamol + 40% Avicel PH-102	0.4826 0.9638 1.446 1.928 2.41 2.892 3.3738 3.8552 4.337 4.818	21.52 18.18 17.04 16.48 16.1 15.9 15.7 15.58 15.5 15.42	0.04 0.232 0.4712 1.0074 2.2028 4.87	361.34 368.28 382.4 409.08 438.8 467.22
80% Paracetamol + 20% Avicel PH-102	0.4822 0.9636 1.4458 1.9282 2.4102 2.892 3.374 3.856 4.337 4.818	21.74 18.22 17.02 16.42 16.06 15.82 15.62 15.5 15.4 15.32	0.038 0.231 0.472 1.0078 2.2036 4.8716	341.48 358.32 375.98 410.72 448.76 485.4
Avicel PH-102	0.483 0.964 1.4453 1.9283 2.411 2.8926 3.374 3.856 4.3373 4.817	15.43 14.43 14.13 13.96 13.86 13.76 13.76 13.7 13.7 13.7	0.03925 0.2315 0.43375 1.1935 2.39825 4.862	354.32 365.5 370.22 380.45 388.25 396.42

4.5 Paracetamol blended with nano silica

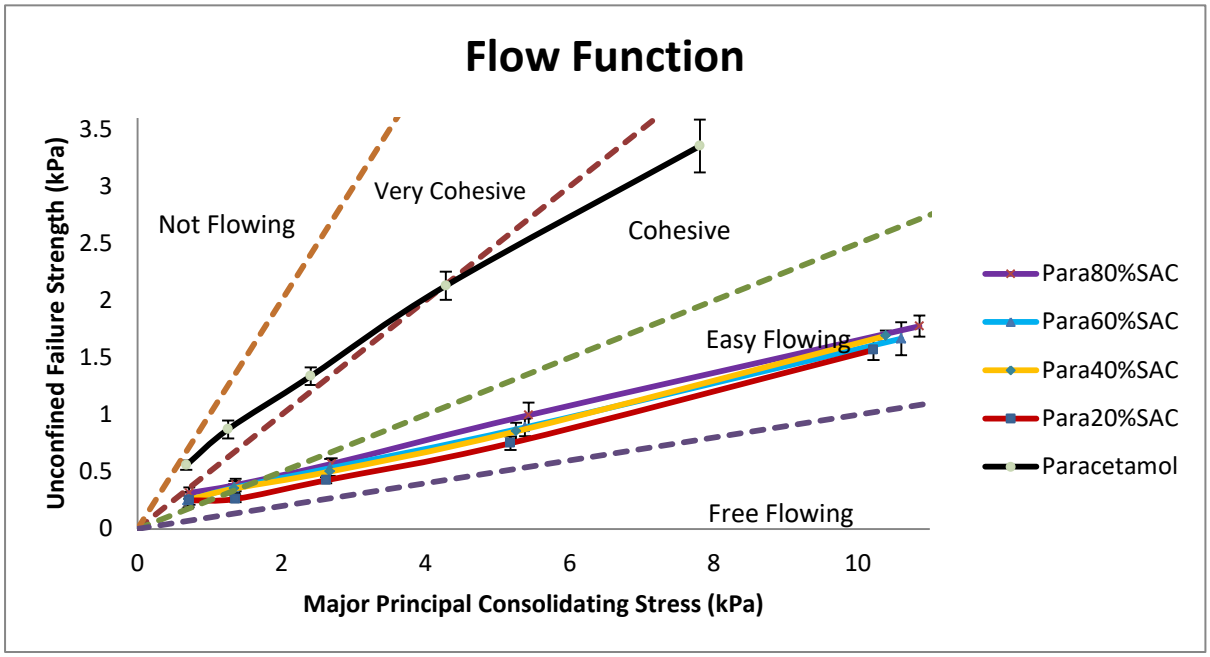

Figure 4.10. Flow function curve of paracetamol blended with Aerosil R972 Pharma

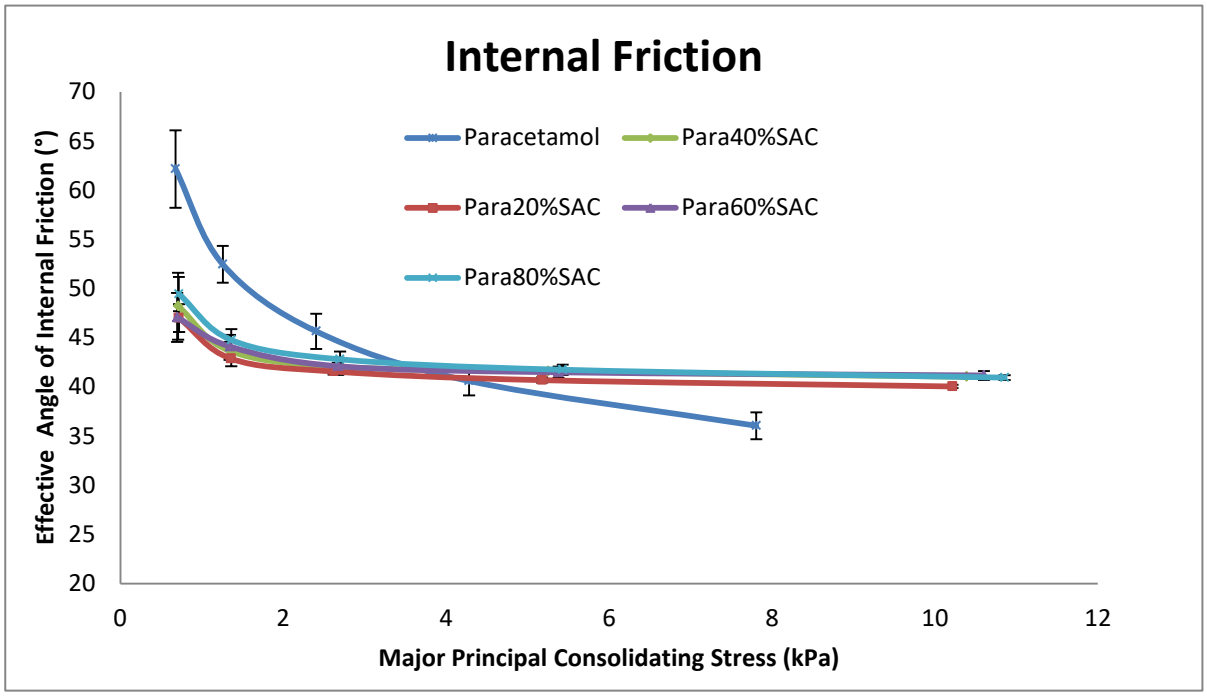

Figure 4.11. Internal friction curve of paracetamol blended with Aerosil R972 Pharma

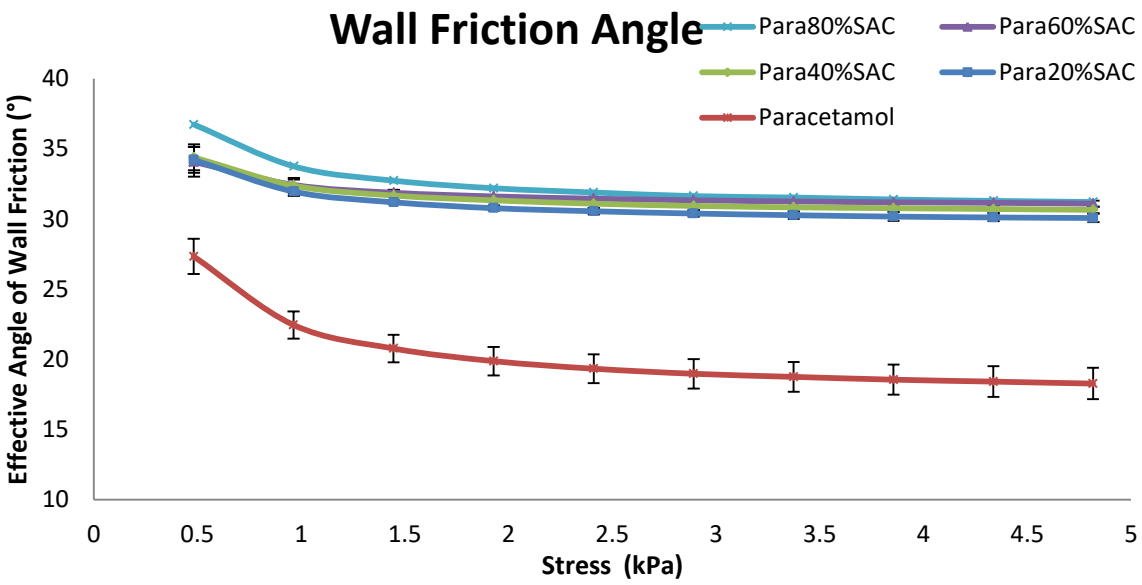

Figure 4.12. Wall friction curve of paracetamol blended with Aerosil R972 Pharma

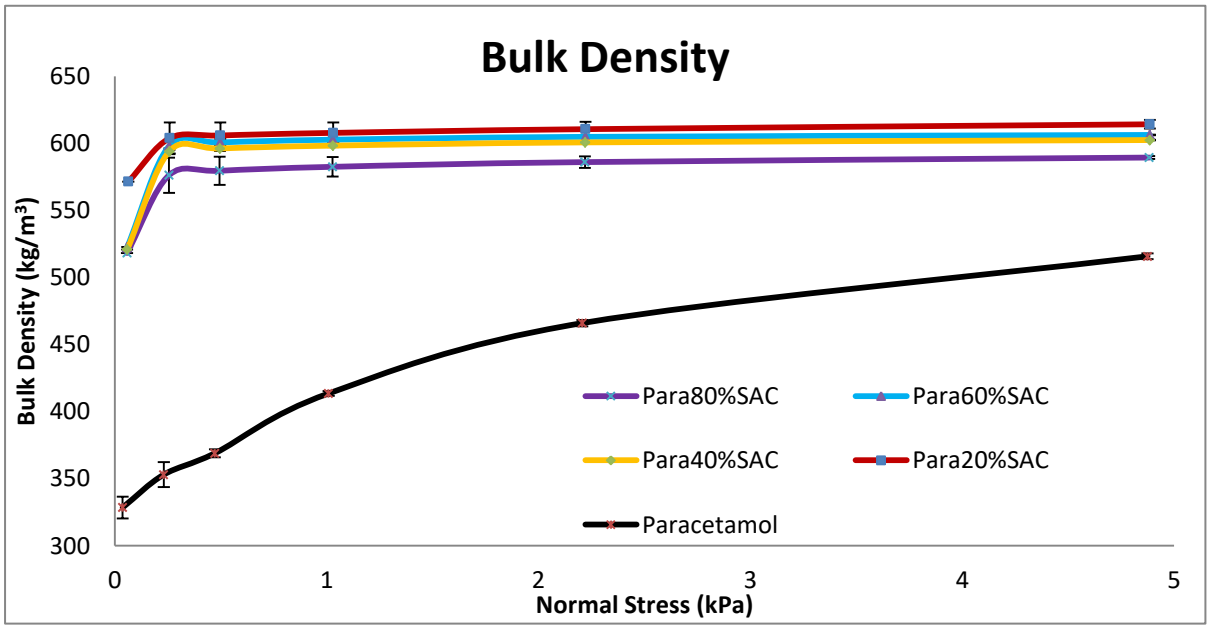

Figure 4.13. Bulk density curve of paracetamol blended with Aerosil R972 Pharma

Paracetamol blended with 20%SAC (0.4945 wt./wt.%) showed maximum improvement in flowability as seen in Figure 4.10. Increasing the wt./wt.% to further increase the SAC resulted in reduction of flowability with 80%SAC sample showing the least flowability improvement. The difference in the flowability of different SAC samples is not that significant but still important because it shows that flowability improved most for the 20%

SAC sample. One reason that can be attributed to the reduction in flowability with increasing wt./wt.% of nano silica is that with increasing nano particles on the host surface, the nanoparticles form agglomerates between themselves and attraction forces between two coated particles increases as the coated particles almost act as a monolayer and not as asperities. The agglomeration can be verified with the SEM image of paracetamol 80%SAC powder.

Wall friction angles did not vary much with the varying concentration of nano silica but still was least for 20%SAC sample and maximum for 80%SAC sample as seen in Figure 4.12. Wall friction angles for pure paracetamol were significantly lower than the nano silica blended samples. As the flowability increases with the de-agglomeration of paracetamol particles, more and more particles come in contact with the wall surface due to which wall friction angle increases on addition of nano silica.

All the four samples showed improved bulk density than pure paracetamol with the 20%SAC sample again showing the best improvement with the least improvement in the 80%SAC sample. This can be attributed to the improved packing of particles. Compressibility was poor for all the samples as is evident from Figure 4.13.

Flowability and bulk density results are well supported by the cohesion and effective angle of internal friction values tabulated in Table 4.7. Lower cohesion means greater flowability. It can be seen that the cohesion values for the nano blended samples were lesser than paracetamol, hence in agreement with the flowability results. There was substantial reduction in cohesion of nano bended samples when compared to paracetamol but no major difference was seen at different SAC's. Internal friction angle gives the friction between the powder particles, a greater variation in internal friction angle means greater compressibility of the powder sample. It is because at increasing stresses the powder particles are compacted and their interlocks are broken which are the primary source of friction. This is the reason the internal friction angle reduces with increasing stress. Range of internal friction angles of nano blended samples was similar to each other but less when compared to paracetamol indicating poor compressibility but improved flowability.

Energy-dispersive X-ray spectroscopy (EDS) (see Table 4.1) and scanning electron microscopy (SEM) confirmed the presence of SiO_2 in the nano blended samples.

Nano silica can be clearly seen on the surface of the paracetamol 80% SAC in Figure 4.14 and its presence can be confirmed by comparison with pure paracetamol.

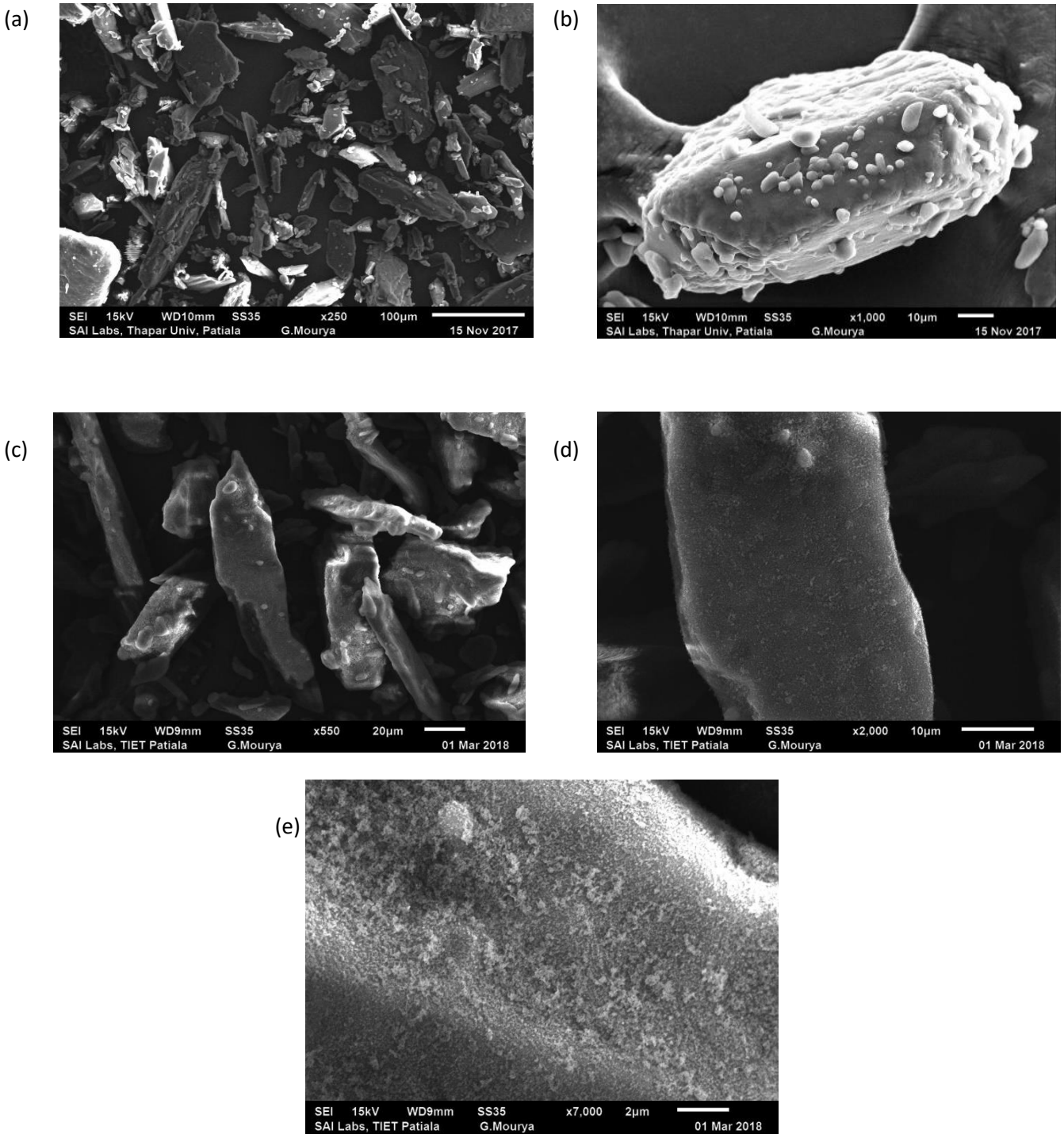

Figure 4.14. SEM images of (a) Paracetamol at magnification of 250x, (b) Paracetamol at magnification of 1000x,(c) Paracetamol 80%SAC at magnification of 550x, (d) Paracetamol 80%SAC at magnification of 2000x, (e) Paracetamol 80%SAC at magnification of 7000x.

Table 4.7. Major principal consolidating stress, unconfined failure strength, effective angle of internal friction and cohesion values of paracetamol nano-silica blends

	Flow Function			
Material	Major principal consolidating Stress (kPa)	Unconfined failure strength (kPa)	Effective angle of internal Friction (°)	Cohesion (kPa)
Paracetamol	0.6774	0.5578	62.15	0.1586
	1.2578	0.8718	52.45	0.2656
	2.4045	1.3372	45.64	0.415
	4.2808	2.1294	40.6	0.6986
	7.8068	3.3534	36.04	1.1332
Paracetamol 20%SAC	0.7208	0.2498	47	0.057
	1.3608	0.2622	42.86	0.067
	2.6192	0.426	41.56	0.114
	5.1776	0.7504	40.68	0.194
	10.2168	1.5674	40.04	0.42
Paracetamol 40%SAC	0.7102	0.2558	48.2	0.061
	1.3426	0.353	43.66	0.0878
	2.669	0.502	42.04	0.1242
	5.2552	0.854	41.58	0.2098
	10.3888	1.6906	41.02	0.4208
Paracetamol 60%SAC	0.6976	0.249	47.06	0.0614
	1.3474	0.3612	44.1	0.0896
	2.674	0.5318	42.1	0.1318
	5.3794	0.8886	41.48	0.219
	10.602	1.666	41.16	0.4116
Paracetamol 80%SAC	0.7186	0.3142	49.44	0.0776
	1.363	0.3844	44.76	0.0944
	2.6968	0.5696	42.8	0.1402
	5.43	0.9958	41.74	0.247
	10.8552	1.7752	40.94	0.4426

Table 4.8. Wall friction and bulk densities values of paracetamol nano-silica blends

	Wall friction		Bulk density	
Material	Stress (kPa)	Effective angle of wall friction (°)	Stress (kPa)	Density (kg/m³)
Paracetamol	0.482	27.34	0.0362	328.42
	0.963	22.46	0.2304	352.96
	1.4452	20.78	0.4716	368.9
	1.928	19.88	1.0088	413.5
	2.4102	19.34	2.2062	465.98
	2.892	18.98	4.8746	515.82
	3.374	18.76		

	3.8556 4.337 4.8172	18.56 18.42 18.28		
Paracetamol 20%SAC	0.483 0.965 1.447 1.929 2.4108 2.892 3.374 3.856 4.3378 4.819	34.22 31.96 31.2 30.78 30.56 30.4 30.28 30.18 30.12 30.08	0.063 0.2586 0.4974 1.0304 2.2218 4.8854	571.5 603.98 605.94 607.88 610.64 614.28
Paracetamol 40%SAC	0.483 0.965 1.4466 1.9286 2.4104 2.8924 3.374 3.856 4.3378 4.8192	34.4 32.38 31.68 31.34 31.1 30.94 30.84 30.78 30.72 30.66	0.058 0.2568 0.496 1.0294 2.2202 4.8852	520.9 594.12 596.26 598.36 600.76 602.5
Paracetamol 60%SAC	0.483 0.9646 1.4464 1.9282 2.4102 2.892 3.374 3.856 4.338 4.819	34.08 32.44 31.88 31.62 31.46 31.34 31.26 31.2 31.16 31.1	0.058 0.2568 0.4974 1.03 2.2216 4.8854	522.7 598.22 600.74 602.8 604.92 606.34
Paracetamol 80%SAC	0.483 0.965 1.4466 1.9286 2.41 2.892 3.374 3.856 4.338 4.819	36.74 33.76 32.74 32.2 31.9 31.64 31.54 31.4 31.3 31.22	0.057 0.2554 0.494 1.0276 2.2186 4.8828	518.3 576.3 579.6 582.56 586.08 589.46

4.6 Ibuprofen blended with Avicel PH-101

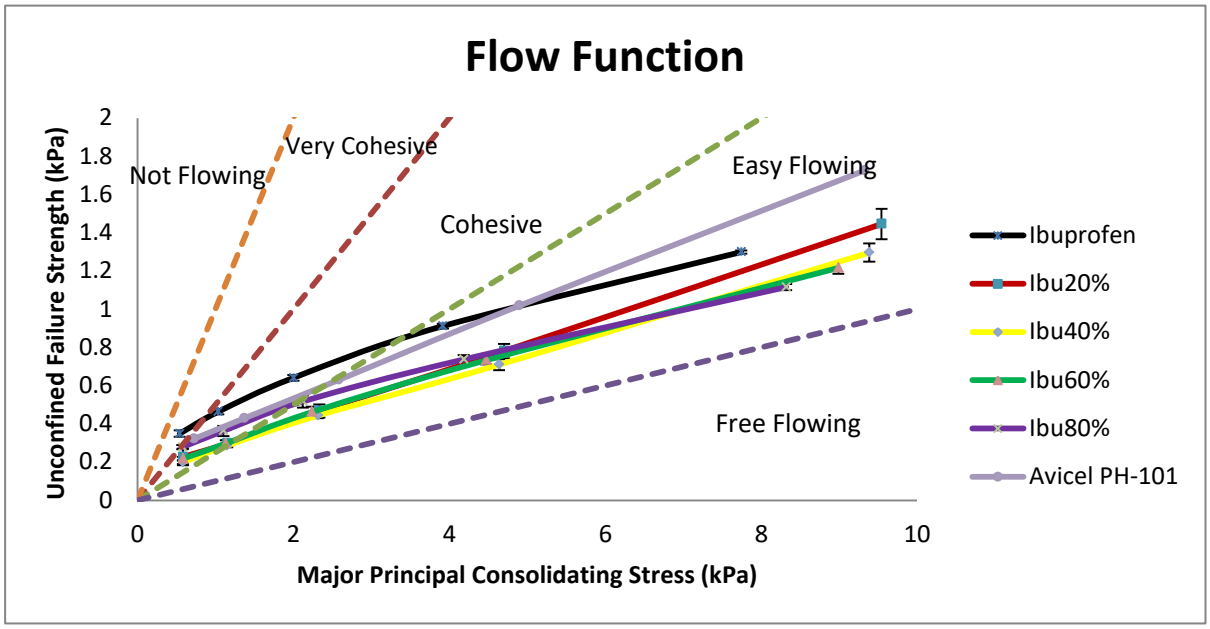

Figure 4.15. Flow function curve of ibuprofen blended with Avicel PH-101

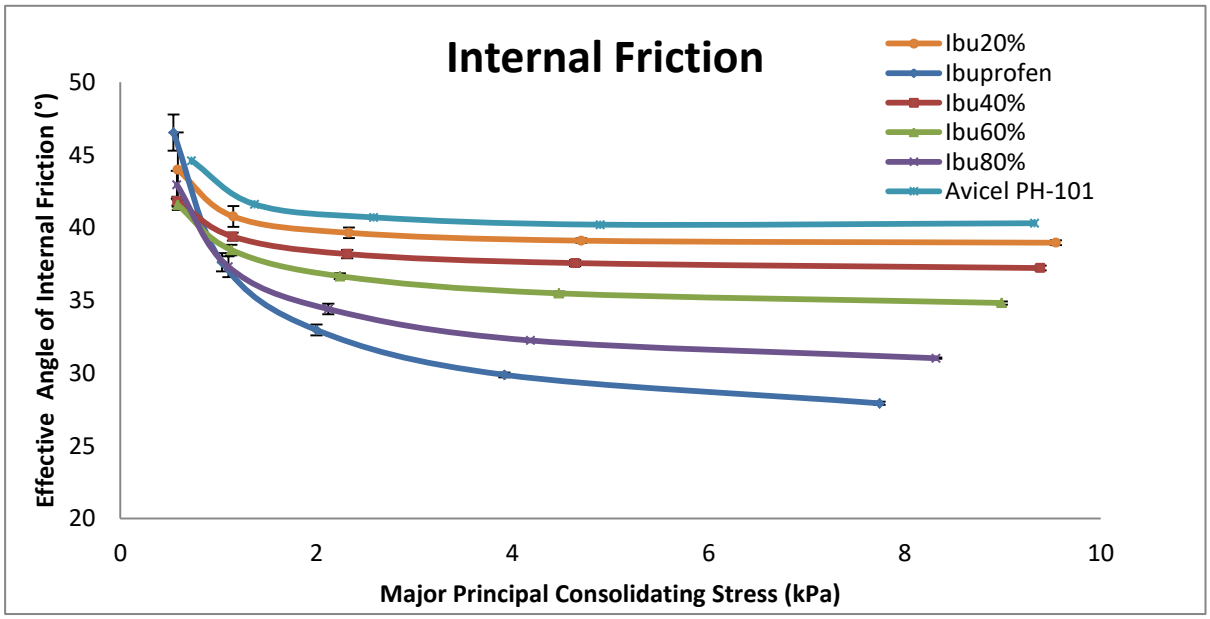

Figure 4.16. Internal friction curve of ibuprofen blended with Avicel PH-101

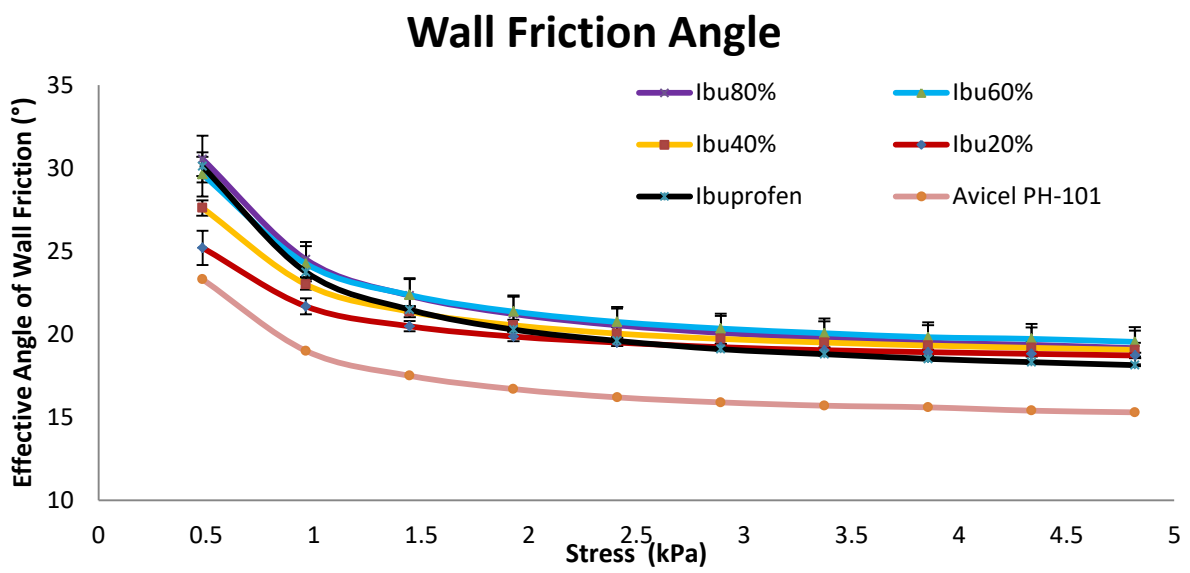

Figure 4.17. Wall friction curve of ibuprofen blended with Avicel PH-101

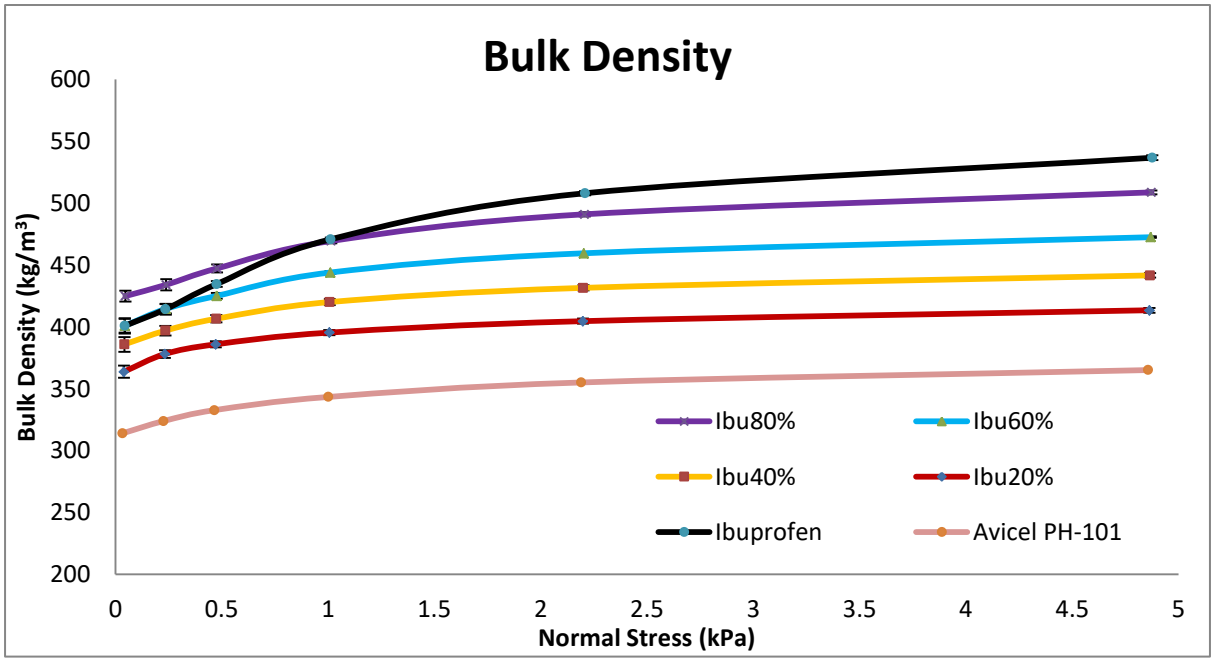

Figure 4.18. Bulk density curve of ibuprofen blended with Avicel PH-101

Ibuprofen blended with Avicel PH-101 showed improved flowability but not as significant as when paracetamol was blended with Avicel PH-101. The flow function curve of Avicel PH-101 was pivotal in determining the improvement in flowability of the various blends. Avicel PH-101 had better flowability than ibuprofen at stress values lower than 5 kPa and the trend reversed at higher stress values as seen in Figure 4.15. Due to this, at stress values lower than 5 kPa the 80% blend (Ibu20%) showed better flowability than the 20% blend (Ibu80%). After 5 kPa, as the flowability of Avicel PH-101 was lower than ibuprofen, 80% blend (Ibu20%) showed decreased flowability and the best improvement was seen in the 20% blend

(Ibu80%). The significant lack in improvement of flowability can be attributed to the fact that ibuprofen was already easy flowing.

There was not a significant change in the wall friction angle after a certain stress value. At low stresses, the 80% blend (Ibu20%) showed the best reduction but after the increase in stress above 2kPa pure ibuprofen showed the least wall friction angle as can be seen in Figure 4.17.

80% blend (Ibu20%) showed the least bulk density followed by densities of 60% (Ibu40%) and 40% blends (Ibu60%) as seen in Figure 4.18. 20% blend (Ibu80%) had the greatest bulk density out of the four blends but still lesser than pure ibuprofen because of lesser bulk density of Avicel PH-101 than ibuprofen. Compressibility of pure ibuprofen was better than the blends.

Flowability and bulk density results are well supported by the cohesion and effective angle of internal friction values tabulated in Table 4.9. Lower cohesion means greater flowability. It can be seen that the cohesion values for the blended samples were lesser than ibuprofen, hence in agreement with the flowability results. The cohesion values agree with the flow function curves as the cohesion values are lesser for the blended samples with increasing ibuprofen content after the stress increases beyond 5 kPa, hence leading to better flowability after 5kPa. Internal friction angle gives the friction between the powder particles, a greater variation in internal friction angle means greater compressibility of the powder sample. It is because at increasing stresses, the powder particles are compacted and their interlocks are broken which are the primary source of friction. This is the reason that the internal friction angle reduces with increasing stress. Range of internal friction angles of blended samples was less as compared to ibuprofen indicating poor compressibility but improved flowability.

Table 4.9. Major principal consolidating stress, unconfined failure strength, effective angle of internal friction and cohesion values of ibuprofen and Avicel PH-101 blends

	Flow function			
Material	Major principal consolidating stress (kPa)	Unconfined failure strength (kPa)	Effective angle of internal friction (°)	Cohesion (kPa)
Ibuprofen	0.5414	0.3492	46.52	0.117
	1.0358	0.4634	37.62	0.153
	2.0012	0.6408	32.96	0.211
	3.918	0.9116	29.88	0.3012
	7.745	1.2992	27.92	0.4288
20% Ibuprofen + 80% Avicel PH-101	0.5848	0.2268	43.98	0.0614
	1.1528	0.2978	40.76	0.079
	2.3324	0.4674	39.64	0.123
	4.7032	0.781	39.1	0.2034
	9.5446	1.4456	38.96	0.3748
40% Ibuprofen +	0.5824	0.1996	41.82	0.0548

60% Avicel PH-101	1.147	0.2858	39.38	0.078
	2.3146	0.4432	38.18	0.1196
	4.6396	0.7096	37.56	0.19
	9.387	1.296	37.22	0.3464
60% Ibuprofen + 40% Avicel PH-101	0.5844	0.2176	41.56	0.0616
	1.1318	0.2968	38.46	0.0834
	2.2388	0.4616	36.66	0.13
	4.4738	0.733	35.48	0.2066
	8.992	1.2164	34.82	0.342
80% Ibuprofen + 20% Avicel PH-101	0.5762	0.278	42.94	0.0842
	1.1022	0.363	37.3	0.1098
	2.1216	0.517	34.4	0.157
	4.1852	0.7372	32.24	0.224
	8.3226	1.1158	31.02	0.3388
Avicel PH-101	0.7258	0.3216	44.6	0.073
	1.37	0.429	41.6	0.1005
	2.582	0.6296	40.7	0.154
	4.8958	1.0178	40.2	0.254
	9.3268	1.7256	40.3	0.457

Table 4.10. Wall friction and bulk densities values of ibuprofen and Avicel PH-101 blends

	Wall friction		Bulk density	
Material	Stress (kPa)	Effective angle of wall friction (°)	Stress (kPa)	Density (kg/m³)
Ibuprofen	0.482	30.1	0.0444	400.9
	0.9638	23.74	0.2366	414.34
	1.446	21.48	0.4772	434.66
	1.9286	20.28	1.0136	470.88
	2.4102	19.6	2.209	508.04
	2.892	19.1	4.8766	536.76
	3.3736	18.8		
	3.8558	18.52		
	4.337	18.32		
	4.818	18.14		
20% Ibuprofen + 80% Avicel PH-101	0.4828	25.2	0.0404	363.8
	0.9632	21.68	0.2328	378.08
	1.4456	20.48	0.4728	385.94
	1.9286	19.86	1.0064	395.4
	2.4104	19.5	2.1988	404.64
	2.892	19.22	4.863	413.46
	3.374	19.04		
	3.8556	18.92		
	4.3374	18.82		
	4.8186	18.72		
40% Ibuprofen +	0.4822	27.6	0.043	385.92

60% Avicel PH-101	0.9632 1.446 1.928 2.4102 2.8924 3.374 3.8558 4.337 4.818	23 21.36 20.54 20.04 19.72 19.5 19.32 19.18 19.06	0.2354 0.475 1.0086 2.2012 4.866	396.96 406.56 420.08 431.56 441.62
60% Ibuprofen + 40% Avicel PH-101	0.4826 0.9636 1.4456 1.9286 2.4102 2.892 3.374 3.856 4.337 4.8172	29.62 24.24 22.36 21.36 20.74 20.34 20.06 19.82 19.72 19.54	0.0442 0.237 0.4768 1.0114 2.2044 4.869	400.9 414.56 425.06 443.98 459.52 472.52
80% Ibuprofen + 20% Avicel PH-101	0.4826 0.9634 1.4458 1.9282 2.41 2.892 3.3734 3.8552 4.3366 4.8178	30.54 24.5 22.32 21.22 20.54 20.08 19.76 19.5 19.36 19.16	0.047 0.2388 0.4786 1.0148 2.2072 4.873	424.92 434.04 447.3 469.42 491.04 508.76
Avicel PH-101	0.483 0.964 1.445 1.928 2.411 2.892 3.374 3.856 4.337 4.817	23.3 19 17.5 16.7 16.2 15.9 15.7 15.6 15.4 15.3	0.035 0.227 0.466 1.0025 2.192 4.857	314.05 323.9 332.7 343.375 355.1 365.1

4.7 Ibuprofen blended with Avicel PH-102

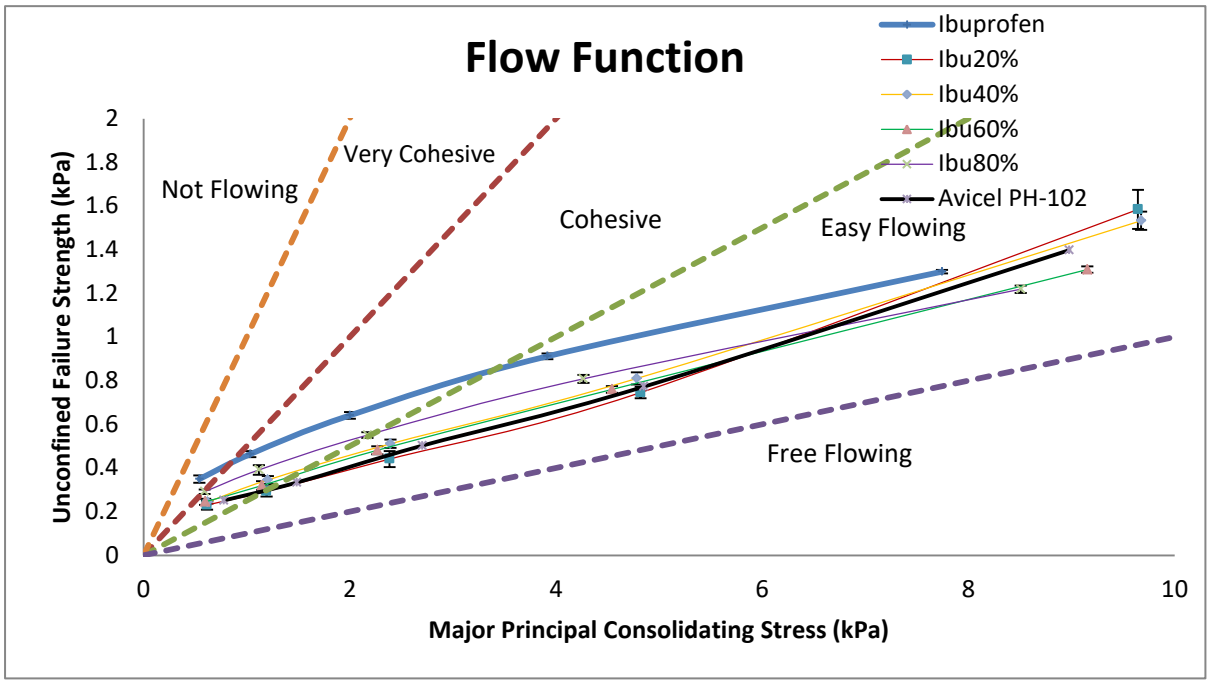

Figure 4.19. Flow function curve of ibuprofen blended with Avicel PH-102

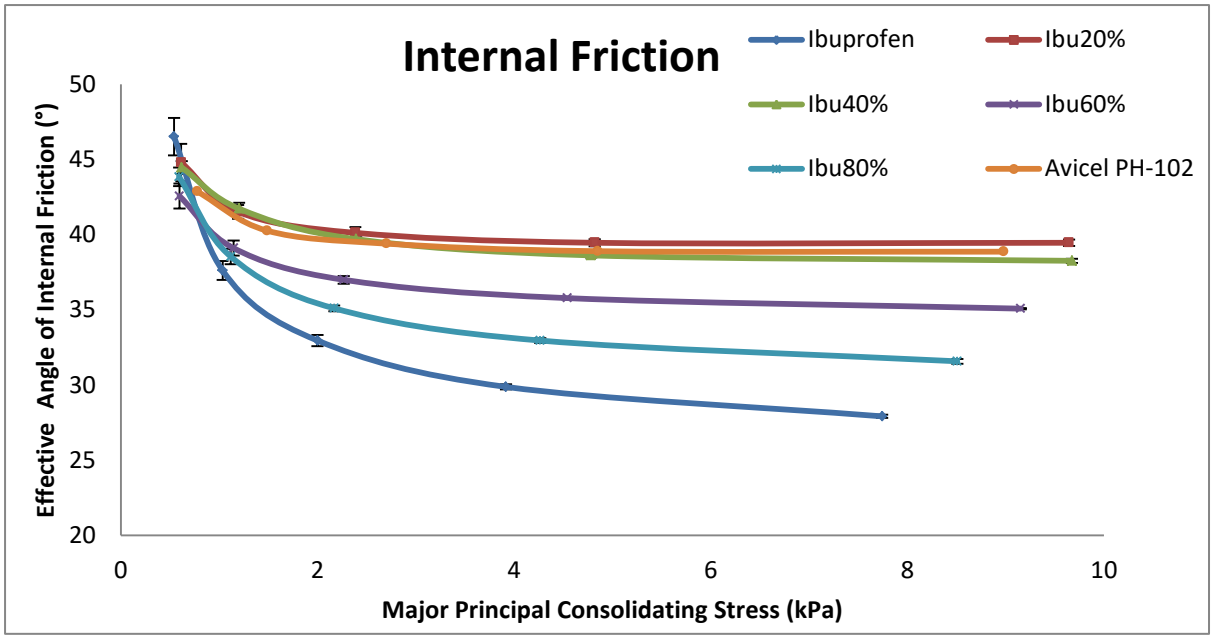

Figure 4.20. Internal friction curve of ibuprofen blended with Avicel PH-102

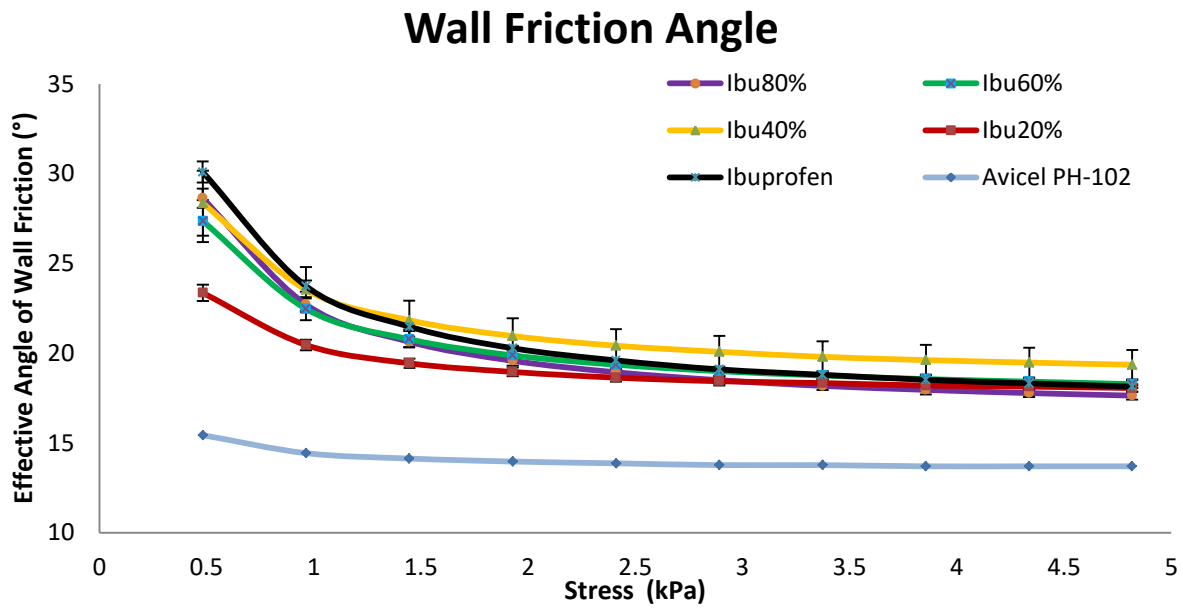

Figure 4.21. Wall friction curve of ibuprofen blended with Avicel PH-102

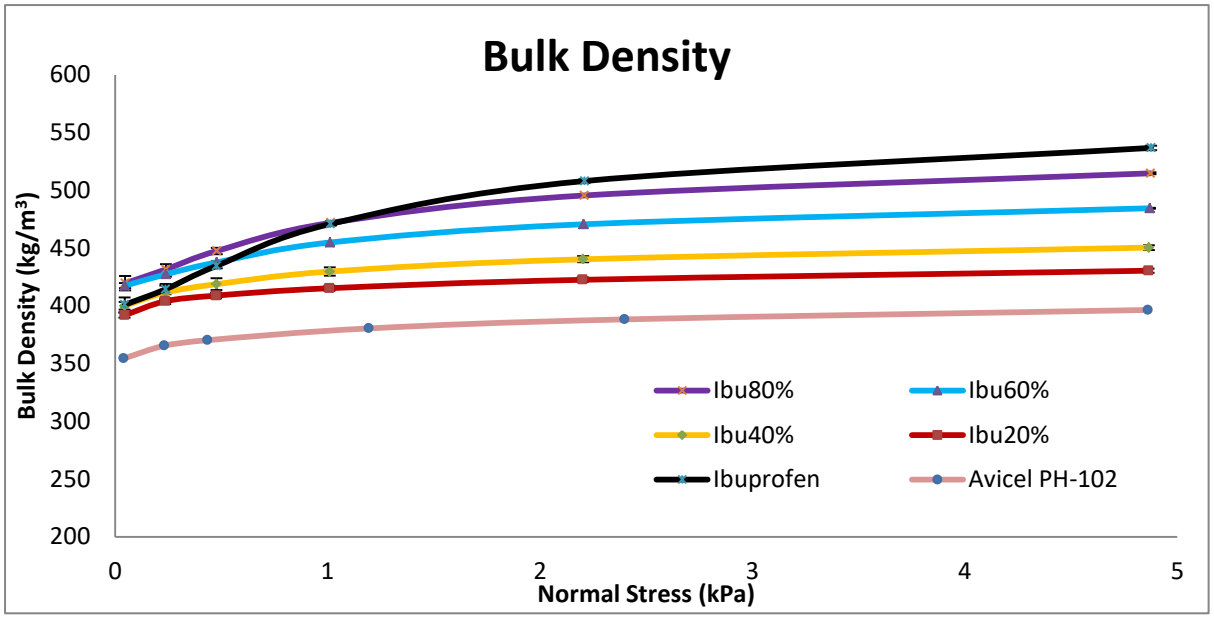

Figure 4.22. Bulk density curve of ibuprofen blended with Avicel PH-102

Blending ibuprofen with Avicel PH-102 gave quite interesting results. 80% (Ibu20%) and 60% (Ibu40%) blends had the best flowability improvement till the major principal consolidating load was 6.5 kPa with the 80% blend (Ibu20%) having better flowability as seen in Figure 4.19. After the 6.5 kPa load the trend reversed and the 20% (Ibu80%) and 40% (Ibu60%) blends showed better flowability than the 60% (Ibu40%) and 80% (Ibu20%) blends with the 20% blend showing best improvement. The reason for this trend can be understood from the flow function curve of Avicel PH-102, around the 6.5 kPa stress point Avicel PH-

102 shows decreased flowability when compared to the flowability exhibited at lower stress points. This causes the decreased flowability of ibuprofen blends as they have larger Avicel PH-102 percentage and the blends constituting lesser Avicel PH-102 show better flowability. Overall there was not a major improvement in flowability as pure ibuprofen had good flowability prior to mixing.

The effective angle of wall friction too showed similar trend to the flowability. Up to stress of 2.5 kPa 80% blend (Ibu20%) had the least wall friction but after 2.5 kPa, 20% blend (Ibu80%) had the lesser wall friction angles as seen in Figure 4.21. Overall there was not a significant change in wall friction angles when compared to pure ibuprofen.

80% blend (Ibu20%) had the least bulk density followed by the 60% (Ibu40%), 40% (Ibu60%) and 20% blends (Ibu80%) in increasing order as seen in Figure 4.22. This can be attributed to greater bulk density of pure ibuprofen than pure Avicel PH-102. Pure ibuprofen had better compressibility than all the blends.

Flowability and bulk density results are well supported by the cohesion and effective angle of internal friction values tabulated in Table 4.11. Lower cohesion means greater flowability. It can be seen that the cohesion values for the blended samples were lesser than ibuprofen, hence in agreement with the flowability results. As discussed in previous paragraphs, flowability of blends with more ibuprofen content increased after 6.5kPa stress as indicated by the cohesion values. Internal friction angle gives the friction between the powder particles, a greater variation in internal friction angle means greater compressibility of the powder sample. It is because at increasing stresses, the powder particles are compacted and their interlocks are broken which are the primary source of friction. This is the reason the internal friction angle reduces with increasing stress. Range of internal friction angles of blended samples was less as compared to ibuprofen indicating poor compressibility but improved flowability.

Table 4.11. Major principal consolidating stress, unconfined failure strength, effective angle of internal friction and cohesion values of ibuprofen and Avicel PH-102 blends

	Flow function			
Material	Major principal consolidating stress (kPa)	Unconfined failure strength (kPa)	Effective angle of internal friction (°)	Cohesion (kPa)
Ibuprofen	0.5414 1.0358 2.0012 3.918 7.745	0.3492 0.4634 0.6408 0.9116 1.2992	46.52 37.62 32.96 29.88 27.92	0.117 0.153 0.211 0.3012 0.4288
20% Ibuprofen + 80% Avicel PH-102	0.6148 1.193 2.3864 4.8208	0.2304 0.2928 0.4408 0.7454	44.8 41.52 40.12 39.46	0.0606 0.076 0.1136 0.1914

	9.6456	1.5842	39.46	0.4088
40% Ibuprofen + 60% Avicel PH-102	0.6198	0.2438	44.46	0.0656
	1.2052	0.345	41.72	0.0916
	2.3944	0.5106	39.7	0.135
	4.7844	0.81	38.62	0.2136
	9.6756	1.5326	38.26	0.405
60% Ibuprofen + 40% Avicel PH-102	0.5972	0.2448	42.56	0.0702
	1.1482	0.3194	39.1	0.0892
	2.268	0.4812	37	0.1352
	4.5436	0.7598	35.78	0.2134
	9.154	1.3088	35.08	0.3674
80% Ibuprofen + 20% Avicel PH-102	0.5922	0.2916	43.84	0.0872
	1.1188	0.391	38.54	0.117
	2.1714	0.5506	35.1	0.1656
	4.2666	0.8084	32.96	0.2442
	8.5088	1.219	31.58	0.368
Avicel PH-102	0.778	0.2512	42.87	0.0580
	1.4872	0.3334	40.27	0.0723
	2.702	0.502	39.40	0.1110
	4.8526	0.7722	38.90	0.1850
	8.98	1.398	38.87	0.3750

Table 4.12. Wall friction and bulk densities values of ibuprofen and Avicel PH-102 blends

	Wall friction		Bulk density	
Material	Stress (kPa)	Effective angle of wall friction (°)	Stress (kPa)	Density (kg/m³)
Ibuprofen	0.482	30.1	0.0444	400.9
	0.9638	23.74	0.2366	414.34
	1.446	21.48	0.4772	434.66
	1.9286	20.28	1.0136	470.88
	2.4102	19.6	2.209	508.04
	2.892	19.1	4.8766	536.76
	3.3736	18.8		
	3.8558	18.52		
	4.337	18.32		
	4.818	18.14		
20% Ibuprofen + 80% Avicel PH-102	0.483	23.36	0.0434	391.86
	0.964	20.46	0.2358	403.96
	1.4466	19.44	0.4754	408.86
	1.9282	18.96	1.0086	415.22
	2.41	18.64	2.2008	422.52
	2.892	18.44	4.8646	430.4
	3.374	18.34		
	3.8556	18.2		
	4.3374	18.14		

	4.8182	18.06		
40% Ibuprofen + 60% Avicel PH-102	0.483 0.9638 1.4454 1.928 2.41 2.892 3.374 3.8554 4.3378 4.8182	28.36 23.54 21.84 20.96 20.42 20.08 19.8 19.62 19.48 19.36	0.0442 0.2362 0.4766 1.01 2.2026 4.867	400.04 411.5 418.72 429.66 440.3 450.44
60% Ibuprofen + 40% Avicel PH-102	0.483 0.9632 1.4454 1.9282 2.4106 2.892 3.374 3.8556 4.3372 4.818	27.36 22.48 20.78 19.88 19.36 19 18.76 18.56 18.42 18.28	0.046 0.2384 0.4782 1.012 2.205 4.871	417.44 427.3 437.62 454.84 470.62 484.48
80% Ibuprofen + 20% Avicel PH-102	0.482 0.9632 1.4456 1.9284 2.41 2.892 3.3738 3.8552 4.337 4.818	28.64 22.72 20.64 19.58 18.94 18.5 18.18 17.96 17.78 17.64	0.0464 0.2388 0.478 1.015 2.2088 4.874	419.54 431.6 447.48 471.86 495.58 514.74
Avicel PH-102	0.483 0.964 1.4453 1.9283 2.411 2.8926 3.374 3.856 4.3373 4.817	15.43 14.43 14.13 13.96 13.86 13.76 13.76 13.7 13.7 13.7	0.03925 0.2315 0.43375 1.1935 2.39825 4.862	354.32 365.5 370.22 380.45 388.25 396.42

4.8 Ibuprofen blended with nano silica

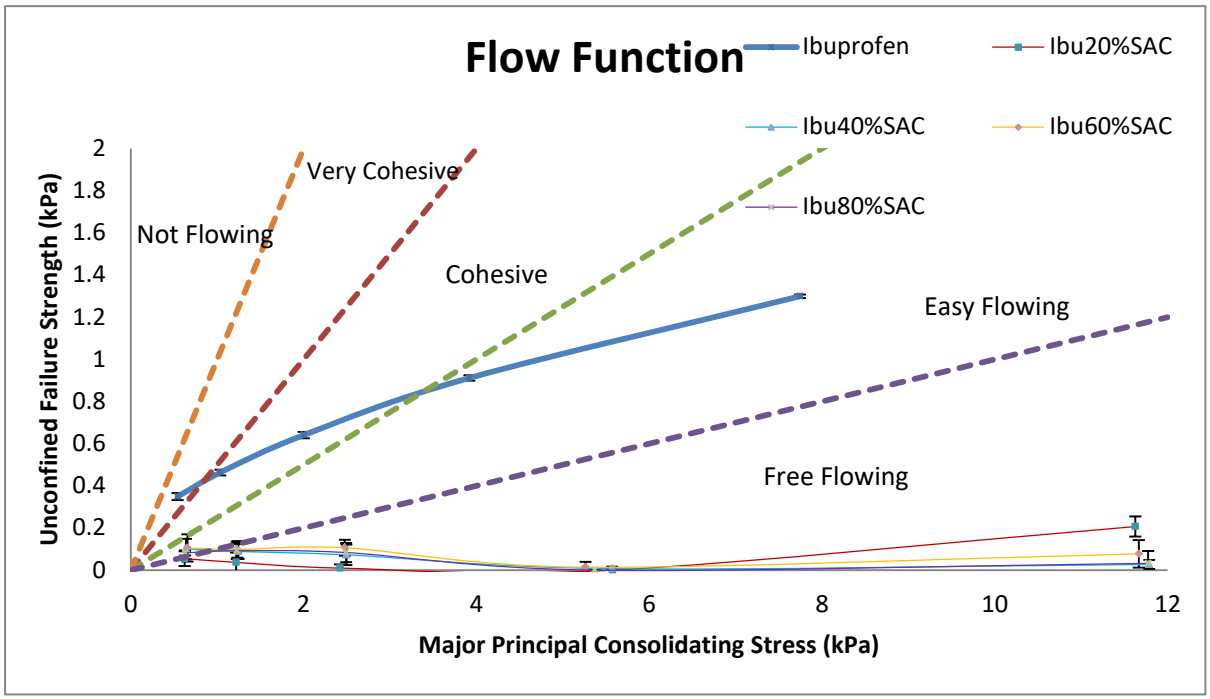

Figure 4.23. Flow function curve of ibuprofen blended with Aerosil R972 Pharma

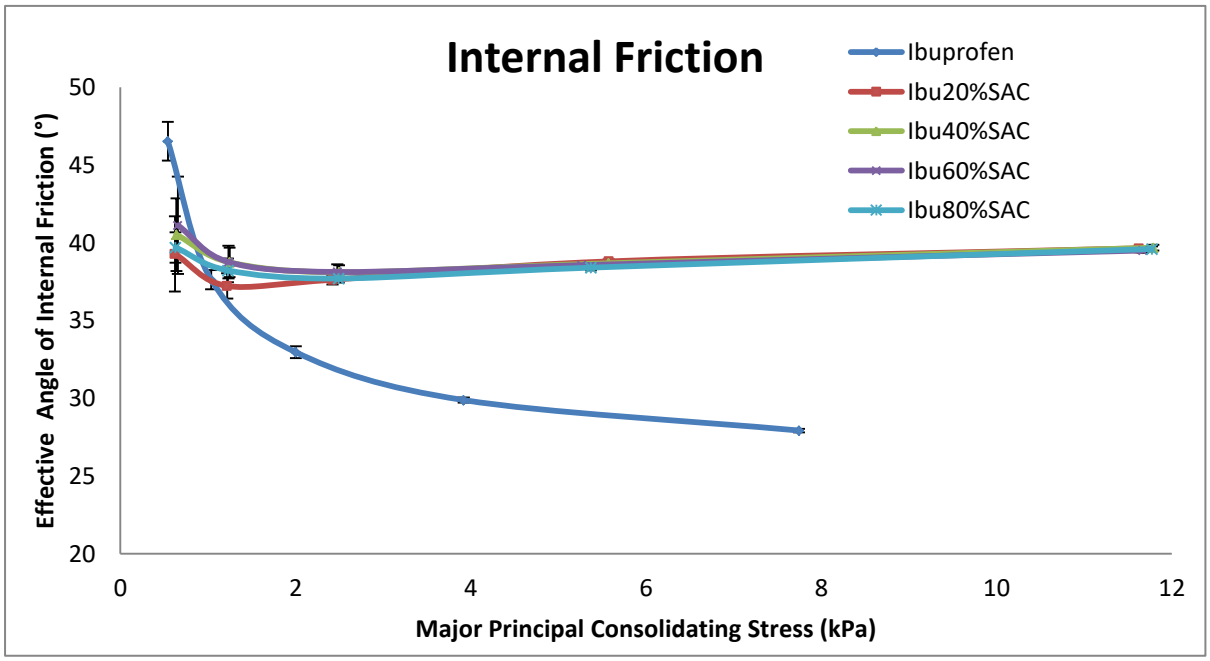

Figure 4.24. Internal friction curve of ibuprofen blended with Aerosil R972 Pharma

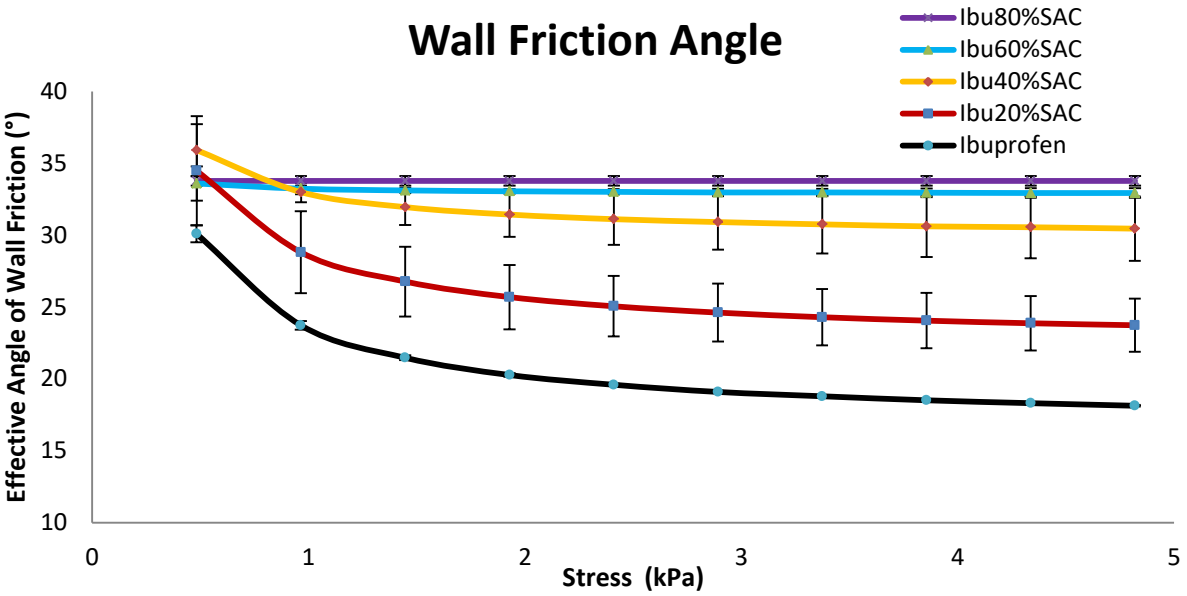

Figure 4.25. Wall friction curve of ibuprofen blended with Aerosil R972 Pharma

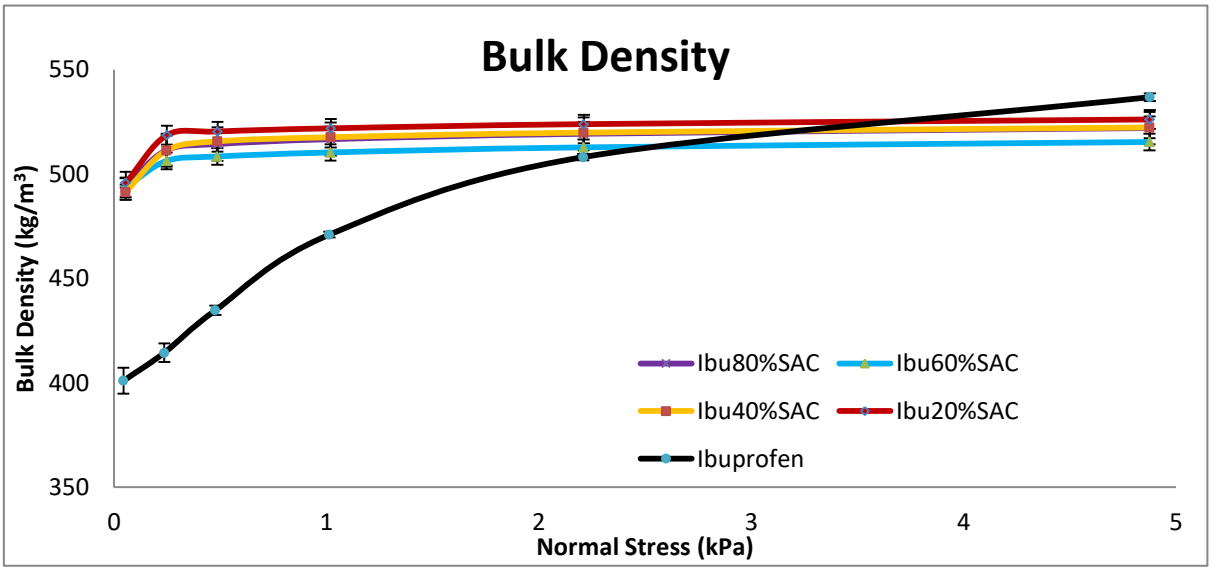

Figure 4.26. Bulk density curve of ibuprofen blended with Aerosil R972 Pharma

Blending with nano silica made the easy flowing ibuprofen into a free flowing one as seen in Figure 4.23. The improvement in flowability was so profound that at some of the major principal consolidation stresses, PFT recorded zero value of unconfined yield strength. All the four samples with SAC's of 20,40,60 and 80% showed free flowing behavior and excellent improvement in flowability just by hand mixing alone.

Pure ibuprofen showed the least wall friction with 20% SAC sample being the closest to pure ibuprofen out of the four SAC samples. The 60 and 80% SAC samples showed no variation in wall friction with increasing stress values as seen in Figure 4.25.

The bulk densities of the four SAC samples were almost same and comparable to the pure ibuprofen sample beyond stress of 3 kPa. The SAC samples had little or negligible compressibility in comparison to the pure ibuprofen sample as seen in Figure 4.26.

Flowability and bulk density results are well supported by the cohesion and effective angle of internal friction values tabulated in Table 4.13. Lower cohesion means greater flowability. It can be seen that the cohesion values for the nano blended samples were almost negligible when compared to ibuprofen, hence in agreement with the immense increase in flowability. There was substantial reduction in cohesion of nano blended samples when compared to ibuprofen but no major difference was seen at different SAC's. Internal friction angle gives the friction between the powder particles, a greater variation in internal friction angle means greater compressibility of the powder sample. It is because at increasing stresses, the powder particles are compacted and their interlocks are broken which are the primary source of friction. This is the reason the internal friction angle reduces with increasing stress. Range of internal friction angles of nano blended samples was similar to each other but extremely less when compared to ibuprofen indicating poor compressibility but improved flowability.

(a)

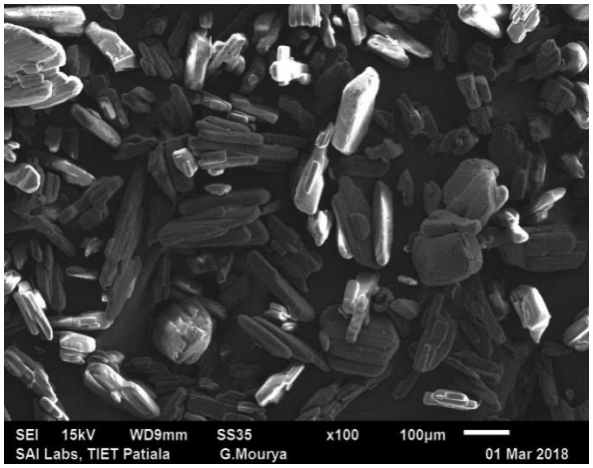

(b)

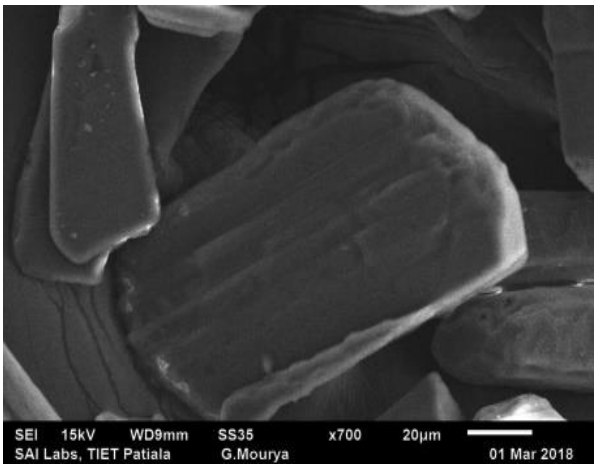

(c)

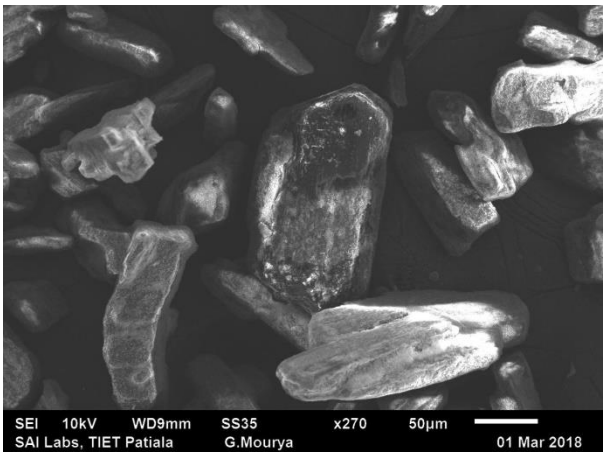

(d)

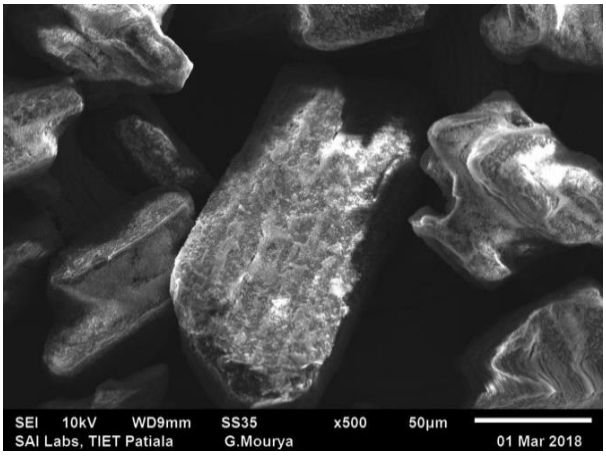

(e)

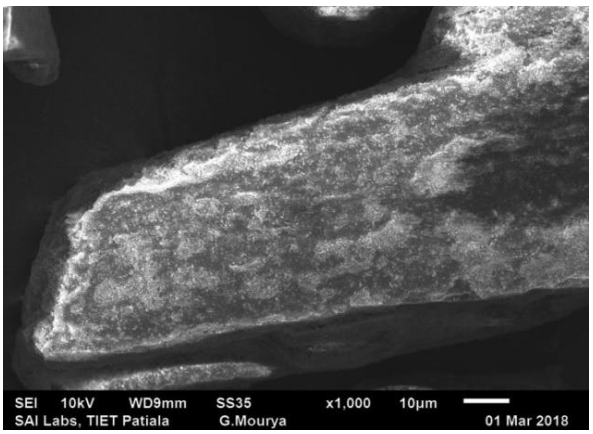

Figure 4.27. SEM images of (a) Ibuprofen at magnification of 100x, (b) Ibuprofen at magnification of 700x, (c) Ibuprofen 80%SAC at magnification of 270x, (d) Ibuprofen 80%SAC at magnification of 500x, (e) Ibuprofen 80%SAC at magnification of 1000x.

Energy-dispersive X-ray spectroscopy (EDS) (see Table 4.2) and scanning electron microscopy (SEM) confirmed the presence of SiO_2 in the nano blended samples.

Nano silica can be clearly seen on the surface of the ibuprofen 80% SAC in Figure 4.27 and its presence can be confirmed by comparison with pure ibuprofen.

Table 4.13. Major principal consolidating stress, unconfined failure strength, effective angle of internal friction and cohesion values of ibuprofen nano-silica blends

	Flow function			
Material	Major principal consolidating stress (kPa)	Unconfined failure strength (kPa)	Effective angle of internal friction (°)	Cohesion (kPa)
Ibuprofen	0.5414	0.3492	46.52	0.117
	1.0358	0.4634	37.62	0.153
	2.0012	0.6408	32.96	0.211
	3.918	0.9116	29.88	0.3012
	7.745	1.2992	27.92	0.4288
Ibuprofen 20%SAC	0.622	0.0546	39.28	0.0132
	1.2178	0.037	37.22	0.0092
	2.421	0.0098	37.62	0.0024
	5.5734	0	38.8	0
	11.6254	0.2068	39.64	0.0492
Ibuprofen 40%SAC	0.6386	0.1002	40.52	0.0252
	1.2464	0.0888	38.74	0.0222
	2.4956	0.0728	38.1	0.018
	5.5696	0.007	38.68	0.0018
	11.7876	0.0272	39.68	0.0064
Ibuprofen 60%SAC	0.6556	0.106	41.12	0.026
	1.2336	0.098	38.76	0.0246

	2.476	0.1064	38.12	0.0262
	5.2632	0.0138	38.56	0.0032
	11.667	0.0772	39.5	0.0182
Ibuprofen 80%SAC	0.6288	0.082	39.7	0.0204
	1.227	0.092	38.22	0.0232
	2.491	0.0836	37.7	0.0208
	5.3708	0	38.4	0
	11.7744	0.0324	39.6	0.0078

Table 4.14. Wall friction and bulk densities values of ibuprofen nano-silica blend

	Wall friction		Bulk density	
Material	Stress (kPa)	Effective angle of wall friction (°)	Stress (kPa)	Density (kg/m^3)
Ibuprofen	0.482	30.1	0.0444	400.9
	0.9638	23.74	0.2366	414.34
	1.446	21.48	0.4772	434.66
	1.9286	20.28	1.0136	470.88
	2.4102	19.6	2.209	508.04
	2.892	19.1	4.8766	536.76
	3.3736	18.8		
	3.8558	18.52		
	4.337	18.32		
	4.818	18.14		
Ibuprofen 20%SAC	0.483	34.48	0.0548	495.66
	0.9642	28.82	0.2488	518.56
	1.4464	26.78	0.4874	520.32
	1.9284	25.7	1.0208	521.84
	2.41	25.06	2.2118	523.84
	2.892	24.62	4.8762	526.08
	3.3734	24.3		
	3.8556	24.06		
	4.3372	23.88		
	4.8188	23.74		
Ibuprofen 40%SAC	0.483	35.92	0.0546	491.3
	0.965	33	0.2472	511.22
	1.4464	31.96	0.4868	515.6
	1.9286	31.44	1.02	517.58
	2.4106	31.12	2.2118	519.8
	2.892	30.92	4.8758	522.26
	3.374	30.76		
	3.856	30.62		
	4.337	30.56		
	4.8188	30.46		
Ibuprofen 60%SAC	0.483	33.6	0.0546	493.58
	0.965	33.24	0.2474	506.24

	1.447 1.9286 2.4104 2.892 3.374 3.856 4.338 4.819	33.12 33.06 33.02 32.98 32.98 32.96 32.94 32.94	0.4862 1.0192 2.2108 4.875	508.34 510.28 512.72 515.28
Ibuprofen 80%SAC	0.483 0.965 1.447 1.9284 2.4106 2.892 3.374 3.856 4.3378 4.819	33.78 33.78 33.78 33.78 33.78 33.78 33.78 33.78 33.78 33.78	0.0548 0.2472 0.487 1.0202 2.2114 4.8758	494.28 511.34 514.3 516.64 519.22 521.96

Chapter 5

Dry Coating

5.1 Introduction

As stated earlier, the coating can be of similar sized particles or smaller particles, in this study we will primarily be focusing on the use of smaller sized particles to enhance flowability. As the cohesiveness of fine particles is a big issue, we will consider the effect of coating nanometer-sized particles on micrometer-sized particles. The smaller particles are generally referred to as guest particles and the primary powder particles as host particles. The technique of ensuring the guest particles stick or adhere to the host particles is called coating. When this coating is done on dry powders and in absence of liquid it is called dry coating (Zhou *et al.*, 2010 a, 2010 b; Qu et al., 2017). The basic idea behind nano-coating is that the guest particles act as roughness on the host particle surfaces and thus increasing the distance between two host particles and hence decreasing the van der Waals forces and in turn cohesivity. Uniform coating of nanoparticles on the host particle surface can cause reduction in cohesiveness as the coating changes the surface properties of the host particle and its interaction or contact nature with other coated particles (Meyer and Zimmermann, 2004; Schulze, 2008; Tomas and Kleinschmidt, 2009)**.** The reduction in cohesive force reduction can be said to be in proportion to the ratio of guest particle size and average asperity radius of host particle (Jallo *et al.*, 2010)**.** The flowability can also be improved by chemical modification of surface. Some literature suggests that lower surface energy increases the flowability (Chen *et al.*, 2010; Jallo *et al.*, 2010)**.**

Dry coating can be done in various wt. / wt.% proportions and is found to decrease the inter-particle forces as well as improve flowability, bulk density and compressibility (Han *et al.*, 2011)**.** The guest particles stay on the host particles if the force of adhesion between them is greater than the guest particles gravity force. The guest and host particles can be blended in a blender but it will not ensure that the guest particles adhere to the host particle surfaces. After blending, coating is extremely essential and in real it enhances flowability (Zhou *et al*., 2010 a, 2010 b; Mullarney et al., 2011).

The dry coating of the guest particles on the host particles can be performed in various machines. Machines such as Mechanofusion, MAIC, FEM and Co-Mill can perform the coating. Basic principle of all these machines is practically similar and involves use of high energy and high shear to coat nanoparticles on the host particles (Zhang *et al.*, 2009; Chen *et al.*, 2010; Jallo *et al.*, 2010, 2012; Zhou *et al.*, 2010 a, 2010 b; Han *et al.*, 2011; Mullarney *et al.*, 2011; Zhou *et al.*, 2011; Karde, Panda and Ghoroi, 2015; Qu *et al.*, 2017)**.**

Host and the guest particles are supplied with high energy inside a mixer or a mill and as a result various collisions take place. These collisions are guest-guest, host-host, guest-host, guest-wall and host-wall. The collisions between guest-guest, host-host, guest-wall and host-wall are responsible for breaking of agglomerates between guest-guest and host-host particles (Zhou *et al.*, 2011)**.** These collisions also result in attrition and the surface modification of the host particles. Size reduction in the host particles can easily be observed as the agglomerates break and the high energy impacts breaks the larger particles (Zhang *et al.*, 2009; Han *et al.*, 2011)**.**

The guest-host collisions are the main contributors towards adhesion of guest particles on the host particles. Another impact of the dry coating process is the reduction in the sharp edges and protrusions of the guest particles also due to high energy impacts (Meyer and Zimmermann, 2004; Mullarney *et al.*, 2011). Sauer *et al.* (2013) encapsulated the recent advances and techniques being used in dry coating. Dry coating techniques such as thermal adhesion, electrostatic coating, liquid assisted coating and film formation coating were discussed. Wei et al. (2002) used various imaging techniques like field emission scanning electron microscope, atomic force microscopy, transmission electron microscopy and energy-dispersive X-ray spectroscopy to distinguish between mixed particles and see their mixing effects. Powders were mixed in three different ways i.e. solvent-based methods, dry powder processing methods and rapid expansion of supercritical solution. Rapid expansion of supercritical solution and hybridizer process performed well enough in comparison to solvent based techniques.

All the dry coating machines mentioned in the above discussions are very expensive, so a need for fabricating a novel and affordable dry coating machine based on the principles of present dry coating machines was felt and therefore a machine was fabricated and tests performed on it for testing its efficacy.

5.2 Background/theory of dry coating

The flow of fine bulk solids mainly depends on the adhesive forces experienced between their individual particles (Schulze, 2008).

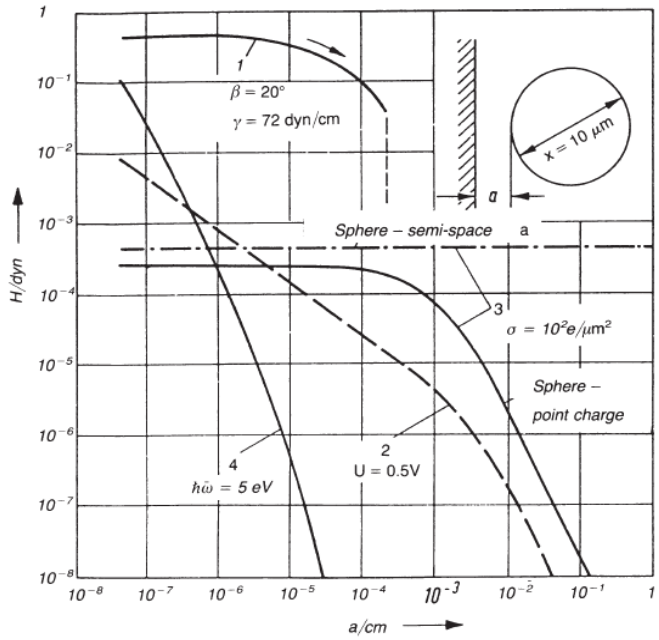

Figure 5.1. Adhesive forces due to various mechanisms of adhesion as a function of the distance *a* between the surfaces of a sphere and a plate: 1, liquid bridges; 2, electrostatic forces for conductors; 3, electrostatic forces for insulators; 4, van der Waals forces. (Rumpf, 2012)

The major forces involved in inter particle adhesive forces are the van der Waals forces, electrostatic forces and the forces due to liquid bridges formed. Liquid bridges are formed by low viscosity fluids that form a bridge or contact between particles. As can be seen in Figure 5.1., all the forces are dependent on the distance between the sphere surface and a plate. The van der Waals force plays a major role when the surfaces are in contact or the distance is very less. Adhesive forces due to liquid bridges are also large at small distance but do not decrease much on increasing distance. Electrostatic forces are smaller than the other two adhesive forces at smaller distances. For dry bulk solids, the adhesive forces due to liquid bridges do not play a major role due to which in a fine and dry bulk solid at low particle distances or where particles are in contact, the van der Waals forces outweigh the electrostatic forces and become the major factor determining the flow of fine and dry bulk solids.

Kendall and Stainton (2001) found that adhesion between particles increases the aggregation with strength directly proportional to adhesion energy. Adhesion causes solidification of aggregates, structure can be looser by reduced packing fraction or slowing structure formation at high packing fractions. Strength of aggregates should increase with adhesion and also depends upon packing, structure of aggregate and particle size.

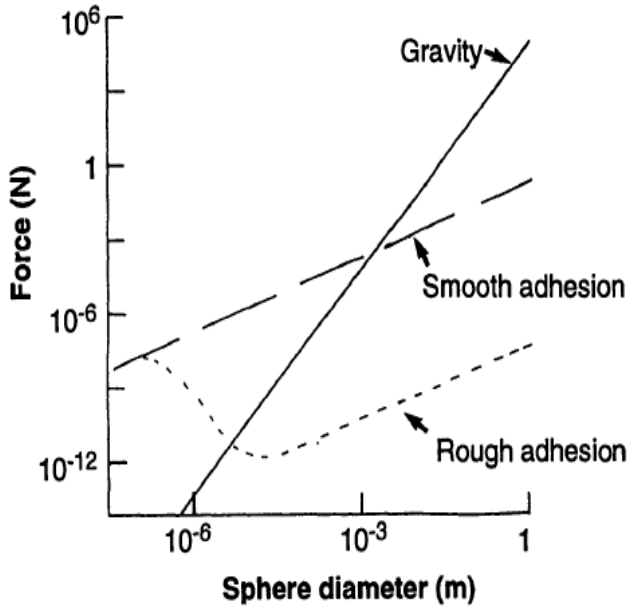

Figure 5.2. Comparison of the adhesion force and gravity for very smooth and rough spheres of different diameters. (Kendall, 1994)

Figure 5.2 between adhesion force and the sphere diameter is very interesting and important to explain some of the behavior of fine particles. As already discussed that for fine dry bulk solids or powders the van der Waals forces are the major dominating forces for the adhesion between two particles, the plot helps us understand the reason for high level of cohesion or adhesion of particles of dry powders. To simply put it, for fine particles of micrometer range, the adhesive forces are really high as compared to gravity force of the particle. The fine powders do not flow and show cohesive nature because their adhesion forces outweigh their gravity forces by about a million times as seen in the above plot. The particles flow under their own weight when the gravity forces outweigh the adhesive or cohesive forces. This theory has been practically observed and authenticated, powder with same particles but of larger size flows more easily than same powder with smaller particles. Through this we can conclude that the van der Waals forces which are the major adhesive forces in dry fine powders cause cohesion between particles and are responsible for poor flow.

Figure 5.3. helps to understand the relation between the various adhesive forces and the sphere diameter when in contact. It can be clearly seen that for particles of micrometer range the adhesive forces due to liquid bridges are most dominant with van der Walls forces being a close second. Electrostatic forces are small as compared to the liquid bridge and van der Waals forces. Gravity forces are really low as the particle size is very small and mass encapsulated in it is very low leading to low gravity force.

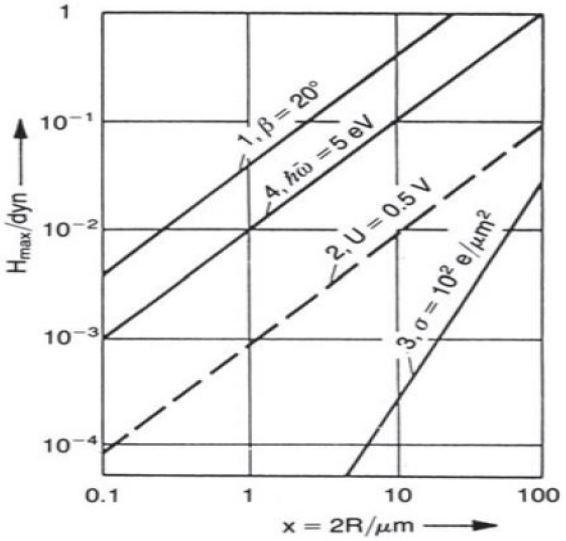

Figure 5.3. Adhesive forces of various mechanisms of adhesion for the sphere plate model (on contact) as a function of the diameter of the sphere: 1, liquid bridges; 2, electrostatic forces for conductors; 3, electrostatic forces for insulators; 4, van der Waals forces. (Rumpf, 2012)

5.3 Reduction in cohesive force by introduction of roughness

To reduce this cohesion between fine particles, there is a simple solution to the problem. As seen in Figure 5.1, the van der Waals forces between a surface and a spherical particles decrease after their distance of separation is increased. It should be clarified here that the model of flat surface and spherical particles is used for calculating various forces, but in actual powders the interaction is mainly between two particles of spherical shape or any other shape which contribute to the cohesion. We can reduce the adhesive or cohesive forces between two particles or a surface and a particle by increasing their distance. This distance can be increased by introducing a surface roughness on the spherical particle. In our study which aims at reducing cohesion in fine particles by dry coating, we basically introduce nanoscale roughness on the surface of particles which is enough to reduce the cohesive forces significantly. The dry coating aims at making the nanoparticles stick or adhere to the host particle surface so they act as a nanoscale roughness. There is plenty of research and deliberation going on about the nature of the roughness required to reduce cohesion i.e. discrete or continuous film of nanoparticles acting as roughness.

The evidence that surface roughness decreases the adhesive or cohesive forces is presented below.

Figure 5.4. describes the various forces of adhesion after the introduction of a surface asperity. H is the adhesive force and r is the radius of the hemispherical asperity introduced

on the spherical particle surface. The distance between the asperity and the plate is kept constant at 4 x 10^{-4} μm. Increase in r leads to increase in distance between plate and spherical particle. As can be seen in the plate as r increases the adhesive forces decrease. Our main focus is on van der Waals forces, they decrease because the asperity increases the distance between plate and spherical plate, van der Waals forces are heavily dependent on distance so the decrease is justified. On increase of asperity radius beyond a limit, the adhesive forces increase as now adhesive forces between hemispherical asperity and wall dominate adhesive forces between plate and spherical particle

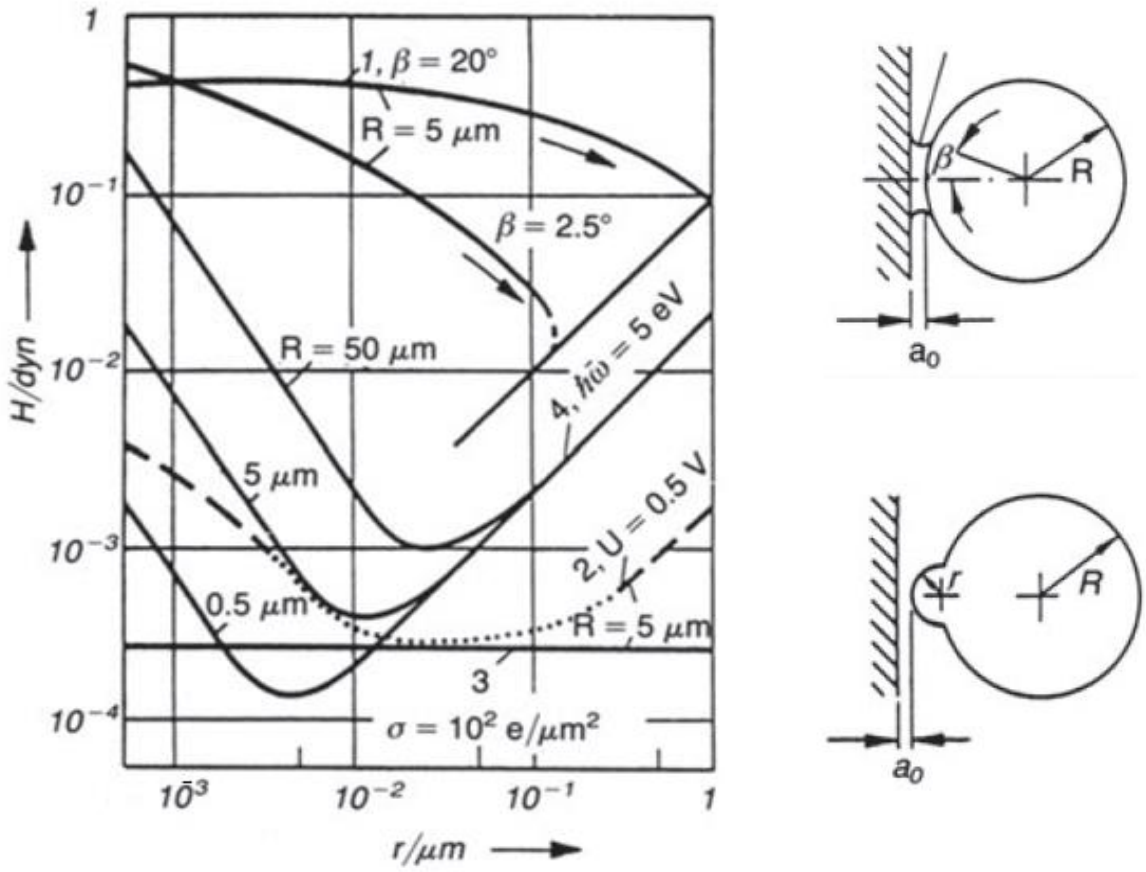

Figure 5.4. Influence of the radius *r* of an asperity on the adhesive forces due to various mechanisms of adhesion for the sphere-plate model (contact gap *a* = ao, ao = 4 x 10^{-4} μm) Adhesive forces of various mechanisms of adhesion for the sphere plate model (on contact) as a function of the diameter of the sphere: 1, liquid bridges; 2, electrostatic forces for conductors; 3, electrostatic forces for insulators; 4, van der Waals forces. (Rumpf, 2012)

Hence, it is established beyond doubt that introduction of surface roughness on the host or primary particles will reduce the adhesive forces.

On careful examination of Figure 5.4. it can be seen that the primary spherical particles of 50, 5 and 0.5 μm are studied and introduction of asperity between 1nm to 30-40nm reduces adhesive forces. Smaller the primary particle, lower the size of asperity needed to reduce the

adhesive value. The asperity or surface roughness in nanoscale can be introduced by dry coating techniques which are extensively discussed in this chapter.

The nanoparticles adhere on the surface of the primary particles because of the high impact force with which they strike the host particles in the dry coating process. The particles do not fall of because the van der Waals forces between the nano and the host particles outweigh the gravity force of the nanoparticles.

Before proceeding to the main part of this chapter there is a need to shed some light on the existing models and the formulas being used for calculating adhesive forces using mathematical formulas.

(Rabinovich *et al.*, 2000 a, 2000 b) in a series of two papers firstly derived a model to predict adhesive force between a plate and a spherical particle with roughness by predicting the size of the asperity based on the root mean square roughness and distance between asperities. Secondly the proposed model was compared to the experimentally determined adhesion force with nanoscale roughness.

According to Rumpf model (Rumpf, 2012) the adhesive force between a plate and a spherical particle with hemispherical asperity is as follows:

$$\mathrm{H} = \frac{h\overline{\omega}}{8\pi}\left(\frac{r}{a^2} + \frac{R}{(r+a)^2}\right) \tag{5.1}$$

H is van der Waals attraction force,
a is gap between the surface of the sphere and the plate,
R is the radius of the sphere,
h is the Lifshitz-van der Waals constant,
$\overline{\omega}$ depends on the dielectric constants of the two bodies and
r is radius of curvature of asperity.

$$F_{ad} = \frac{A\,R}{6\,H_0^2}\left[\frac{1}{1+\left(\frac{32Rk_1rms}{\lambda^2}\right)} + \frac{1}{\left(1+\frac{k_1rms}{H_0}\right)^2}\right] \tag{5.2}$$

(Rabinovich *et al.*, 2000 a)

F_{ad} is adhesion force between adhering particle and a nanoscale roughness surface,
Root mean square roughness is rms,
λ is peak to peak distance between hemispherical asperity,
A is Hamaker constant,

k_1 is coefficient for establishing relationship between rms and maximum value of peak height of hemispherical asperity,
R is radius of adhering particle and
H_o is distance of closest approach between surfaces.

Rabinovich et al. (2000 b) found that the nanoscale roughness plays a dominant role in adhesion interaction even if the surface has a large rms roughness. Roughness as small as 1.6 nm reduced the force of adhesion by nearly five times. Radius of the sphere in contact with the surface plays a major role in force of adhesion, larger radius led to larger reduction of adhesive force. By incorporating the height and breadth of the asperities and then applying to van der Waals approach the values of experimentally determined adhesion were within a 50% range of the theoretical value, earlier models miscalculated the adhesion forces by a factor as much as 10-50 times. The model conceptualized reduced the error in prediction greatly, which was not done until now. Deformations of asperities and the spheres are also incorporated and results compared. The work by the author is genuinely path breaking and shows that a very small nano-scale roughness can greatly reduce adhesion forces.

In the study by Tomas and Kleinschmidt (2009), various models to ascertain van der Waals forces were discussed together with the effect of coating induced variations on surface of powder and their effect on van der Waals forces. The total adhesion force between two particles is the summation of van der Waals force, surface tension and capillary force. The flow properties of powders improve upon coating by additives. The efforts of the writer should be lauded to compile multiple theories and explanations of van der Waals forces into one paper.

Mangal *et al.* (2016) defined cohesive adhesive balance as a balance between the adhesive forces between small and large particles and cohesive forces as force of cohesion between small particles. De-agglomeration and adhesion of small particles on large particles is favoured when adhesive forces are larger than the cohesive forces in the cohesive adhesive balance model. Interactive mixtures have high chance of formation when adhesion forces exceed or equal cohesion forces. At higher excipient loading, tensile strength results circumvented CAB concept. Bulk density improvement for higher concentrations of excipients, can be attributed to better coverage by excipients on host particle surfaces. In summation, if the adhesive forces exceed cohesive forces the mixture is more strong or its tensile strength increases together with bulk density and tapped density. If the guest or excipient adhere on the API surface, they will reduce original interaction and hence cohesivity. The CAB model proved to be an effective tool for predicting properties and behavior of mixture. Phase diagrams linking cohesive and adhesive forces with other properties should be constructed together with tests with different guest and host particles.

The mass percentage of guest particles required for 100% surface coverage of host particles with guest particles monolayer was given by Yang *et al.* (2005). It is assumed that guest and host particles are spherical and all guest particles are of same size. Guest and host particles do

not deform during coating process. Weight percentage of guest particles (Gwt.%) for 100% surface coverage is:

$$\text{Gwt\%} = \frac{(\text{Nd}^3\rho_\text{d})}{(\text{D}^3\rho_\text{D}) + (\text{Nd}^3\rho_\text{d})} \times 100 \quad (5.3) \qquad N = \frac{4(\text{D} + \text{d})^2}{\text{d}^2} \quad (5.4)$$

ρ_d= Particle density of guest particles, ρ_D= Particle density of host particles
D= Diameter of host particles, d= Diameter of guest particles

We will now look at the aspect of the surface area of the host particles coated/covered with guest particles and its corresponding effect on the reduction in cohesiveness of powders.

Chen *et al.* (2010) proposed a model to encapsulate the effect of surface area coverage. A case where three small guest particles supported two spherical host particles was considered. Figure 5.5 below describes the model.

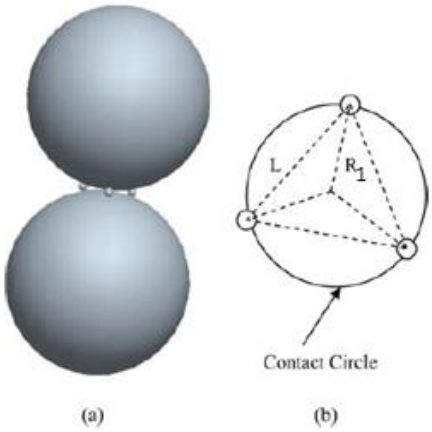

Figure 5.5. (a) Contact of two-coated cohesive particles and (b) Location of guest particles.
It was assumed that guest particles were monosized spheres and were coated evenly on the host surface. Between the two host particles, the guest particles are assumed to lie on the vertices of an equilateral triangle.

Contact circle radius

$$R_1^2 = \left(\frac{D+d}{2}\right)^2 - \left(\frac{D+H_0}{2}\right)^2 \quad (5.5)$$

Area of the three coated particles triangle

$$S = \frac{3\sqrt{3}}{4} R_1^2 \quad (5.6)$$

Relation between number of coated particles and area of triangle S can be expressed as follows:

$$N = \frac{\pi D^2}{2S} = \frac{2\sqrt{3}\pi D^2}{9R_1^2} \tag{5.7}$$

Surface area coverage or SAC then becomes:

$$SAC = \frac{N \times \frac{\pi D^2}{4}}{4\pi\left(\frac{d+D}{d}\right)^2} \times 100\% = \frac{N \times d^2}{4(d+D)^2} \times 100\% \approx \frac{N \times d^2}{4(D)^2} \times 100\% \tag{5.8}$$

According to Rumpf (2012) adhesive force between two rough particles is the summation of attraction between asperity and host particle and adhesion between two host particles. Adhesive force between two coated particles was calculated as:

$$F_{ad} = \frac{A}{12\, z_0^2}\left[\frac{3dD}{d+D} + \frac{D}{2\left(\frac{H_0}{z_0}\right)^2}\right] \approx \frac{Ad}{4(z_0)^2} + \frac{AD}{24(H_0)^2} \tag{5.9}$$

Host-host distance can be related to SAC, D and d as follows:

$$H_1 = \sqrt{(D+d)^2 - \frac{1.21d^2}{SAC}} - D \tag{5.10}$$

The following is the expression linking surface coverage area of guest particles on the host particles to the adhesion force between the two host particles.

$$F_{ad} = \frac{A\, d}{4\, z_0^2} + \frac{A}{24\left(\sqrt{\left(1+\frac{d}{D}\right)^2 - \frac{1.21}{SAC}\left(\frac{d}{D}\right)^2} - 1\right)^2 D} \tag{5.11}$$

A = Hamaker constant,
D = Diameter of host particle,
d = Diameter of guest particle,
z_0 = Default distance between two surfaces in contact,
H_1 = Distance between two coated host particles,
S = Area of the contact circle,
R_1 = Radius of the contact circle, respectively and
N = Number of guest particles coated on the surface of each host particle.

5.4 Techniques/machines used for dry coating

An effort has been made to accumulate and compare results of the effects of dry coating on cohesive powders with the help of widely used machines and techniques for dry coating such as Co-Mill, Fluid Energy Mill, Magnetic Assisted Impact Coater, Mechanofusion, LabRAM, Hybridizer and Cyclomix.

The effects of dry coating technique on different powders has been discussed together with a comparison and effectiveness of different techniques. This study tries to establish the relative advantages and disadvantages of a certain technique for certain applications and tries to encapsulate the general effect of dry coating on fine cohesive powders.

We will proceed in the following order:

5.4.1 Co-Mill
5.4.2 Fluid Energy Mill
5.4.3 Magnetic Assisted Impact Coater
5.4.4 Mehanofusion
5.4.5 Hybridizer and Cyclomix
5.4.6 LabRAM
5.4.7 Random techniques

5.4.1 Co-Mill

The cone mill has a conical chamber and product enters through the feed hopper. Rotating impeller imparts a vortex flow to the product and centrifugal forces continuously force it to a zone between impeller and conical chamber screen. Particles become trapped between screen and impeller edge and experience high shear stresses which causes de-agglomeration of host and guest particles.

The high shear stresses experienced cause the host and guest particles interaction and eventually lead to coating. Proper residence time ensures repeated collisions between host and guest particles and ensures uniform coating. The screen size ensures the desired size reduction and the finished product is discharged at the bottom of the milling chamber.

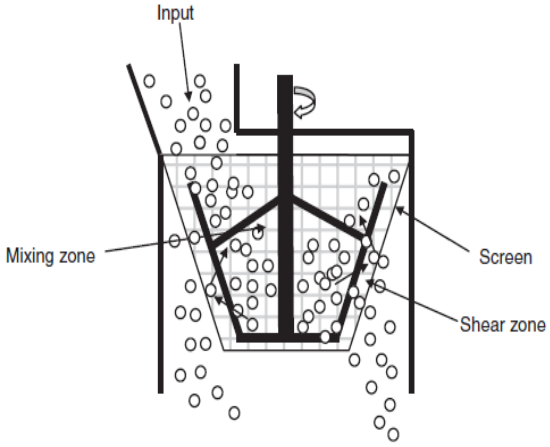

Figure 5.6. Co-Mill (Mullarney *et al.*, 2011)

No substantial micronization.
Prior blending preferred.
Low temperature and low dust generation.

Operating parameters and effects

(a) Comilling cycles

Comilling cycles effect the coating efficiency and flowability improvement greatly, after optimum cycles the guest particles tend to be lost within inner surface of Co-Mill and entrapment in grooves and crevices of host particles.

(b) Operating speed

Operating speed does not have a major impact on the coating performance and efficiency.

(c) Powder feeding rate

As the feed rate increases, comilling cycles have to be increased so as to de-agglomerate host and guest particles and to aid proper dispersion of guest particles on the host particles surface.

(d) Screen and impeller

The shape and size of screen, impeller blade design was found not to be significant in determining the coating performance.

In the study conducted by Chattoraj, Shi and Sun (2011) it was proposed that a continuous layer of guest particles on the host particles was similar to increasing the diameter of the host particle by a small diameter and only contributed to little reduction of cohesivity. If the guest particles are separated by a discreet nanoparticle asperity it leads to a larger reduction in cohesion in comparison to a continuous film. Avicel PH105 was coated with 1% wt. / wt. silica nanoparticles and optimum milling cycles for optimum surface coverage and improvement in flowability were found. 40 milling cycles were found to be optimum for improvement in flowability as after this the flow function decreased. At 40 cycles the silica loading was incremented from 0 to 1% wt./wt. and flowability improved with increasing wt./wt.% of silica, the simply blended samples showed very poor flowability comparable to Avicel 105 emphasizing the role of milling. The tabletability defined as the effect of compaction pressure on tensile strength of tablets decreased after dry coating probably due to reduction in bonding areas between the host Avicel particles due to coating of silica particles.

Mullarney *et al.* (2011) hypothesized that the surface roughness, hydrophilicity, charge, particle shape and size play a major role in influencing the bulk density and flow of the powders and thus it is difficult to generalize or recommend a single regime for improving flow of the cohesive powders. The major finding of this study was that simple blending was insufficient in improving flow, comilling process is necessary and secondly that the comilling process can be scaled up for industrial and practical use as the improvements in flow and bulk density were similar for large and small batch size (5kg and 20g). The guest particles increase the distance between the host particles due to which van der Waals forces reduce leading to decrease in cohesivity and hence improving the flow.

Zhou et al. (2012) tried to develop coating parameters so as flowability is improved and tabletability is not affected much. Discrete surface coating was thought to be effective in improving flow. Silica loading was varied between 0-2% wt./wt. and comilling cycles from 0 to 40 while not changing other parameters. As the silica loading increased the optimum number of comilling cycles to improve flow properties increased as certain number of cycles is necessary to break the agglomerates of guest particles and aid their proper spread on host particles. The reduction in flowability was attributed to the loss of silica within inner surface of Co-Mill and silica trapped between grooves and crevices of host particles. The larger wt./wt.% of silica improved flowability because more silica content improved surface coverage and the direct contacts between host particles were reduced. The coating of silica with different wt./wt.% on microcrystalline cellulose decreased both tabletability (dependence of tablet tensile strength on compaction pressure) and compactibility (dependence of tablet tensile strength on tablet porosity) of the tablets manufactured. The author suggested a 0.5 wt./wt.% of silica as optimum for improving flow and without effecting tabletability.

Yuan *et al.* (2013) studied the manufacturing of danshen, notoginseng and borneol mixture coated with colloidal silica and its flowability. The bulk and tap densities of individual powders and there mixtures after coating increased together with the reduction in angle of repose except borneol which showed increase in AOR. The compressibility also decreased for all the three powders and there mixture. The milling of powders helped in better particle

size distribution as the small particles underwent agglomeration and large particles underwent size reduction. The hygroscopicity of the powders was not affected much but the tabletability improved in comparison to uncoated powders.

Zhou *et al.* (2013) used ibuprofen blend and evaluated the effects of dry coating on flowability and tabletability. The increase in moisture content on the flowability of ibuprofen blend had a non-significant impact on flowability because of low hygroscopicity of ibuprofen. The flowability of 0.1% and 0.5% wt./wt. silica coated blends increased in comparison to uncoated blends. The impeller speed, type of impeller, screen size and design had little effect in enhancing the flow of the blend. Blending alone is insufficient in breaking the agglomerates of the host and guest particles and leads to ineffective coating, comilling overcomes the deficiencies of simple blending. Coating of ibuprofen blend with silica improved the tabletability and compactibility in comparison to uncoated blend and particle size distribution of the coated and uncoated blends showed that particle attrition did not take place. The higher tensile strength can be attributed to the higher bonding strength between silica and ibuprofen as compared to lubricated particles in the blend. The author states that tabletability increases in ibuprofen because the guest particles sink in the surface and there is no net decrease in bonding areas between ibuprofen particles but in microcrystalline cellulose the tabletability decreases as the particles are harder and they do not conform to the shape of the silica particles hence causing a decrease in the bonding area. This logic is a little contradictory because if the bonding area between the ibuprofen particles did not change after coating then why did the flowability increase, as we consider that the guest coating decreases the contact area between host particles and reduces cohesivity.

The use of comilling technique improved the flow of each and every powder tested indicated by various flow properties in the above studies, but the properties required for manufacturing tablets like tabletability and compactibility showed no fixed trend and varied from a case to case basis. There is some agreement between the studies, i.e. guest coating increases the inter particle distance of host particles, promotes guest-guest interaction and reduces bonding area between host particles, all leading to reduction on cohesivity and hence increase in flowability.

5.4.2 Fluid Energy Mill

Fluid Energy Mill or FEM comprises a shallow cylindrical grinding chamber into which through specially designed nozzles which are spaced around the circumference of the chamber, high pressure compressible fluid is introduced which creates a high velocity vortex. Product to be processed is introduced through a separate venturi system guided by feed air.

The product is sucked into the vortex and due to the relative velocities of the particles they strike each other and also the walls of the chamber causing de-agglomeration of host and guest particles and coating of guest particles on the host particle surface. The grinding fluid imparts different velocities to the powder particles due to which they have different momentum and strike each other causing high energy particle-wall and particle-particle collisions which cause particle size reduction and attrition.

Fluid energy mill has no moving parts and the particles take a spiral path from chamber periphery to central outlet.

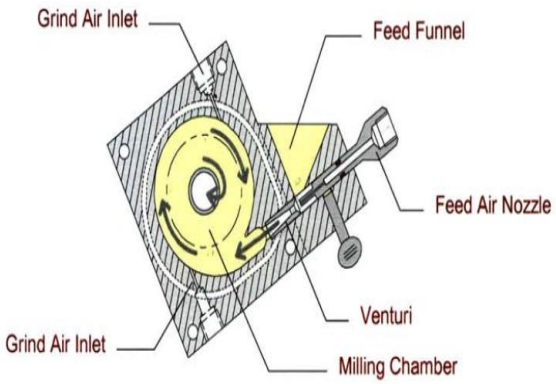

Sturtevant Qualification FEM

Figure 5.7. Fluid Energy Mill (Teng *et al.*, 2009)

Substantial micronization.
Prior blending preferred.
Process takes place without attritional heat so heat sensitive materials can be successfully reduced. As no moving parts minimum contamination.

Operating parameters and effects

(a) Solid feeding rate

Increase in solid feeding rate does not have a monotonous effect on the median particle size after milling. Large solid feed rate may increase collision frequencies resulting in smaller average size and on the other hand may provide less specific energy per particle and hence larger average size.

(b) Feeding pressure

Feeding pressure does not have a major impact on the median particle size and the coating performance as it just provides it with absolute velocity.

(c) Grinding pressure

Pressure of the grinding fluid entering into the chamber imparts relative velocities to the particles which causes high energy particle-wall and particle-particle interactions. Increasing grinding pressure beyond optimal level causes guest coating to come off leading to decrease in flowability and breakage of host particles and subsequent shape change.

Teng *et al.* (2009) commented on the benefits of FEM and listed them to be narrow PSD, no heat accumulation, less contamination. Increasing the grinding nozzles increases the energy input and reduces the concentrated erosion on the wall. Study suggested that the particle wall collisions are significant for particle size reduction. Grinding pressure has a far major impact on particle size reduction than feed pressure. The reason for the insignificance of feed pressure can be attributed to the fact that feed pressure air only increases the velocity of particles but does not change the relative velocity of particles which are real contributors to particle size reduction. The increase in solid feed rate causes shorter residence time of particles as well as low specific energy per particle causing increase in mean particle size, the effect of solid feed rate is not monotonous always. The simulations performed helped in understanding the working of FEM and corroborated some phenomena's observed in the study.

Han *et al.* (2011) observed that increasing the grinding pressure while keeping solid feed rate constant decreased the median particle size and increasing the solid feed rate by keeping the grinding pressure constant led to increase in median particle diameter. Rod shaped ibuprofen particles were converted to spherical shape particles after processing in FEM, micronized uncoated ibuprofen formed irregular shaped agglomerates whereas the cohesion reduced in coated ibuprofen and so did the agglomerating tendency. Flow of coated powders improved and cogrinding with glidant further increased bulk density. The surface energy of particles reduced after coating. Dry coated ibuprofen showed low compressibility indicating efficient packing and minimum excess air probably because the inertial forces of the powder dominated the reduced cohesion forces. Dissolution improved due to hydrophilic silica improving wettability together with better dispersibility of coated powder.

Qian, Wang and Gogos (2012) proposed that solid feeding rate and grinding pressure have major impact on the size and particle size distribution after milling. Solid feed rate does not have a monotonous effect on the particle size, as a large solid feed rate may increase collision frequencies resulting in smaller average size and on the other hand may provide less specific energy per particle and hence larger average size. Increase in grinding pressure leads to lower mean particle size. Polymer composite made by mixing homopolymer and calcium carbonate showed that mixing milled+coated and milled+uncoated samples improved the impact strength of composite in comparison to un-milled composite. The milled+coated composite showed better elongation at break than milled+uncoated composite. It is because the milled+uncoated particles form agglomerates which decreases their distribution, aspect ratio becomes larger than 1 which causes stress concentration and agglomerates causes large voids which act as initiation sites for fracture. The flowability of the coated particles increased as expected and seen in similar studies.

Ghoroi, Han, *et al.* (2013) linked dispersibility with dry coating and dispersion effects on flowability. Small particles are generally more cohesive than larger particles and have poor dispersibility. In the study MAIC was used for dry coating and FEM for simultaneous micronization and coating. Micronized acetaminophen without coating showed agglomeration whereas Leucine coated showed rough surface on SEM analysis and little agglomeration. The micronized dry coated powders showed improved dispersibility and required much lesser energy to achieve fully dispersed state in comparison to uncoated micronized powders indicating that the dry coating reduced cohesive forces and hence made it easier to disperse the powder. All coated powders showed improved flow and bulk densities indicating better packing which can be linked to better dispersibility caused by reduction in cohesion. Coated powders showed improved fluidization over the uncoated ones.

Han *et al.* (2013) investigated the effect of surface area coverage of guest particles on the host particles and previous studies showed that a SAC of 20% or preferably 40% is required to minimize the host-host and host-guest interactions. Uncoated ibuprofen processed in fluid energy mill was micronized and the shape of particles changed from rod or flake like structures to round shape particles. Micronization of ibuprofen led to severe agglomeration and the reason was thought to be introduction of high energy sites because of micronization. Coated ibuprofen showed little aggregation after micronization. The ibuprofen coated with hydrophobic nano-silica showed better bulk density than uncoated ibuprofen and coated with hydrophilic silica. The surface energy values of coated ibuprofen were similar to the surface energy of the nano silica indicating that dry coating helps in covering or suppression of high energy sites on ibuprofen particles after coating. The improvement in flowability was attributed to the nano roughness introduced on the particles together with lowering the surface energy which was linked with aggregation tendency. Dry coating helped in surface energy homogeneity and passivation of high energy sites.

All the studies conducted tended to agree on broadly some of the following points. Solid feed rate and grinding pressure are the most important parameters in determining the median particle size after milling. Solid feed rate did not show a monotonous trend whereas grinding pressure did. Feeding pressure was relatively insignificant. Fluid energy milling helps in combining two processes of micronization and dry coating into a simple one step process which can be used to simultaneously decrease the average size of particles and improving the flow by dry coating. The usage of FEM often causes change of shape in particles which can sometimes be undesirable. The FEM is a process which has very low powder contamination levels, low heat accumulation and narrow PSD.

5.4.3 Magnetic Assisted Impact Coater

As the name suggests in MAIC the coating of guest particles on the host particles is assisted by impaction caused by magnetic assistance. Processing vessel is surrounded by a series of electromagnets. Magnetic field created by the electromagnets agitates the magnetic particles present in the vessel along with powder.

These agitated magnetic particles transfer their energy to the host and guest particles by collisions, hence promoting inter particle and particle wall collisions. These collisions cause de-agglomeration and high energy impaction of guest particles on host particles leading to coating. Magnetic particles are generally coated to prevent contamination.

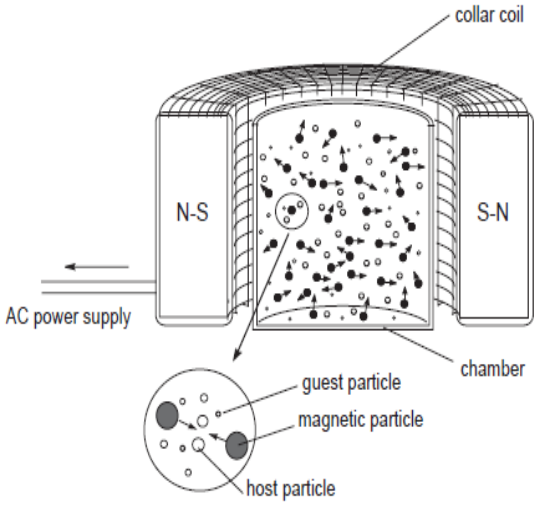

Figure 5.8. Magnetic Assisted Impact Coater (Yang *et al.*, 2005)

No substantial micronization and low particle attrition.
Prior blending preferred.
No heating of product but contamination tendency due to uncoated magnetic particles.

Operating parameters and effects

(a) Magnetic particle size

Increased particle size of the magnetic particles leads to better surface coverage probably due to better dispersibility of guest particles.

(b) Magnet to powder mass ratio

Increasing the magnet to powder mass ratio increases collision frequency and leads to shorter processing times to achieve similar coating conditions.

(c) Processing time

The coating efficiency and effectiveness increased with increasing processing time as indicated by improving flowability. Increasing processing time beyond optimal led to reduction in flowability attributed to the destruction of coating and change in shape and size of host particles due to continuous collisions and high energy impactions.

(d) Current and frequency

Increase in current till optimal level led to linear increase in surface coverage. Frequency variations showed periodic fluctuations in surface coverage results.

Yang *et al.* (2005) used varying sizes of guest particles to ascertain their impact on reduction of cohesive forces between particles. Magnetic particles of 1.4-1.7 mm range, magnet to powder mass ratio 3:1 and processing time of 10 minutes in MAIC were used. V blender is not able to break agglomerates of host and guest particles and also has poor performance in dispersion of guest particles. This study proposed that for a fixed host particle size the reduction in cohesive force between the host particles was inversely proportional to the guest particle size. It essentially means lower the guest particle size, greater the reduction of cohesive forces between host particles. This theory was backed with favourable results with improvement in flow with reducing guest particle sizes. Hydrophobic coating improved flow better than hydrophilic coating as the former reduces water adsorption and water bridge formation.

Chen *et al.* (2010) linked the improvement in flowability to Bond number. Bond number is the ratio of particle adhesion force to the particle weight. Flow of cohesive powders increases when Bond number decreases. Powders were silane treated and dry coated. Silane treatment lowers the surface energy which helps in lowering cohesion and better de-agglomeration or fine detachment which decreases the average particle size. Silane treatment smoothens the surface and lowers the roughness whereas dry coating does not reduce the roughness that much but reduces the average particle size more than silane treatment.` The study showed that silane treatment reduced the Bond number greatly in comparison to dry coating samples.

Jallo *et al.* (2012) emphasized that impact of coating on flow and other properties should not come at a cost of changed particle size and shape. Surface coverage of 10-20% and discrete coverage of guest particle can be enough to improve the flowability. Elasticity and hardness of particles were major factors influencing particle attrition as a magnet to powder mass ratio of 2:1 or 3:1 caused high particle attrition. Dry coating improved the flowability of all the powders tested. Lower cohesive forces in dry coated powders leads to formation of weaker structures which collapse easily during angle of repose testing. The coating reduces the direct contacts between host particles and increases there inter particle distance causing reduction in van der Waals forces. The operating parameters of MAIC for surface coverage and minimum particle attrition vary for different powders.

Ghoroi, Gurumurthy, *et al.* (2013) used MAIC and found that coated nanoparticles imparted nano scale roughness on the guest particles and that reduces host-host particle contact, hence reducing cohesivity and agglomeration tendency thus increasing the dispersibility. Attrition of the particles was minimum. Surface coated API's and excipients generally showed improvement in flowability in comparison to uncoated ones. Powders which have good flow generally pack better because of the low cohesion forces due to which the structure collapses during settling of particles. The dry coated API's showed improved bulk densities. It was found that dynamic powder properties such as aeratability cannot be linked directly to powder properties like conditioned bulk density, Carr's index and angle of repose. The author plotted conditioned bulk density and flow function coefficient and defined two regions i.e. "probable" and "definite". The regions were defined for the ability of direct compaction of powders with powders falling in definite region being fit for direct compaction and those

falling in probable region could be direct compacted. Barring one API used in this study, all other dry coated API's fell in one of the two regions indicating that dry coating can aid in direct compaction.

The studies using MAIC techniques showed that magnet to powder mass ratio, magnetic particle size and operating time were the main factors influencing working and performance of MAIC machinery. There is an urgent need of verifying the effect of surface energy reduction on improvement in flowability. Also some researchers prefer discrete guest coatings while others prefer continuous or complete surface coverage. Proper research should be conducted to encapsulate the effects of both and a model should be proposed suggesting optimal surface coverage requirement bearing in mind the factors like cost and time. Another area of interest is the roughness induced by the guest particles, i.e. how much surface roughness is ideal that contributes to optimum cohesion reduction.

5.4.4 Mechanofusion

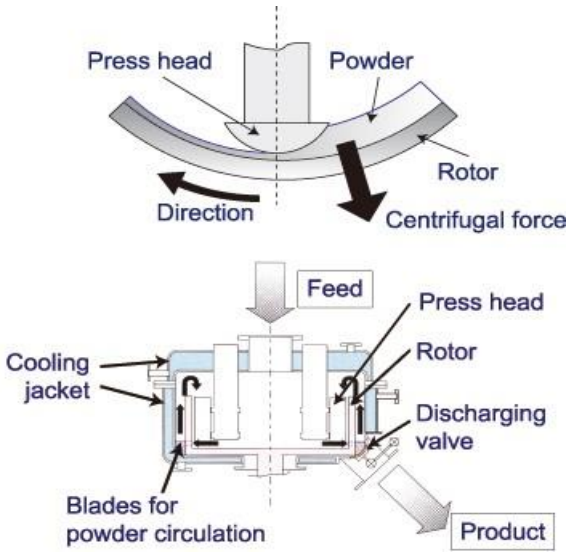

Figure 5.9. Mechanofusion, Hosokawa Micron Corporation

Mechanofusion is a device that mechanically coats the guest particles on the host particles. It is typically a cylindrical vessel comprising of an axial shaft with series of paddles extending from the shaft at alternating angles to each other. The paddles along the length of the axial shaft extend very close to the vessel wall with an approximate distance of about 1mm.

The rotation of the shaft causes the paddles or blades to sweep very close to the vessel wall and ensure constant violent motion of powder. Due to the high rpm of paddles, powder is pushed towards the wall and experiences very high shear forces at paddle face and compressive stresses between paddle and wall. The energy thus gained by the powder is sufficient to break the agglomerates and subsequent coating to take place.

No substantial micronization and shape change of particles.

Prior blending preferred.
No heating of product during granulation / sizing operation, due to better air circulation & lesser impact action.

Operating parameters and effects

(a) Processor rotation speed

Flow properties improve with an increase in rotational speed because host and guest particles de-agglomerate and with increase in rotational speed the guest particles spread or disperse more evenly on the host particle surface. Increasing processor rotation speed further than the optimal speed does not have an adverse impact on properties.

(b) Processing time

Similar to the parameter discussed above, a minimum amount of processing time is required so that host and guest particle agglomerates are broken and the guest particles get enough time for coating on the host particle surfaces. Increasing processing time does not improve or deteriorate flow properties to a great extent because mechanofusion is a process in which there is no major particle attrition indicating energy of the process does not break the particles or micronize them.

Zhou *et al.* (2010 a) studied the effects of using mechanofusion technique on lactose monohydrate powder by coating it with MgSt and fumed silica. Batch mechanofused with fumed silica showed rough surfaces similar to batch mechanofused without fumed silica. Mixing was unable to disperse MgSt particles on lactose, but mechanofused sample showed rounded edges attributed to the same reason as explained by Zhou *et al.* (2010 b). Batch mechanofused with MgSt showed a lower angle of repose indicating better flow. Poured density showed no major impact of mechanofusion whereas tap density improved. Compressibility after mechanofusion decreased because of improved packing and lesser voidage due to the reduced cohesion values.

Zhou et al. (2011) studied the effect of process head speed and time on coating. Mechanofusion process did not lend a hand in particle attrition but rounds off the sharp edges. All the samples that were mechanofused with MgSt showed varying degrees of improved flowability. Control on energy input is better in mechanofusion system than in conventional milling methods. The poured and the tapped densities increased when rpm were 3000 and 2000 respectively but did not improve further on increasing the rpm of the process head indicating at an optimum rpm. The cohesion values reduced and ffc increased for speeds in the range of 4000-5000 rpm. Study found that beyond a certain operating time the effects on flowability were minimal, that value is about 10 minutes for this study. Coating helped to reduce cohesion between particles that led to lower agglomerates formation and ultimately better packing. Mechanofusion helped to improve powder properties but not at the expense of particle size change. Processing speed and time were the major parameters effecting the coating performance.

Qu et al. (2017) tried to develop a process to optimize tensile strength and dissolution of the tablet together with improving flowability of the mixture all in a single step. MgSt was chosen to have the dual effect of acting as flow-aid and also as a lubricating agent, lubrication is required to prevent adhesion to the dies during high speed tableting of powders. The reduction in tensile strength was attributed to the decrease in bond formation of ibuprofen

powders due to coating with MgSt whereas an increase in tensile strength when coated with silica was attributed to the stronger inter-particle strength between silica and ibuprofen than between ibuprofen powders. There was an interesting result in this study, silica improved the flow the most but its tensile strength also improved. Generally improvement in flow is attributed to reduction in cohesive forces and improvement in tensile strength to the increase in cohesive forces. Cohesion reduction mainly depends upon the interaction between host particles whereas tensile strength depends upon the dominant cohesion force of either host-host or host-guest interactions. In conclusion silica mechanofused sample had best flowability, MgSt coated tablet showed minimum tensile strength, L-leucine was the best optimized coating for improving flow, tensile strength, providing lubrication as well as good dissolution rate. Particle attrition was not of high order. The study emphasized that direct compression can lead to elimination of special excipients related to direct compression hence reducing the cost and size of the tablets manufactured.

Mechanofusion is a technique which can be used for dry coating without changing the median particle size to a great extent. It has relatively few parameters effecting performance namely processing speed and time as compared to other dry coating machines. Mechanofusion aids in breaking agglomerates of host particles and distributes the guest particles effectively. Mechanofusion process is stated as a thermo-mechanical process which means temperature can play a part in the coating. For cases where low melting point powders are used, undesirable effects can be seen. On the other side heat can improve the performance of coating materials like wax to spread better and effectively coat host surface area. Mechanofusion like other techniques can be used for direct compaction and tableting purposes.

5.4.5 Laboratory scale Resonant Acoustic Mixer

Laboratory scale Resonant Acoustic Mixer or LabRAM is a relatively new device that is being used for coating of guest particles on the surface of the host particles.

LabRAM works at the resonant frequency at which amplitude of vibration is maximum. There are three forces in the system (a) inertial force due to plate mass, (b) damping force due to powder mass and (c) spring force due to the springs. Force applied to the plates at resonant frequency leads to cancellation of inertial and spring forces by each other and only damping forces exists. Damping forces are characterized in LabRAM as the forces used for mixing.

At resonance the amplitude of vibration is maximum and the powder is mixed through transfer of mechanical forces of system into acoustic pressure wave which are sent through the mixing vessel. The energy transferred to the loose mass by the acoustic pressure wave ensures proper mixing through creation of micro-mixing zones throughout the vessel and also promoting bulk flow simultaneously.

The most important parameter in LabRAM is the mixing intensity. The mixing intensity can be controlled by the energy supplied by the load plates to the vessel. Amplitude of the mechanical vibration translates into the acceleration the mixing vessel experiences.

Coating is achieved by the collisions between the guest and host particles during the high energy mixing process. De-agglomeration of host and guest particles take place when they collide with the vessel base and with each other.

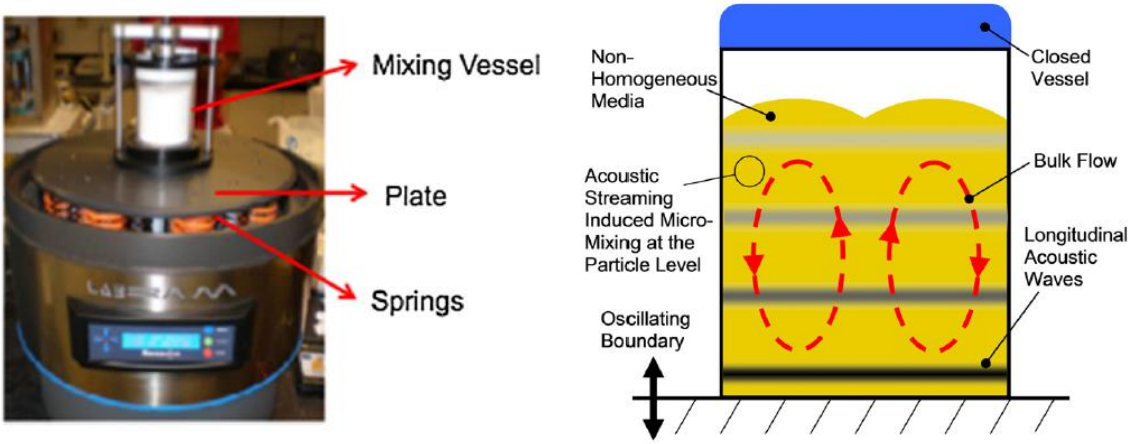

Figure 5.10. LabRAM (Osorio and Muzzio, 2015)

No substantial micronization and shape change of particles.
Prior blending not required.
Powder bed can get heated at higher accelerations and greater blending time. Powder properties should be properly analyzed before deciding the working conditions in order to avoid melting.

Operating parameters and effects

(a) Acceleration

It is one of the most vital parameter effecting the coating performance and the blend homogeneity. At low mixing times the higher acceleration of the mixing vessel translates to

more energy transfer to the powder mixture hence increasing the coating performance and blend homogeneity.

(b) Mixing time

Mixing time effects the performance of LabRAM immensely. A low mixing time can lead to poor blend homogeneity. At a given acceleration proper mixing time is required so that coating takes place and also a homogeneous blend is obtained. Mixing beyond the optimal time can lead to particle attrition and heat accumulation. The level to which the vessel was filled did not have an impact on the mixing performance.

Huang *et al.* (2015) conducted the flowing study, various blends of API and excipients together with disintegrant and MgSt were blended and tested. Nano guest particles were coated on API and excipients in LabRAM and mixed in blends. Blends with uncoated API and excipients added with silica were also tested. Resonant acoustic mixer was successful in breaking the guest particle agglomerates and distributing them over host particles, the nano scale roughness was thus created and the cohesion reduced. Use of LabRAM improved the flow and decreased compressibility of coated powders. The % API in blend plays a major role in the compaction and strength properties. At maximum loading of coated API the packing and flow properties improved, the excipient size did not play a major role. API coated blend with fine excipients showed better tableting properties.

Osorio and Muzzio (2015) studied the effects of fill level, acceleration and blending time on the mixing performance of LabRAM. LabRAM is a device which uses the concepts of mechanical engineering to its advantage. There are three forces in the system (a) inertial force due to mass, (b) damping force due to powder mass and (c) spring force due to the springs. Force applied to the plates at resonant frequency leads to cancellation of inertial and spring forces by each other and only damping forces exists. At resonance the amplitude of vibration is maximum and the powder is mixed through transfer of mechanical forces of system into acoustic pressure wave which are sent through the mixing vessel. Better mixing performance was seen at higher acceleration, blending time required for proper mixing and homogeneity was different at different accelerations but fill level did not have any influence on the mixing performance which is not the case in most blenders.

Wang *et al.* (2017) used a controlled shear system and LabRAM to compare the different mixing processes and their effect on lubrication. Both devices basically give control of the strain or energy and the strain rate. Lubrication by MgSt significantly improved the flow of the pharmaceutical blend. Analysis of variance technique helped to deduce that the most important factor effecting lubrication was shear or the energy supplied and not the shear rate or the rate at which energy is supplied to the blend.

5.4.6 Hybridizer and Cyclomix

Ouabbas *et al.* (2009) conducted a study in which MgSt was coated on silica gel in hybridizer and cyclomix in wt./wt.% of 5 and 15 and then compared with the results of mixing in turbula mixer. Stability and quality of coated powders changes with change in storage conditions, particularly relative humidity plays a major role in pharmaceutical and food powder handling and storage. Hybridizer performs coating by high impaction forces and friction heat, high impaction is caused by interaction of powder with blades and wall. High speeds up to 16000 rpm can be achieved in hybridizer which makes the processing time short. In cyclomix the powder is pushed to the top by the rotating paddles and conical shape of vessel, during the upward motion particles are intensively mixed due to friction with vessel walls. Cyclomix processing changed the shape of particles whereas hybridizer did not. Hybridizer improved the flow of coated silica but the Cyclomix reduced the flowability attributed mainly to breaking of silica particles (fine particles have larger cohesive force). Turbula mixer did not improve flow. Processing silica with MgSt increased the hydrophobicity in all three machines. Interestingly after storage for a specific time under specific humidity conditions, the MgSt layer disappeared once again exposing the silica surface.

Lefebvre, Galet and Chamayou (2011) found out that surface coating of talc with silica helped in increasing the hydrophobicity of talc, coating also varied the dispersion rate of talc in water. One good way of checking the surface wettability is to drop small droplets on the surface and calculate it's angle of contact with the surface. If the drop maintains its shape, it means that the surface is hydrophobic, if the drop gets absorbed by the surface, it indicates hydrophilicity. Between the two extremes we can determine the effect of coating on hydrophobicity or hydrophilicity by calculating the angle of contact of the surface. Angle of contact lesser than 90º indicates hydrophilicity and greater than 90º hydrophobicity. Work of adhesion linked to the affinity of particles with water, decreased with an increase in silica concentration.

Sato *et al.* (2013) varied the operating conditions of the Cyclomix and its effect on coating and subsequent properties studied. Discrete element method simulation of Cyclomix to estimate factors like collision frequency, distribution of collision forces and average rotational distance was done to measure the coating efficiency. Coating performed at 500 rpm and 60 seconds covered the entire surface. Flow improves with increasing operating time at 500rpm. If the speed and the time duration are increased beyond a certain level flow again starts to decrease which can be attributed to the breakage or fragmentation of host particles due to high shear and impaction forces. Wettability of Suglet powder decreased when coated with MgSt. The increase in rotational speed improves the coating performance. The rotational speed of 500 rpm gave best improvement in flow and hydrophobicity. Increasing the rpm to near 1500 led to breakage of coating and exposure of host particle surface. The number of collisions per particle and the colliding force of particles increased with increasing rotational speed or rpm.

Devices like Hybridizer and Cyclomix improve the flowability of fine cohesive powders and also improve their properties for tablet manufacturing, their dissolvability and

hydrophobicity. From literature it can be seen that the effect of parameters greater than the optimum parameters can greatly reduce the enhancements in properties made by Cyclomix coating. Cyclomix is a very energy rich mechanism in which operating parameters are to be strictly controlled in order to achieve desired results. Increasing the operating parameters beyond optimum parameters does not cause such degradation in properties as seen in devices like FEM, Co-Mill, MAIC and Mechanofusion.

5.4.7 Random techniques

Pingali *et al.* (2009) blended three micronized API powders with additives and lubricants in a V-blender. After mixing with additives the flow of all three API's improved although to different levels. The addition of all three additives in the powder improved the flow the most. Adjusted flow index (flow index/dynamic density) showed similar curves for all three API's when plotted against impedance and dilation. Also flow index and dilation and flow index and impedance show a linear relation. The stand out feature of this study was to link flow index with impedance. More cohesive powders have a lower density leading to less frequent particle to particle contacts necessary for transferring charge due to which they have low conductivity or high impedance. High impedance powders are thought to have less conductivity or high capacitance which leads to electrostatic charge acquired which leads to poor flow. There is a need for clarification on the types of contacts, it is well established that cohesivity is reduced by minimizing particle contact. In poor packed powders although there are host-host particle contacts but due to a number of voids transmission of current is difficult making impedance high. In coated powders host-host particle interactions are suppressed by guest particles but due to better packing the voids are less and the contacts between coated particles are more and of continuous nature which leads to more charge transfer and lower impedance. For more cohesive powders the dilation increases as more mass of powder is required to overcome the stronger cohesive forces.

Huang, Zhang and Zhu (2010) used patented blending method for blending nanoparticles with the host particles. The powder blended with different nanoparticles showed improved flowability and fluidization, however to different degrees. The surface coverage area was different for different nanoparticles at same concentration. Increasing the concentration of nanoparticles above certain limit decreased flowability. To achieve the same level of improvement in flowability different wt./wt.% of different guest particles was required, this can be explained by the different physical properties of different nanoparticles due to which the change in surface coverage areas was observed. The technique of calculating the surface coverage was not discussed. Castellano's model was cited which states that if the guest nanoparticles cover more than 20% of the host particles, the contact between two host particles becomes nanoparticle to nanoparticle contact which reduces the curvature of host particle and increases the hardness which sum up to decrease inter particle forces. One major finding of this study was that the effect of multiple types of guest particles on the flow properties was not the simple summation of their individual effects.

5.5 Novel dry coating technique

A dry coating machine has been fabricated trying to use the same fundamentals as fluid energy mill and other turbulence generating dry coating machines.

The design of the machine includes two S.S. 304 hoppers. The hoppers have been joined with S.S. 304 pipe. Both hoppers are cylindrical and have conical outlets. The upper hopper is larger than the lower hopper to allow the upper hopper to store the conveyed powder. The lower hopper primarily acts as a connector to the conveying line. The upper and the lower hopper are joined by a 2 inch N.B. S.S. 304 pipe and have a flow valve between them to regulate the flow. The outlet of lower hopper is kept at 1 inch and is connected to the suction pipe by a 1 inch flow valve. The pipe used is 1 inch N.B. S.S. 304 pipe. The main conveying line is connected to the suction line by a 1 inch to 0.75 inch reducer. The main conveying line comprises of 0.75 inch N.B. S.S. 304 pipes. The single element of the conveying line consists of a section of 300mm pipe, then a pipe of 565mm at an angle of 45° to the 300mm pipe and then again a 300mm pipe connected parallel to the ground to the end of 565mm pipe. The connections are made by welding the pipes at the joints. The total section length comes to be 1165mm or 1.165m. 8 such identical sections have been made thus comprising a total length of 9.32m. Each section has T.C. clamp face welded at both ends of the 300mm pipe. T.C. clamps help in fast engagement and disengagement of the sections and also provides leak free joints. The sections of the conveying line are connected to each other by a vertical bend. The conveying line starts from the reducer at the suction line and ends at 0.75 inch to 1 inch reducer welded to 1 inch pipe connected to the upper hopper. The 0.75 inch pipe is chosen to increase the particle interactions with the wall as a larger diameter pipe would have been less successful in this as most of the particles would have stayed down on the pipe surface due to gravity and not strike the upper and the lower wall surface essential for dry coating. The upper hopper deposits the conveyed powder material by the help of 5μm bag filter fastened to it through a clamp. The bag filter helps in accumulating powder material in the upper hopper and lets the air pass through it.

The suction line uses normal pressure and kinetic energy conversions for generating the suction. The suction line has inside it a pipe of small diameter. As the cross sectional area of pipe reduces, its pressure decreases and the velocity increases. This exact concept is applied here. As the pipe inside the 1 inch suction line has lower diameter, suction is generated at the cross section where the lower hopper and suction line are joined. This helps in sucking the powder easily into the suction line. Once the powder is sucked in the suction line, the low diameter pipe ends and the pressure increases as the cross section area increases. This increase in pressure acts as the pressure responsible for conveying the powder in the loop and hence for dry coating.

The dry coating machine fabricated has no moving part and uses compressed air to convey the powder. The turbulence created with high pressure coupled with multiple bends helps in the following particle interactions, guest-guest, host-host, guest-host, guest-wall and host-wall. The collisions between guest-guest, host-host, guest-wall and host-wall are responsible

for breaking of agglomerates between guest-guest and host-host particles. The guest-host collisions are the main contributors towards adhesion of guest particles on the host particles and thus the host particles are coated with guest particles.

The machine has a possibility of working with the following three different loop lengths i.e.

(a) 8 Sections + Bend
(b) 4 Sections + Bend
(c) 0 Sections + Bend

Such an arrangement helps to change the distance the powder travels and the length can be optimized for various powders for optimum coating performance.

Two inputs, namely the input pressure at start of the conveying line and the total conveying time of the powder can be changed. The input pressure can directly influence the coating efficiency as it controls the turbulence of powder particles and their collisions and also high pressure often leads to particle attrition. The conveying time at a particular pressure can also influence the coating efficiency as optimum coating performance is often seen at an optimum time and if the time increases further, reduction in coating efficiency can be seen.

The powder mixture comprising the host and guest particles can be input into the upper hopper whilst the valve connecting the upper and lower hopper is closed. The upper hopper can be then fastened with a bag filter with the help of a hose clamp. After selecting suitable conveying length, the sections can be fastened with T.C. clamps to make the connections leak proof and to complete the loop.

The compressor is switched on together with the air dryer to prevent any moist air to enter the conveying line. The compressed air is then stored in an air receiver whose outlet is equipped with pressure regulator and non-return valve. The pressure to be used in the conveying line can be regulated through a pressure control valve (controls gauge pressure) and then passed through a non-return valve to prevent any back flow of powder into the air receiver. Now the valve connecting the upper and the lower hopper is opened and this is preceded by the opening of the valve connecting the lower hopper and the suction line. The powder is sucked into the suction line because of generation of suction pressure and then is conveyed in the conveying line. After completing its travel in the loop, the powder goes into the upper hopper after filtering action by the bag filter. As the valves are opened, the powder falls into the lower hopper due to gravity and again gets sucked into the suction line and thus again conveyed and so on. The conveying time can easily be controlled by removing the supply of compressed air. At the end of the conveying time the valve connecting the lower hopper and the conveying line can be closed to collect the powder. The suction line is detachable from the lower hopper through the help of T.C. clamp which enables easy discharge of dry coated powder once the valve is opened.

Drafts of dry coating machine (dimensions in mm, angles in degree)

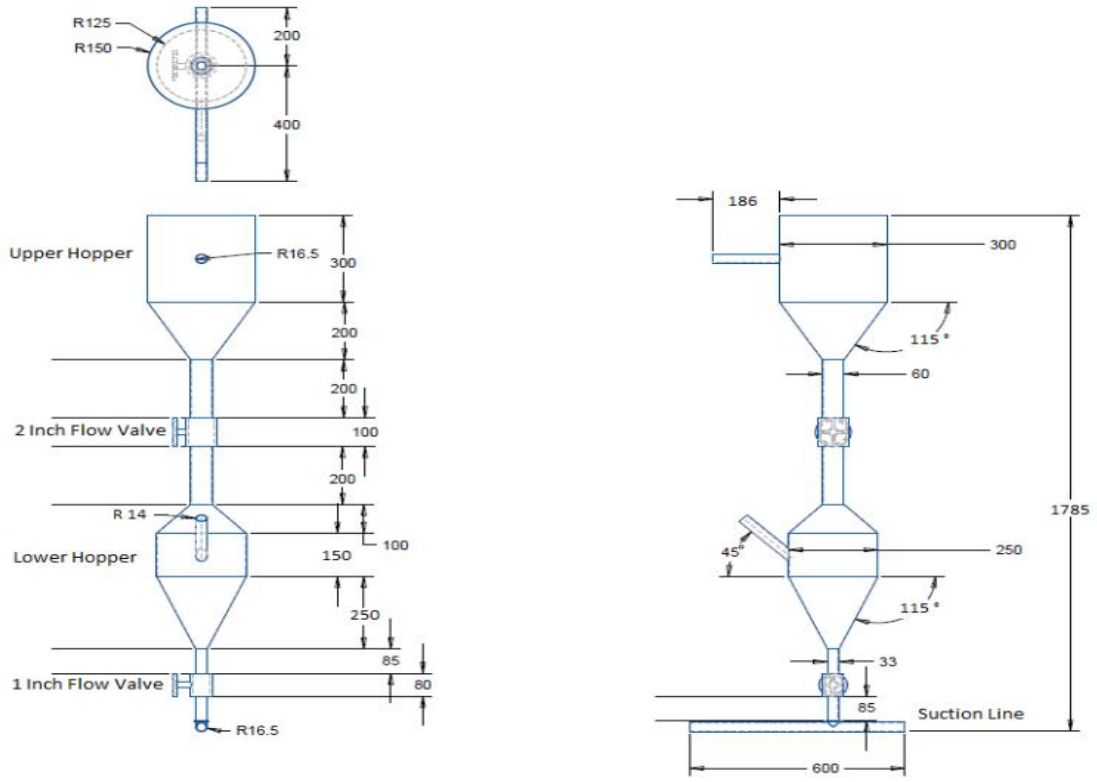

Figure 5.11. Draft of the dry coating machine without supports

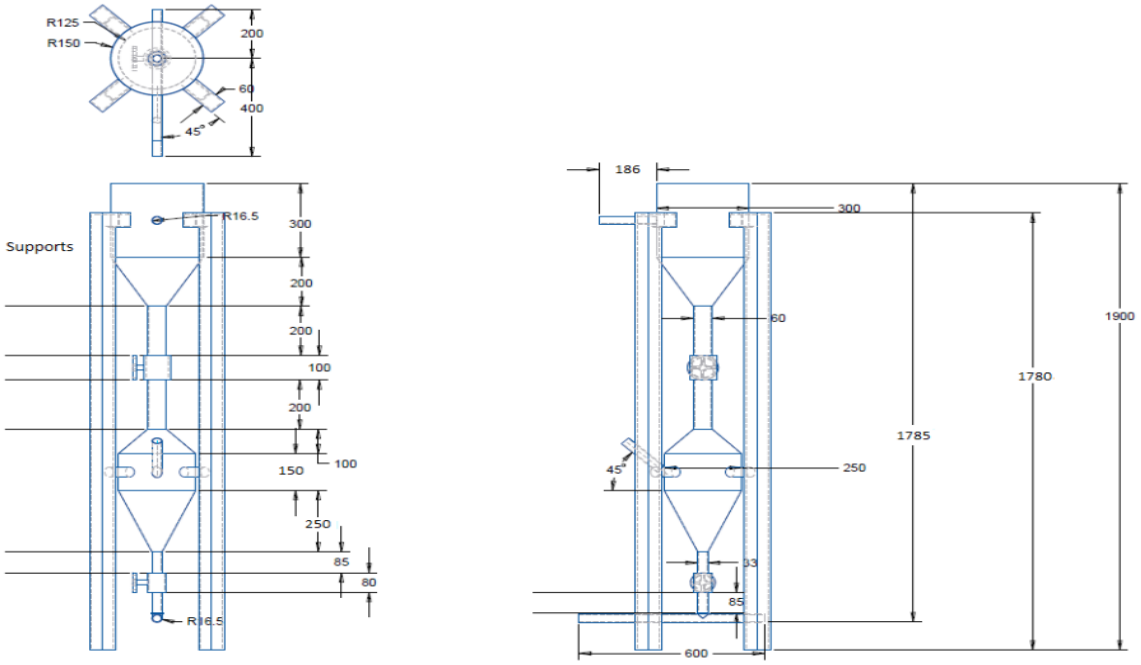

Figure 5.12. Draft of the dry coating machine with supports

(a) (b)

Figure 5.13. (a) Dry coating machine working with bend and bag filter attached to the upper hopper, (b) Connection from the air receiver to the suction line through yellow pipe

Figure 5.14. Pressure in pressure regulator set as 4 kg/cm^2 .

(a)

(b)

Figure 5.15. (a) Non return valve & pressure regulator, (b) Air receiver, (c) Air dryer (d) Compressor

(c)

(d)

5.6 Dry coating results with paracetamol

The following are the results of the samples which were dry coated. Paracetamol 20%SAC was chosen to be experimented and dry coated first as it had the best flowability improvement out of the 20,40,60 & 80% SAC samples. Firstly, the paracetamol sample was mixed with 0.49 wt.% Aerosil R972 pharma in a plastic container and then poured in the upper hopper of the dry coating machine. The mixing was done by rapidly shaking the container by hand for approximately 10 minutes.

Dry coating machine was operated at 3, 4 & 5 kg/cm^2 operating pressure (gauge pressure) and 10 & 20 minute of processing times. Samples processed for 10 minutes under a particular pressure were processed again for 10 minutes to create the 20 minute processing time sample. The 4 kg/cm^2 20 minute sample was processed again for 10 minutes to create a 30 minute processed sample. Further paracetamol 80%SAC samples were processed at 4 kg/cm^2 and 6 kg/cm^2 for 10 minutes each to see the impact of 80%SAC wt.% of nano silica.

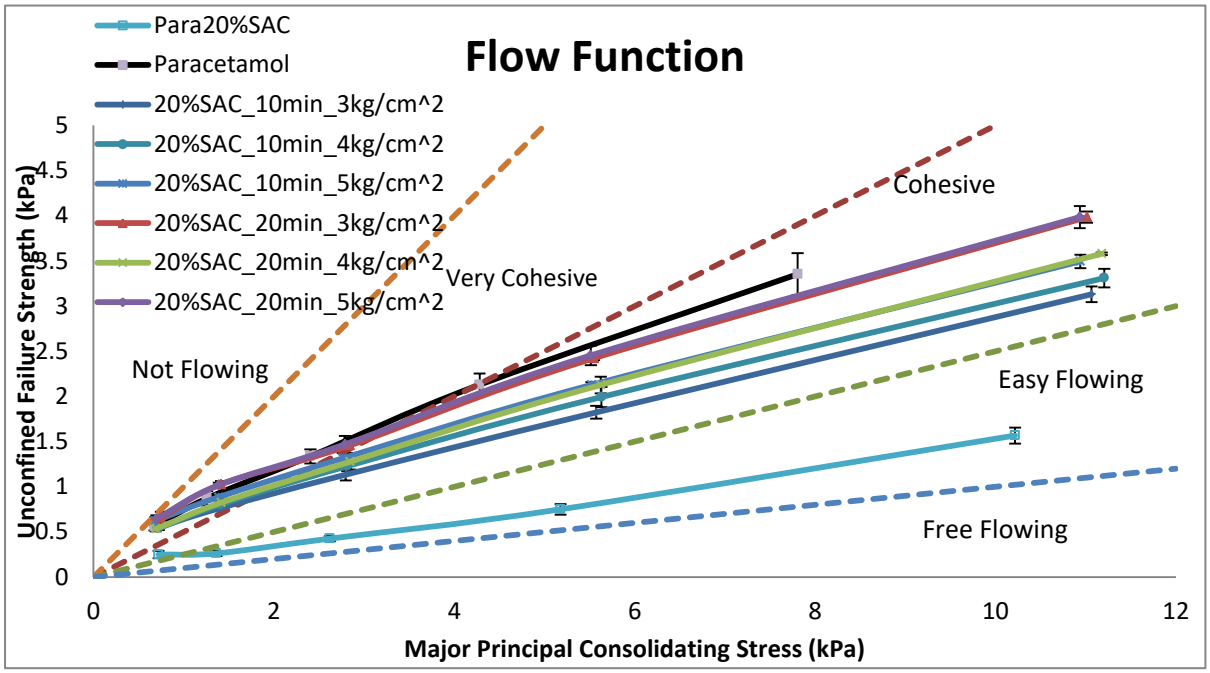

Figure 5.16. Flow function curve of paracetamol dry coated with 20%SAC (0.49 wt./wt.% Aerosil R972 Pharma) at different pressures and processing times

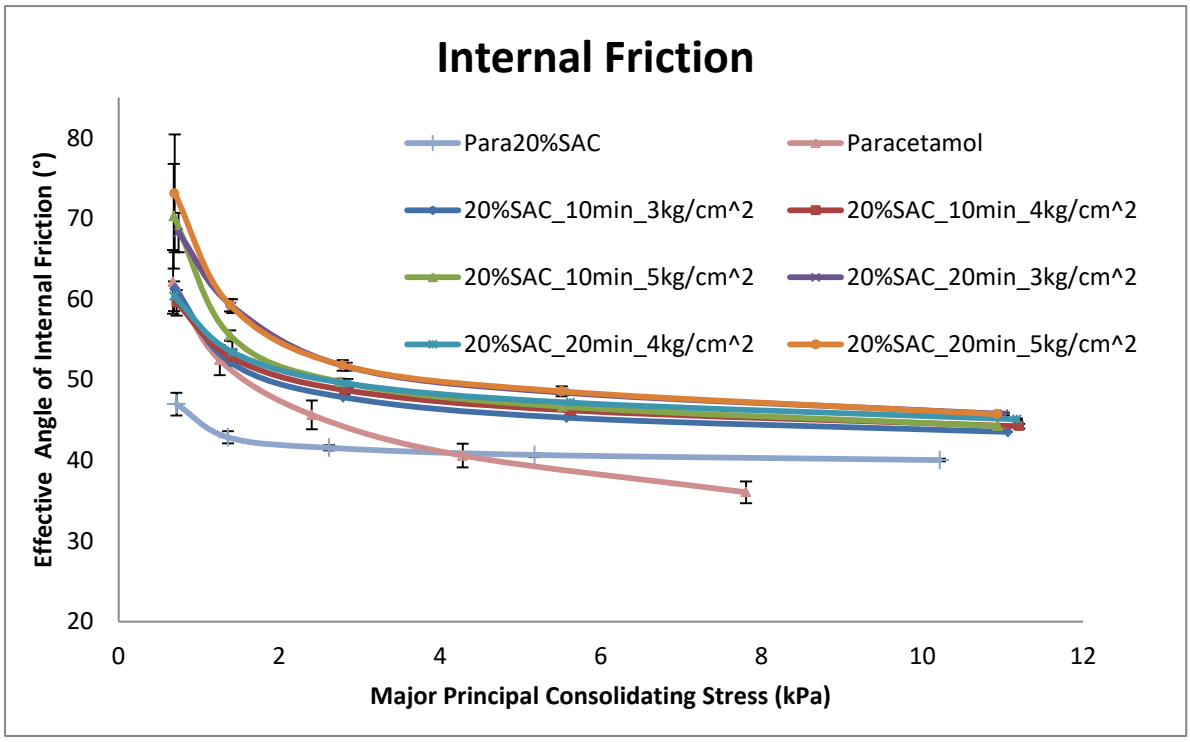

Figure 5.17. Internal friction curve of paracetamol dry coated with 20%SAC (0.49 wt./wt.% Aerosil R972 Pharma) at different pressures and processing times

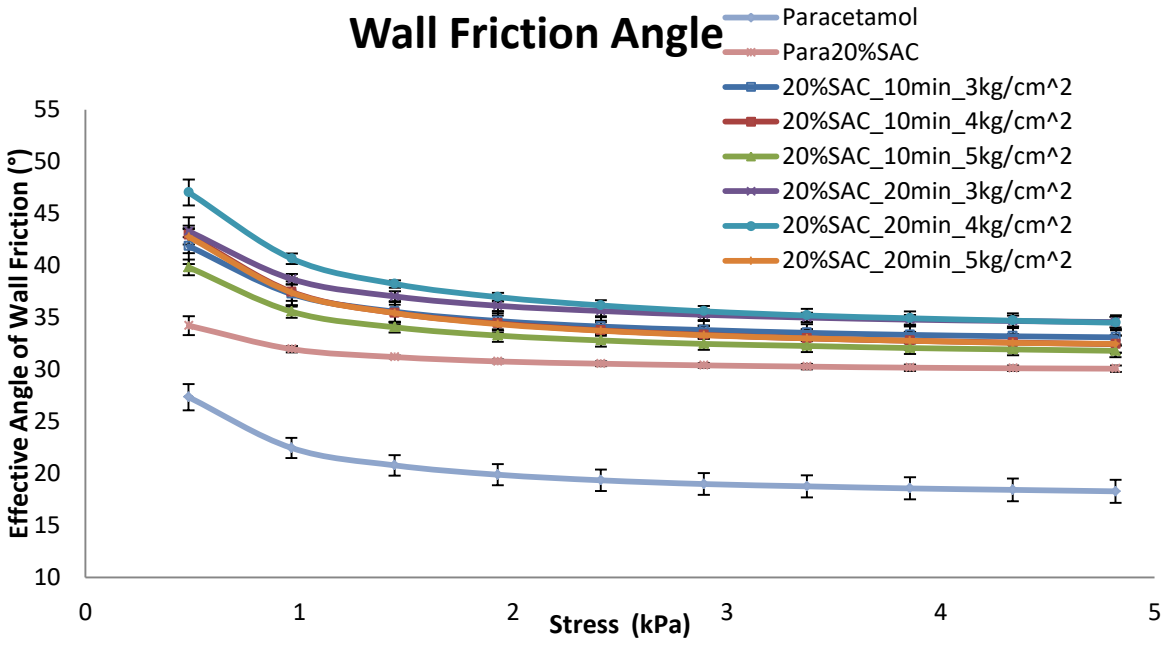

Figure 5.18. Wall friction curve of paracetamol dry coated with 20%SAC (0.49 wt./wt.% Aerosil R972 Pharma) at different pressures and processing times

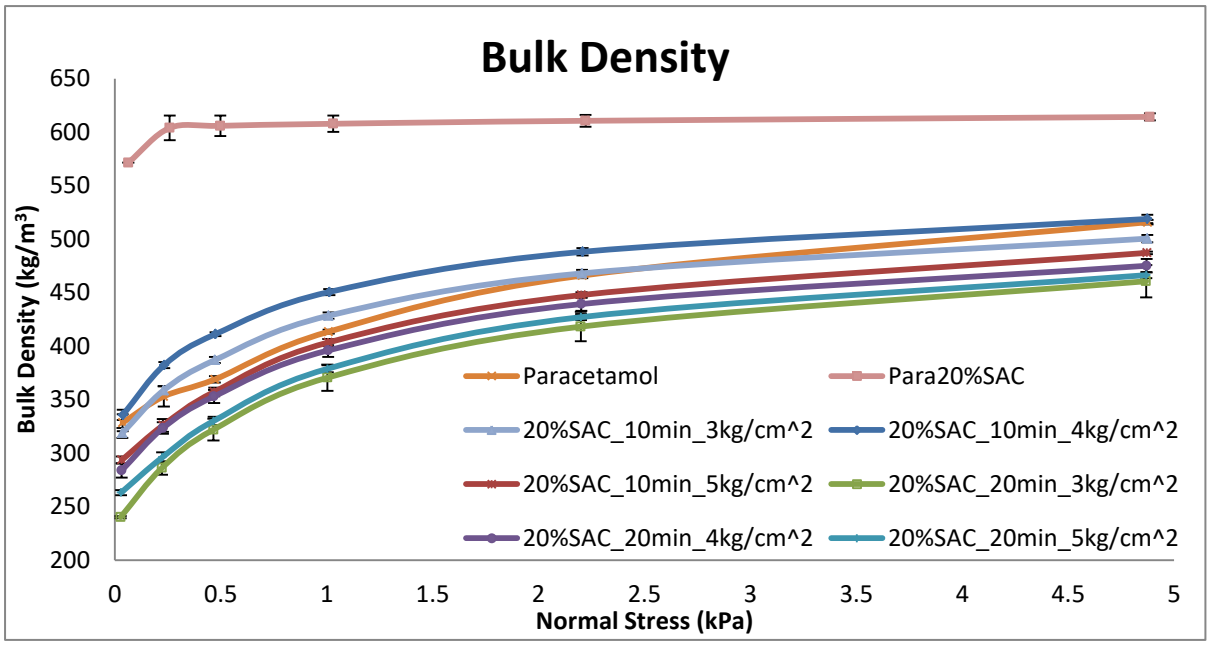

Figure 5.19. Bulk density curve of paracetamol dry coated with 20%SAC (0.49 wt./wt.% Aerosil R972 Pharma) at different pressures and processing times

5.6.1 Paracetamol dry coated with 20%SAC (0.49 wt./wt.% Aerosil R972 Pharma) at 3 kg/cm^2 pressure and 10 and 20 min processing times

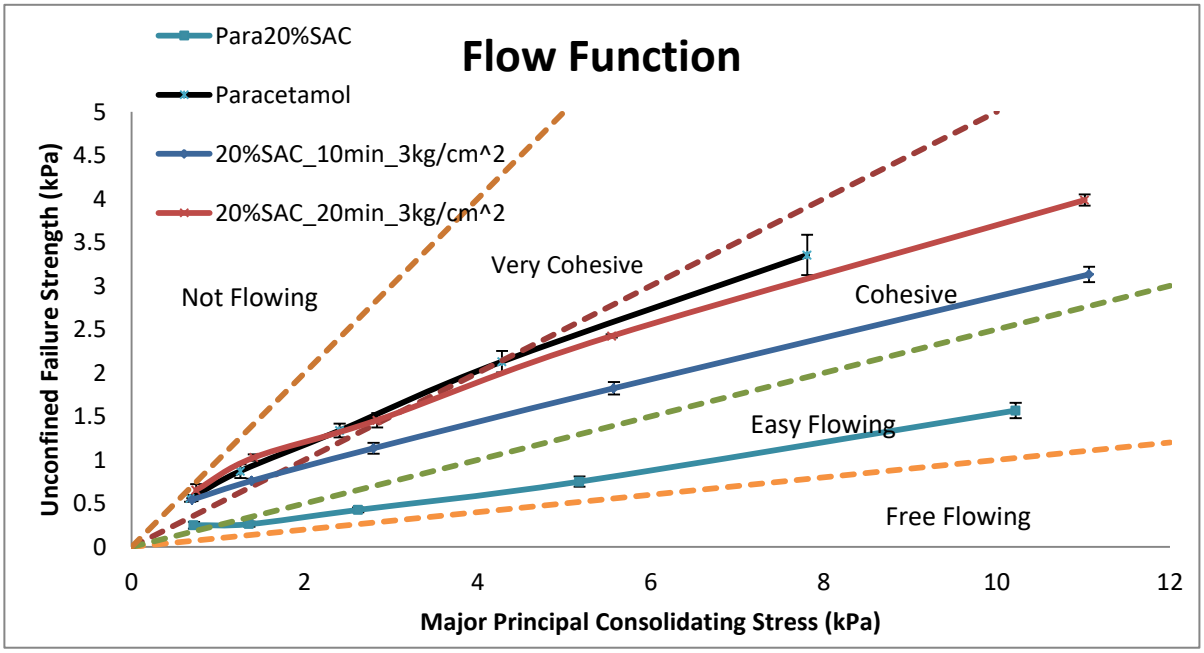

Figure 5.20. Flow function curve of paracetamol dry coated with 20%SAC (0.49 wt./wt.% Aerosil R972 Pharma) at 3 kg/cm^2 pressure and 10 and 20 min processing times

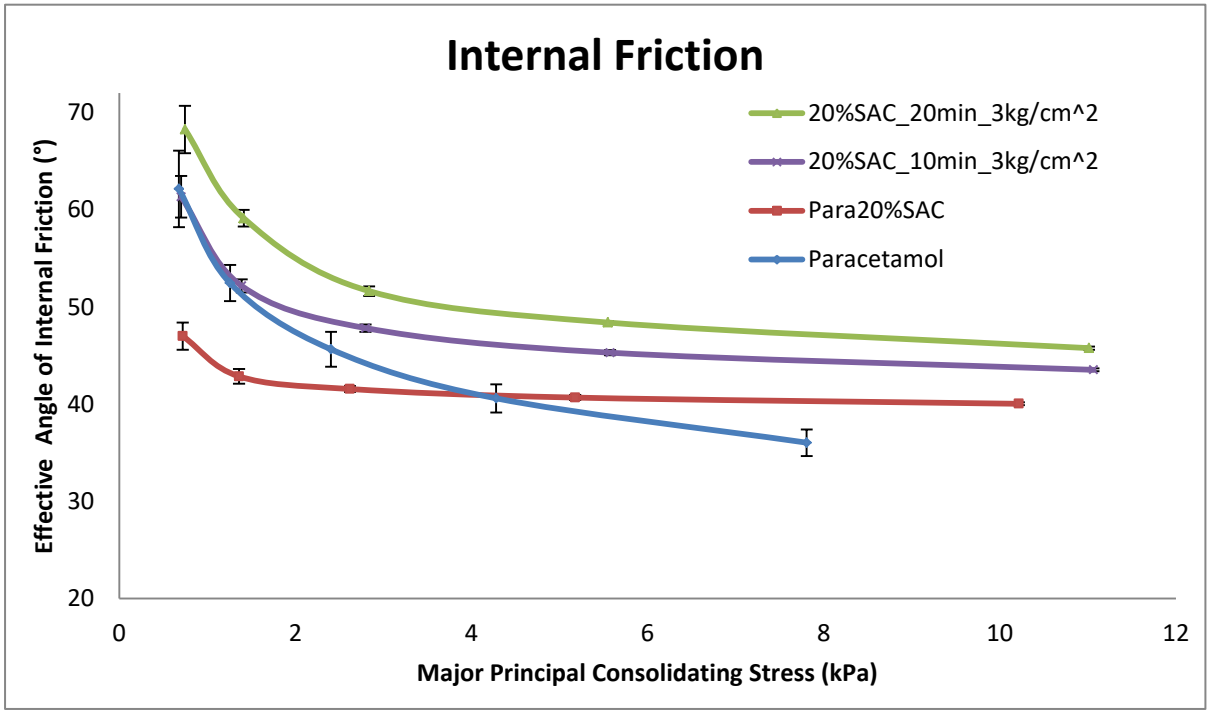

Figure 5.21. Internal friction curve of paracetamol dry coated with 20%SAC (0.49 wt./wt.% Aerosil R972 Pharma) at 3 kg/cm^2 pressure and 10 and 20 min processing times

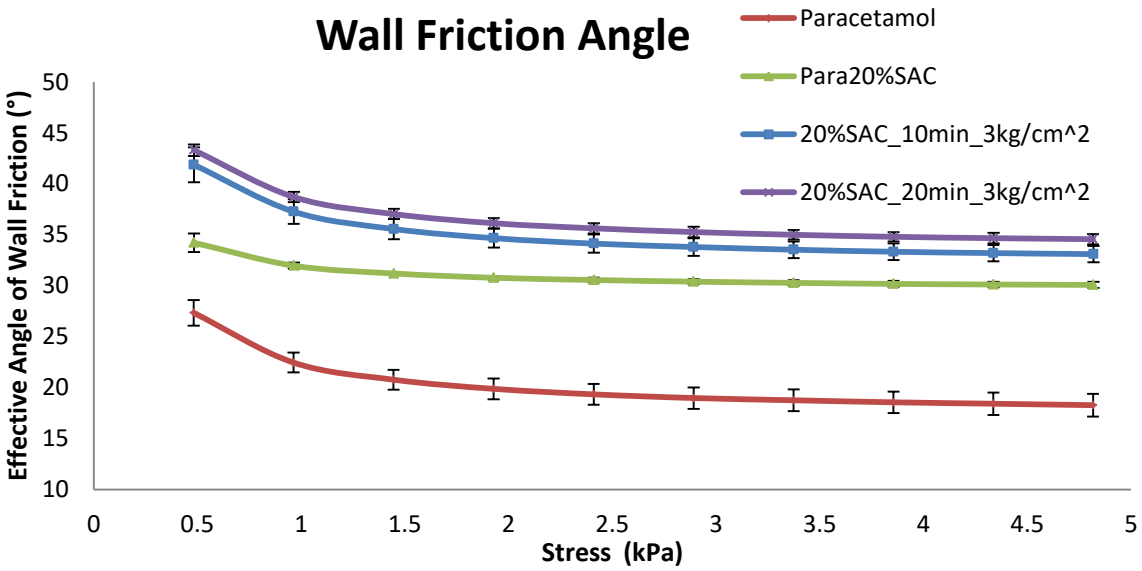

Figure 5.22. Wall friction curve of paracetamol dry coated with 20%SAC (0.49 wt./wt.%

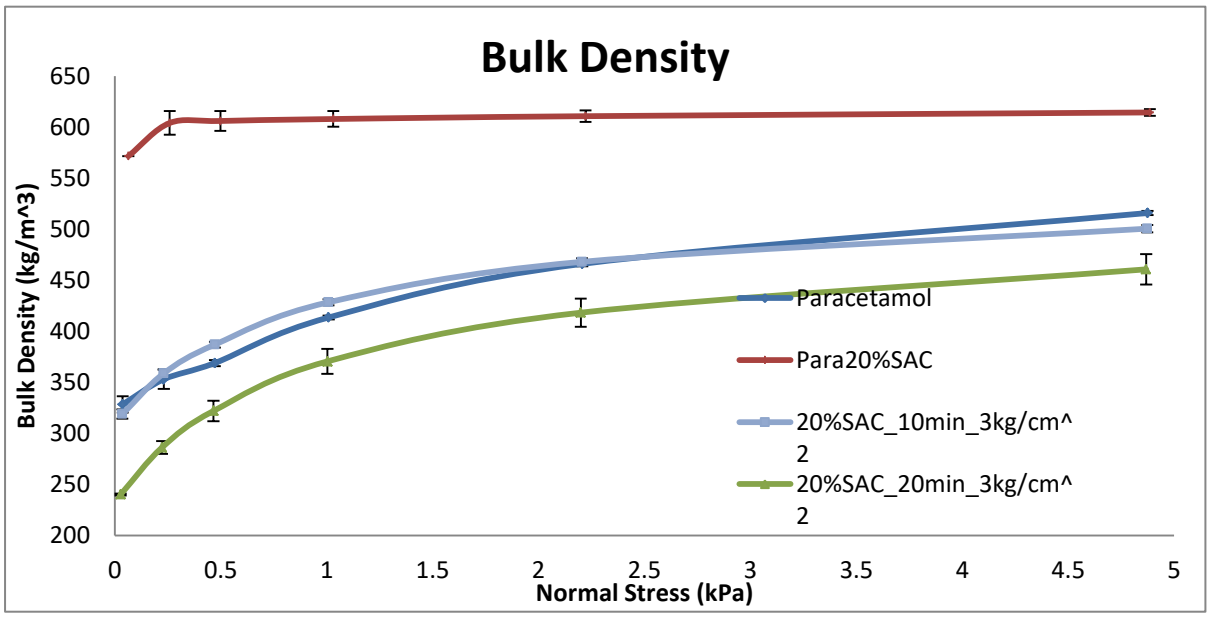

Figure 5.23. Bulk density curve of paracetamol dry coated with 20%SAC 0.49 wt./wt.% Aerosil R972 Pharma at 3 kg/cm^2 pressure and 10 and 20 min processing times

As seen in Figure 5.20, the flowability of 3 kg/cm^2 10 minute processed sample was better than the flowability of 20 minute processed sample. The flowability of the 20 min processed sample approached that of the pure paracetamol sample. The 10 minute processed sample had improved flowability but the flowability of 20%SAC hand blended sample is better. This can be attributed to the entrapment of silica particles in the dry coating machine in various corners and crevices and possibly to the particle attrition of paracetamol particles. With increase in processing time, flowability worsened indicating increased entrapment of particles and particle attrition.

Wall friction increased for the dry coated samples in comparison to the nano hand blended sample as seen in Figure 5.22. The wall friction angles for 20 minute processed sample were marginally higher than the 10 minute processed sample. Wall friction angles for paracetamol were lesser than the dry coated and hand blended samples.

Paracetamol nano hand blended sample had the greatest bulk density out of the four samples tested as seen in Figure 5.23. Bulk density of the 10 minute processed sample is similar to paracetamol and the 20 minute processed sample showed lesser bulk density than the two. Compressibility for the nano hand blended sample is poor but is comparable to paracetamol for the dry coated samples.

Flowability and bulk density results are well supported by the cohesion and effective angle of internal friction values tabulated in Table 5.1. Lower cohesion means greater flowability. It can be clearly seen that the cohesion values for the dry coated samples were greater than the hand blended sample but lesser than paracetamol, hence in agreement with the flowability results. Internal friction angle gives the friction between the powder particles, a greater variation in internal friction angle means greater compressibility of the powder sample. It is

because at increasing stresses the powder particles are compacted and their interlocks are broken which are the primary source of friction. This is the reason the internal friction angle reduces with increasing stress. As can be seen the range of internal friction angle of nano blended sample was the least indicating poor compressibility but improved flowability as the angle was lower than paracetamol indicating reduced friction between particles.

Table 5.1. Major principal consolidating stress, unconfined failure strength, effective angle of internal friction and cohesion values of paracetamol 20% SAC (0.49 wt./wt.% Aerosil R972 Pharma) dry coated samples at 3 kg/cm^2 operating pressure and 10 and 20 minutes processing time

	Flow function			
Material	Major principal consolidating stress (kPa)	Unconfined failure strength (kPa)	Effective angle of internal friction (°)	Cohesion (kPa)
Paracetamol	0.6774	0.5578	62.15	0.1586
	1.2578	0.8718	52.45	0.2656
	2.4045	1.3372	45.64	0.415
	4.2808	2.1294	40.6	0.6986
	7.8068	3.3534	36.04	1.1332
Paracetamol 20%SAC	0.7208	0.2498	47	0.057
	1.3608	0.2622	42.86	0.067
	2.6192	0.426	41.56	0.114
	5.1776	0.7504	40.68	0.194
	10.2168	1.5674	40.04	0.42
Paracetamol 20%SAC Dry coated 3 kg/cm^2 10min	0.7020	0.5437	61.33	0.1477
	1.3903	0.7603	52.17	0.1940
	2.7967	1.1340	47.83	0.2837
	5.5737	1.8237	45.30	0.4573
	11.0657	3.1310	43.53	0.7940
Paracetamol 20%SAC Dry coated 3 kg/cm^2 20min	0.7457	0.6533	68.27	0.1793
	1.4133	1.0273	59.13	0.2720
	2.8380	1.4570	51.63	0.3640
	5.5490	2.4233	48.40	0.6133
	11.0147	3.9853	45.77	1.0140

Table 5.2. Wall friction and bulk densities values of paracetamol 20% SAC (0.49 wt./wt.% Aerosil R972 Pharma) dry coated samples at 3 kg/cm^2 operating pressure and 10 and 20 minutes processing time

	Wall friction		Bulk density	
Material	Stress (kPa)	Effective angle of wall friction (°)	Stress (kPa)	Density (kg/m^3)
Paracetamol	0.482	27.34	0.0362	328.42

	0.963 1.4452 1.928 2.4102 2.892 3.374 3.8556 4.337 4.8172	22.46 20.78 19.88 19.34 18.98 18.76 18.56 18.42 18.28	0.2304 0.4716 1.0088 2.2062 4.8746	352.96 368.9 413.5 465.98 515.82
Paracetamol 20%SAC	0.483 0.965 1.447 1.929 2.4108 2.892 3.374 3.856 4.3378 4.819	34.22 31.96 31.2 30.78 30.56 30.4 30.28 30.18 30.12 30.08	0.063 0.2586 0.4974 1.0304 2.2218 4.8854	571.5 603.98 605.94 607.88 610.64 614.28
Paracetamol 20%SAC Dry coated 3 kg/cm^2 10min	0.4830 0.9643 1.4467 1.9290 2.4107 2.8920 3.3740 3.8560 4.3373 4.8193	41.87 37.27 35.57 34.67 34.13 33.80 33.53 33.33 33.20 33.10	0.0353 0.2297 0.4717 1.0083 2.2047 4.8733	318.87 358.63 386.97 428.40 468.00 500.5
Paracetamol 20%SAC Dry coated 3 kg/cm^2 20min	0.4830 0.9650 1.4470 1.9283 2.4107 2.8920 3.3740 3.8560 4.3377 4.8167	43.30 38.70 37.03 36.13 35.63 35.27 35.00 34.80 34.67 34.57	0.027 0.222 0.465 1.003 2.199 4.868	240.17 286.13 321.93 370.50 418.20 460.67

5.6.2 Paracetamol dry coated with 20%SAC (0.49 wt./wt.% Aerosil R972 Pharma) at 4 kg/cm^2 pressure and 10, 20 and 30 min processing times

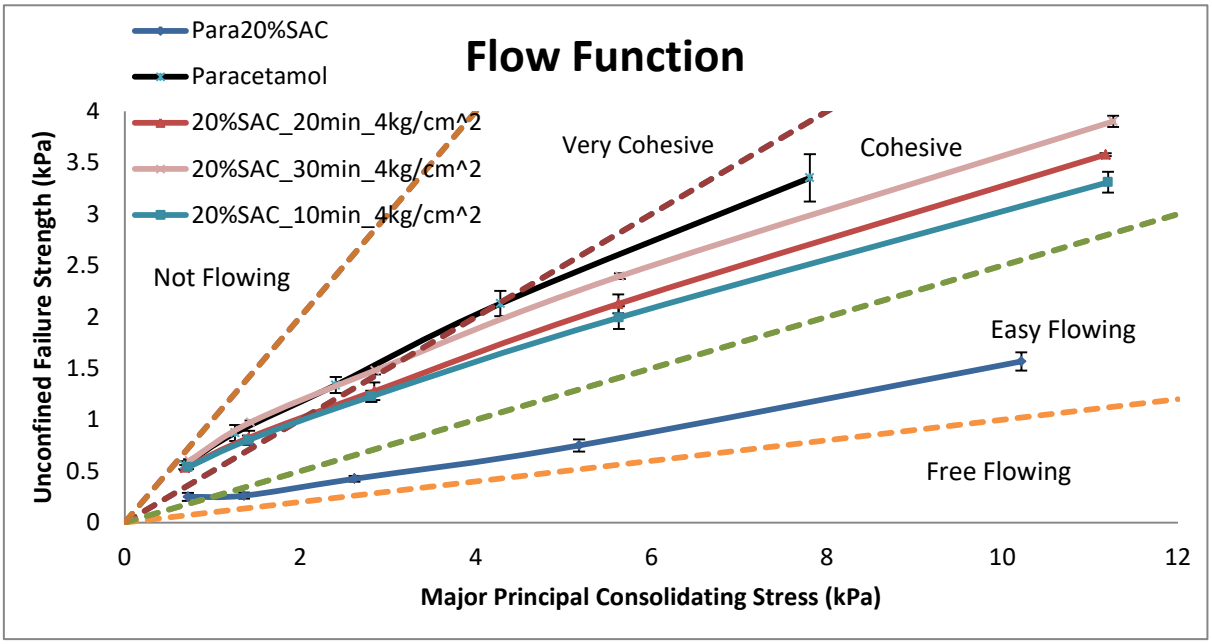

Figure 5.24. Flow function curve of paracetamol dry coated with 20%SAC (0.49 wt./wt.% Aerosil R972 Pharma) at 4 kg/cm^2 pressure and 10,20 and 30 min processing times

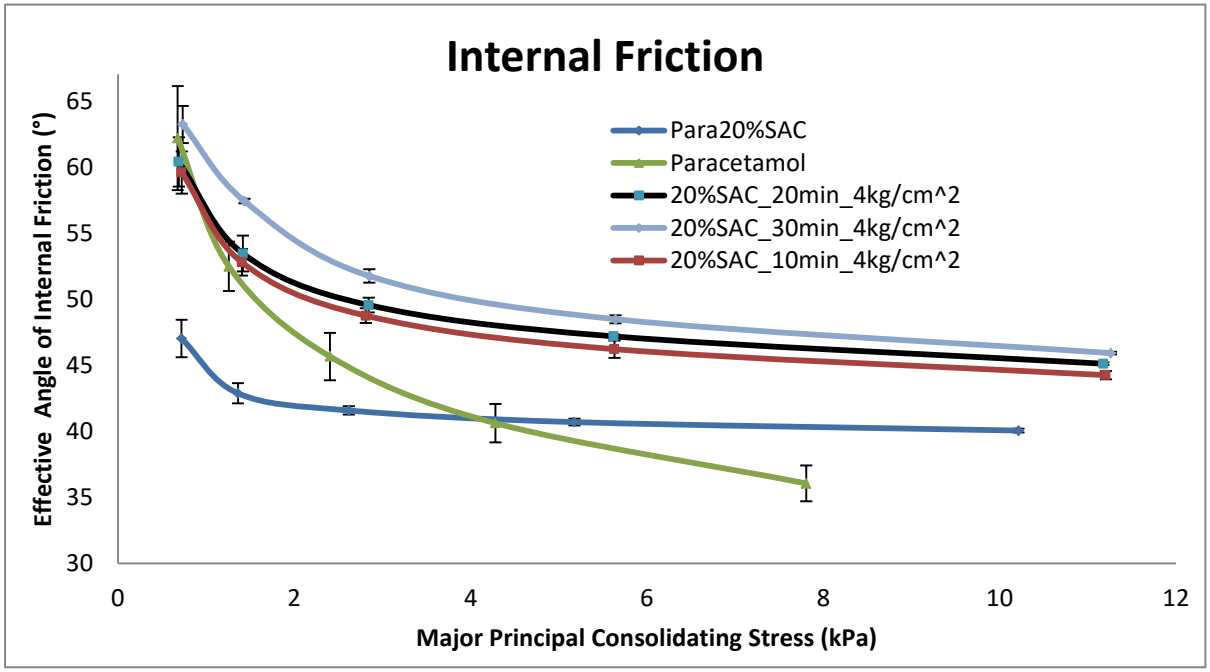

Figure 5.25. Internal friction curve of paracetamol dry coated with 20%SAC (0.49 wt./wt.% Aerosil R972 Pharma) at 4 kg/cm^2 pressure and 10,20 and 30 min processing times

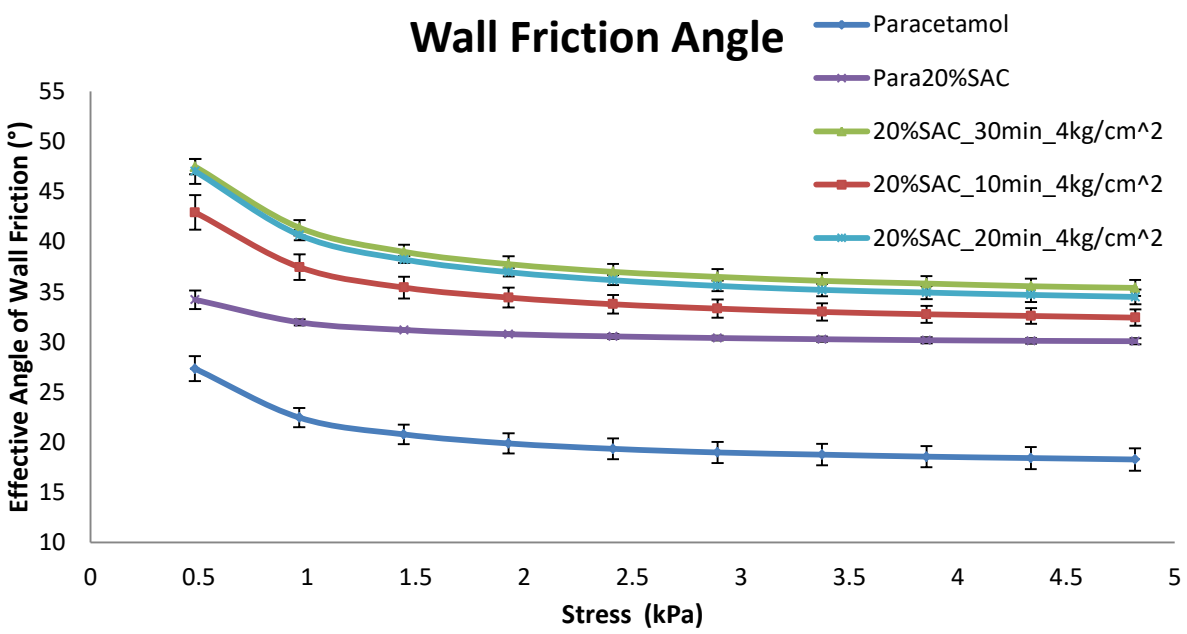

Figure 5.26. Wall friction curve of paracetamol dry coated with 20%SAC (0.49 wt./wt.% Aerosil R972 Pharma) at 4 kg/cm^2 pressure and 10,20 and 30 min processing times

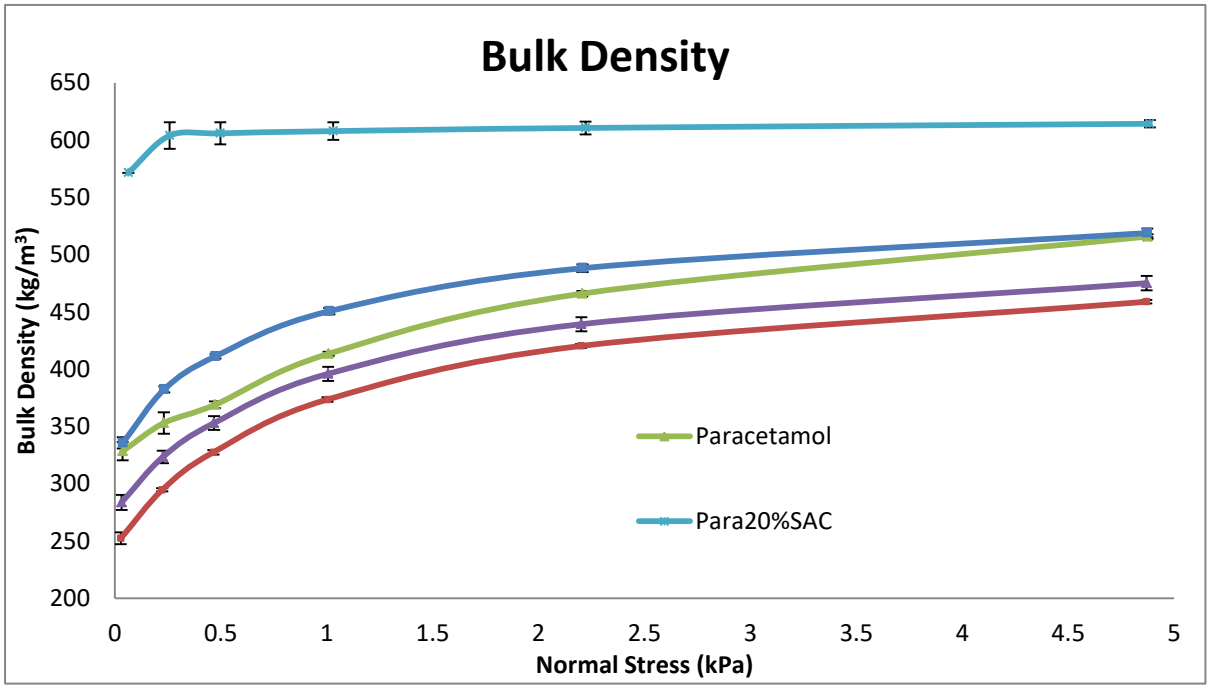

Figure 5.27. Bulk density curve of paracetamol dry coated with 20%SAC (0.49 wt./wt.% Aerosil R972 Pharma) at 4 kg/cm^2 pressure and 10,20 and 30 min processing times

As seen in Figure 5.24, the flowability of 4 kg/cm^2 10 minute processed sample was better than the flowability of 20 & 30 minute processed samples. The flowability of the 30 min processed sample was lesser than the 20 minute sample and approached that of the pure paracetamol sample. The 10 minute processed sample had improved flowability but the flowability of 20%SAC hand blended sample was better. This can be attributed to the entrapment of silica particles in the dry coating machine in various corners and crevices and possibly to the particle attrition of paracetamol particles. With increase in processing time, flowability worsened indicating increased entrapment of particles and particle attrition.

Wall friction increased for the dry coated samples in comparison to the nano hand blended sample as seen in Figure 5.26. The wall friction angles for 20 min and 30 min processed samples were almost equal and marginally higher than the 10 min processed sample. Wall friction angles for paracetamol were lesser than the dry coated and hand blended samples.

Paracetamol nano hand blended sample had the greatest bulk density out of the four samples tested as seen in Figure 5.27. Bulk density of the 10 minute processed sample was similar to paracetamol and the 20 minute and 30 minute processed samples showed lesser bulk density than the two. Compressibility for the nano hand blended sample was poor but was comparable to paracetamol for the dry coated samples. Compressibility of the dry coated samples was similar to paracetamol sample.

Flowability and bulk density results are well supported by the cohesion and effective angle of internal friction values tabulated in Table 5.3. Lower cohesion means greater flowability. It can be clearly seen that the cohesion values for the dry coated samples were greater than the hand blended sample but lesser than paracetamol, hence in agreement with the flowability results. The cohesion values of the 10 minute sample was greater than the 20 and 30 minute processed samples and again in tune to the flowability results. Internal friction angle gives the friction between the powder particles, a greater variation in internal friction angle means greater compressibility of the powder sample. It is because at increasing stresses the powder particles are compacted and their interlocks are broken which are the primary source of friction. This is the reason the internal friction angle reduces with increasing stress. As can be seen the range of internal friction angle of nano blended sample was the least indicating poor compressibility but improved flowability as the angle was lower than paracetamol indicating reduced friction between particles. The internal friction angles of the 3 dry coated samples were almost similar.

Table 5.3. Major principal consolidating stress, unconfined failure strength, effective angle of internal friction and cohesion values of paracetamol 20% SAC (0.49 wt./wt.% Aerosil R972 Pharma) dry coated samples at 4 kg/cm^2 operating pressure and 10, 20 and 30 minutes processing time

	Flow function			
Material	Major principal consolidating stress (kPa)	Unconfined failure strength (kPa)	Effective angle of internal friction (°)	Cohesion (kPa)
Paracetamol	0.6774	0.5578	62.15	0.1586
	1.2578	0.8718	52.45	0.2656
	2.4045	1.3372	45.64	0.415
	4.2808	2.1294	40.6	0.6986
	7.8068	3.3534	36.04	1.1332
Paracetamol 20%SAC	0.7208	0.2498	47	0.057
	1.3608	0.2622	42.86	0.067
	2.6192	0.426	41.56	0.114
	5.1776	0.7504	40.68	0.194
	10.2168	1.5674	40.04	0.42
Paracetamol 20%SAC Dry coated 4 kg/cm^2 10min	0.7227	0.5390	59.57	0.1460
	1.4060	0.8017	52.77	0.2063
	2.8110	1.2273	48.73	0.3080
	5.6313	1.9937	46.20	0.4983
	11.2057	3.3107	44.23	0.8323
Paracetamol 20%SAC Dry coated 4 kg/cm^2 20min	0.6893	0.533	60.37	0.1490
	1.4167	0.825	53.43	0.2127
	2.8443	1.277	49.53	0.3177
	5.6243	2.1273	47.17	0.5293
	11.1783	3.58	45.10	0.8970
Paracetamol 20%SAC Dry coated 4 kg/cm^2 30min	0.7353	0.6023	63.20	0.1690
	1.4347	0.9757	57.40	0.2523
	2.8513	1.4793	51.73	0.3703
	5.6430	2.3967	48.47	0.5990
	11.2633	3.9027	45.90	0.9773

Table 5.4. Wall friction and bulk densities values of paracetamol 20% SAC (0.49 wt./wt.% Aerosil R972 Pharma) dry coated samples at 4 kg/cm^2 operating pressure and 10, 20 and 30 minutes processing time

	Wall friction		Bulk density	
Material	Stress (kPa)	Effective angle of wall friction (°)	Stress (kPa)	Density (kg/m^3)
Paracetamol	0.482	27.34	0.0362	328.42
	0.963	22.46	0.2304	352.96
	1.4452	20.78	0.4716	368.9
	1.928	19.88	1.0088	413.5

	2.4102 2.892 3.374 3.8556 4.337 4.8172	19.34 18.98 18.76 18.56 18.42 18.28	2.2062 4.8746	465.98 515.82
Paracetamol 20%SAC	0.483 0.965 1.447 1.929 2.4108 2.892 3.374 3.856 4.3378 4.819	34.22 31.96 31.2 30.78 30.56 30.4 30.28 30.18 30.12 30.08	0.063 0.2586 0.4974 1.0304 2.2218 4.8854	571.5 603.98 605.94 607.88 610.64 614.28
Paracetamol 20%SAC Dry coated 4 kg/cm^2 10min	0.483 0.9647 1.4463 1.9287 2.4107 2.892 3.374 3.856 4.338 4.819	42.93 37.47 35.43 34.43 33.77 33.33 33.00 32.77 32.60 32.43	0.0373 0.2327 0.4743 1.0120 2.2073 4.8737	335.67 382.33 411.23 450.63 488.17 518.90
Paracetamol 20%SAC Dry coated 4 kg/cm^2 20min	0.4830 0.9650 1.4470 1.9290 2.4100 2.8920 3.3740 3.8560 4.3373 4.8193	47.03 40.67 38.23 36.97 36.17 35.60 35.20 34.93 34.70 34.50	0.0317 0.2263 0.4677 1.0063 2.2017 4.8703	283.73 323.37 352.97 395.97 439.30 475.13
Paracetamol 20%SAC Dry coated 4 kg/cm^2 30min	0.4830 0.9643 1.4463 1.9283 2.4103 2.8920 3.3740 3.8557 4.3377 4.8180	47.50 41.40 39.00 37.77 37.00 36.50 36.10 35.83 35.57 35.40	0.0277 0.2230 0.4647 1.0033 2.1997 4.8687	252.33 294.60 327.43 373.53 420.27 458.87

5.6.3 Paracetamol dry coated with 20%SAC (0.49 wt./wt.% Aerosil R972 Pharma) at 5 kg/cm^2 pressure and 10 and 20 min processing times

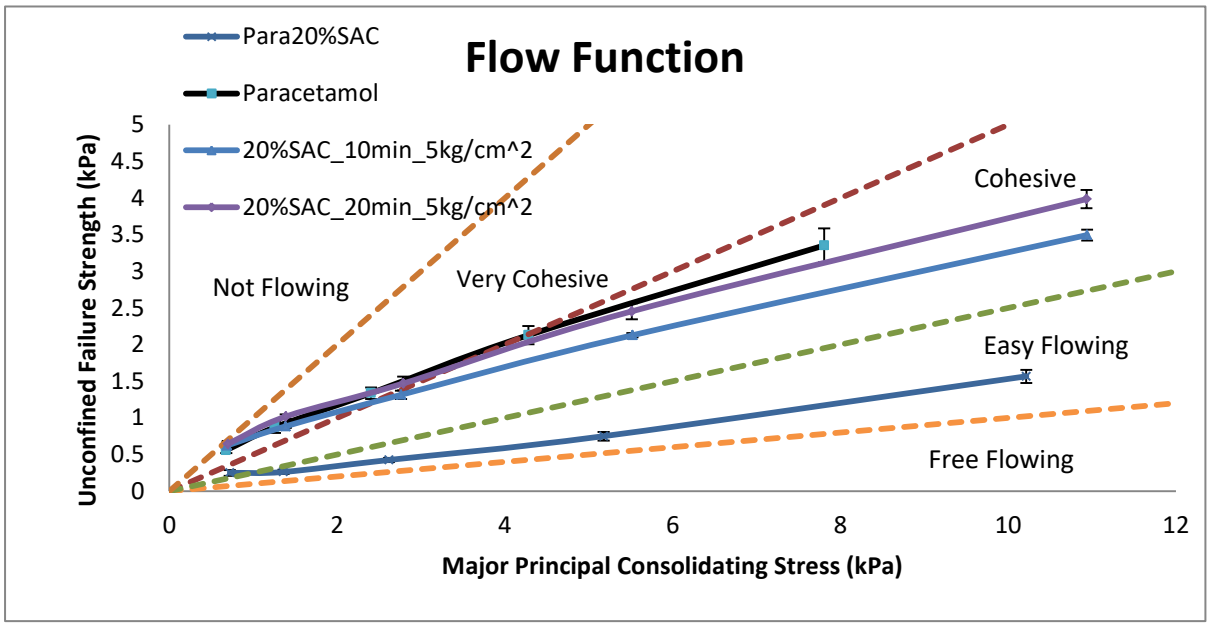

Figure5.28. Flow function curve of paracetamol dry coated with 20%SAC (0.49 wt./wt.% Aerosil R972 Pharma) at 5 kg/cm^2 pressure and 10 and 20 min processing times

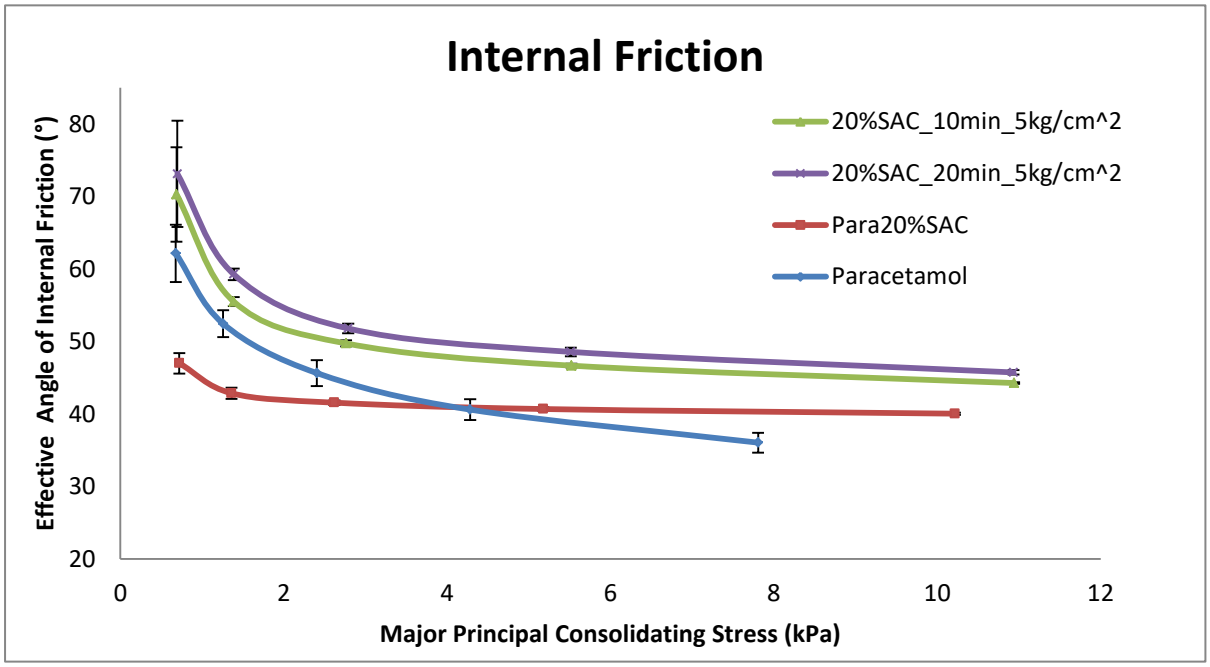

Figure 5.29. Internal friction curve of paracetamol dry coated with 20%SAC (0.49 wt./wt.% Aerosil R972 Pharma) at 5 kg/cm^2 pressure and 10 and 20 min processing times

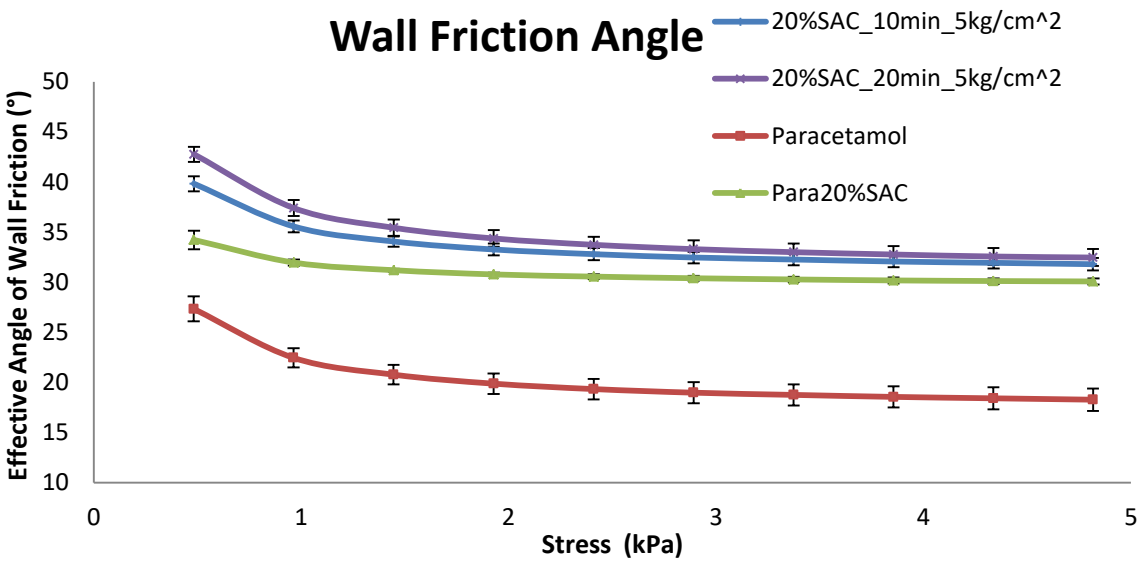

Figure 5.30. Wall friction curve of paracetamol dry coated with 20%SAC (0.49 wt./wt.% Aerosil R972 Pharma) at 5 kg/cm^2 pressure and 10 and 20 min processing times

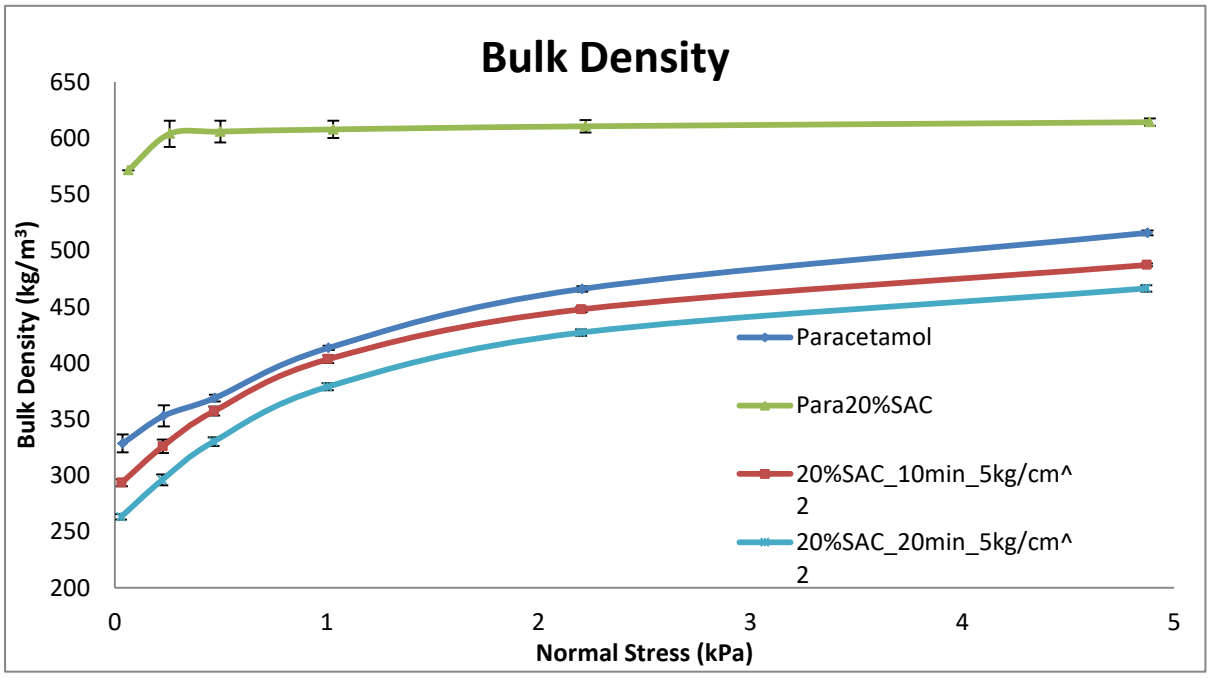

Figure 5.31. Bulk density curve of paracetamol dry coated with 20%SAC (0.49 wt./wt.% Aerosil R972 Pharma) at 5 kg/cm^2 pressure and 10 and 20 min processing times

As seen in Figure 5.28 the flowability of 5 kg/cm^2 10 minute processed sample was better than the flowability of 20 minute processed sample. The flowability of the 20 min processed sample approached that of the pure paracetamol sample. The 10 minute processed sample had improved flowability but the flowability of 20%SAC hand blended sample was better. This can be attributed to the entrapment of silica particles in the dry coating machine in various

corners and crevices and possibly to the particle attrition of paracetamol particles. With increase in processing time flowability worsened indicating increased entrapment of particles and particle attrition.

Wall friction increased for the dry coated samples in comparison to the nano hand blended sample as seen in Figure 5.30. The wall friction angles for 20 min processed sample were marginally higher than the 10 min processed sample. Wall friction angles for paracetamol were lesser than the dry coated and hand blended samples.

Paracetamol nano hand blended sample had the greatest bulk density out of the four samples tested as seen in Figure 5.31. Bulk density of the 10 minute processed sample was lesser than paracetamol and the 20 minute processed sample showed lesser bulk density than the two. Compressibility for the nano hand blended sample was poor but was comparable to paracetamol for the dry coated samples.

Flowability and bulk density results are well supported by the cohesion and effective angle of internal friction values tabulated in Table 5.5. Lower cohesion means greater flowability. It can be clearly seen that the cohesion values for the dry coated samples were greater than the hand blended sample but lesser than paracetamol, hence in agreement with the flowability results. Internal friction angle gives the friction between the powder particles, a greater variation in internal friction angle means greater compressibility of the powder sample. It is because at increasing stresses, the powder particles are compacted and their interlocks are broken which are the primary source of friction. This is the reason the internal friction angle reduces with increasing stress. As can be seen the range of internal friction angle of nano blended sample was the least indicating poor compressibility but improved flowability as the angle was lower than paracetamol indicating reduced friction between particles.

If we compare the different operating pressures and processing times, best improvement in flowability was seen in the 3 kg/cm^2 and 4 kg/cm^2 operating pressure and 10 minute processing time each. Increasing the pressure and processing time reduced the flowability. Bulk density for 3 kg/cm^2 and 4 kg/cm^2 processed for 10 minutes each was almost similar to paracetamol and all other samples showed improved compressibility but a little reduction in bulk density. Wall friction and internal friction angle variation among the various dry coated samples was not much.

Table 5.5 Major principal consolidating stress, unconfined failure strength, effective angle of internal friction and cohesion values of paracetamol 20% SAC (0.49 wt./wt.% Aerosil R972 Pharma) dry coated samples at 5 kg/cm^2 operating pressure and 10 and 20 minutes processing time.

	Flow function			
Material	Major principal consolidating stress (kPa)	Unconfined failure strength (kPa)	Effective angle of internal friction (°)	Cohesion (kPa)
Paracetamol	0.6774	0.5578	62.15	0.1586
	1.2578	0.8718	52.45	0.2656
	2.4045	1.3372	45.64	0.415
	4.2808	2.1294	40.6	0.6986
	7.8068	3.3534	36.04	1.1332
Paracetamol 20%SAC	0.7208	0.2498	47	0.057
	1.3608	0.2622	42.86	0.067
	2.6192	0.426	41.56	0.114
	5.1776	0.7504	40.68	0.194
	10.2168	1.5674	40.04	0.42
Paracetamol 20%SAC Dry coated 5 kg/cm^2 10min	0.6867	0.6220	70.30	0.1807
	1.3877	0.8857	55.50	0.2297
	2.7623	1.3147	49.73	0.3337
	5.5213	2.1280	46.67	0.5397
	10.9410	3.4953	44.27	0.8930
Paracetamol 20%SAC Dry coated 5 kg/cm^2 20min	0.6973	0.6447	73.13	0.1887
	1.3880	1.0180	59.27	0.2710
	2.7887	1.4700	51.80	0.3700
	5.5133	2.4543	48.57	0.6233
	10.9350	3.9860	45.73	1.0167

Table 5.6. Wall friction and bulk densities values of paracetamol 20% SAC (0.49 wt./wt.% Aerosil R972 Pharma) dry coated samples at 5 kg/cm^2 operating pressure and 10 and 20 minutes processing time

	Wall friction		Bulk density	
Material	Stress (kPa)	Effective angle of wall Friction (°)	Stress (kPa)	Density (kg/m^3)
Paracetamol	0.482	27.34	0.0362	328.42
	0.963	22.46	0.2304	352.96
	1.4452	20.78	0.4716	368.9
	1.928	19.88	1.0088	413.5
	2.4102	19.34	2.2062	465.98
	2.892	18.98	4.8746	515.82
	3.374	18.76		
	3.8556	18.56		
	4.337	18.42		

	4.8172	18.28		
Paracetamol 20%SAC	0.483 0.965 1.447 1.929 2.4108 2.892 3.374 3.856 4.3378 4.819	34.22 31.96 31.2 30.78 30.56 30.4 30.28 30.18 30.12 30.08	0.063 0.2586 0.4974 1.0304 2.2218 4.8854	571.5 603.98 605.94 607.88 610.64 614.28
Paracetamol 20%SAC Dry coated 5 kg/cm^2 10min	0.4827 0.9640 1.4457 1.9283 2.4107 2.8920 3.3740 3.8560 4.3377 4.8170	39.83 35.57 34.07 33.27 32.80 32.47 32.27 32.07 31.93 31.80	0.0327 0.2263 0.4687 1.0067 2.2023 4.8713	293.57 325.87 357.20 403.40 447.77 487.20
Paracetamol 20%SAC Dry coated 5 kg/cm^2 20min	0.4830 0.9643 1.4463 1.9283 2.4107 2.8920 3.3740 3.8557 4.3373 4.8173	42.77 37.40 35.43 34.37 33.73 33.30 33.00 32.77 32.57 32.47	0.0290 0.2233 0.4660 1.0040 2.2000 4.8690	263.07 295.97 330.03 378.83 427.10 466.37

5.6.4 Paracetamol dry coated with 80%SAC (1.98 wt./wt.% Aerosil R972 Pharma) at 4 kg/cm^2 and 6 kg/cm^2 pressure and 10 min processing time

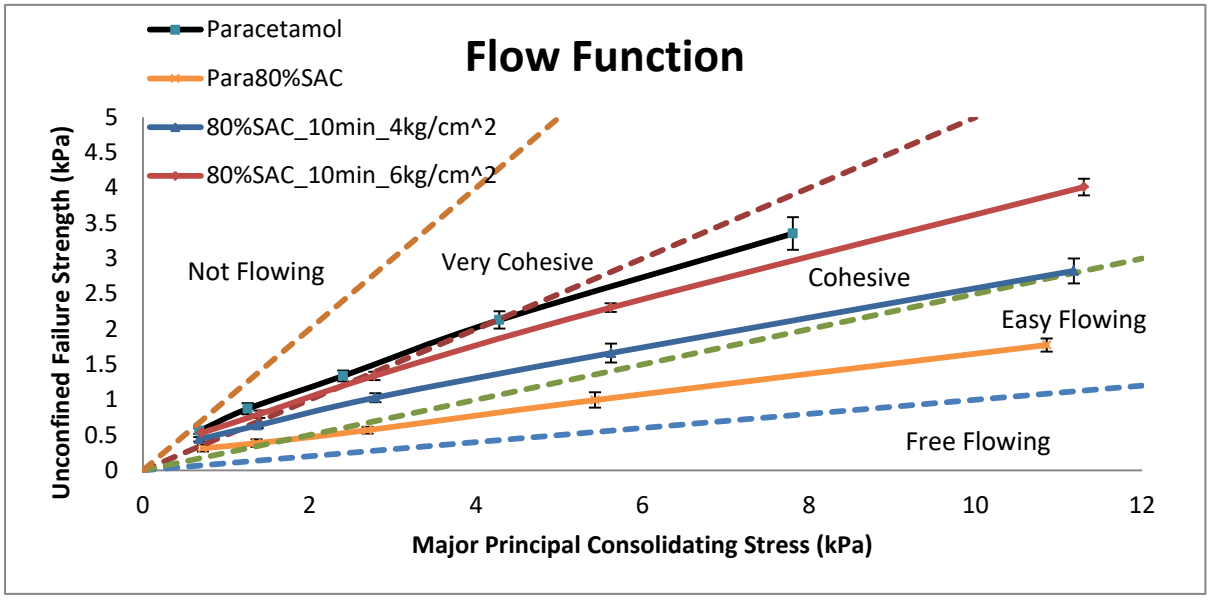

Figure 5.32. Flow function curve of paracetamol dry coated with 80%SAC (1.98 wt./wt%. Aerosil R972 Pharma) at 4 kg/cm^2 and 6 kg/cm^2 pressure and 10 min processing time

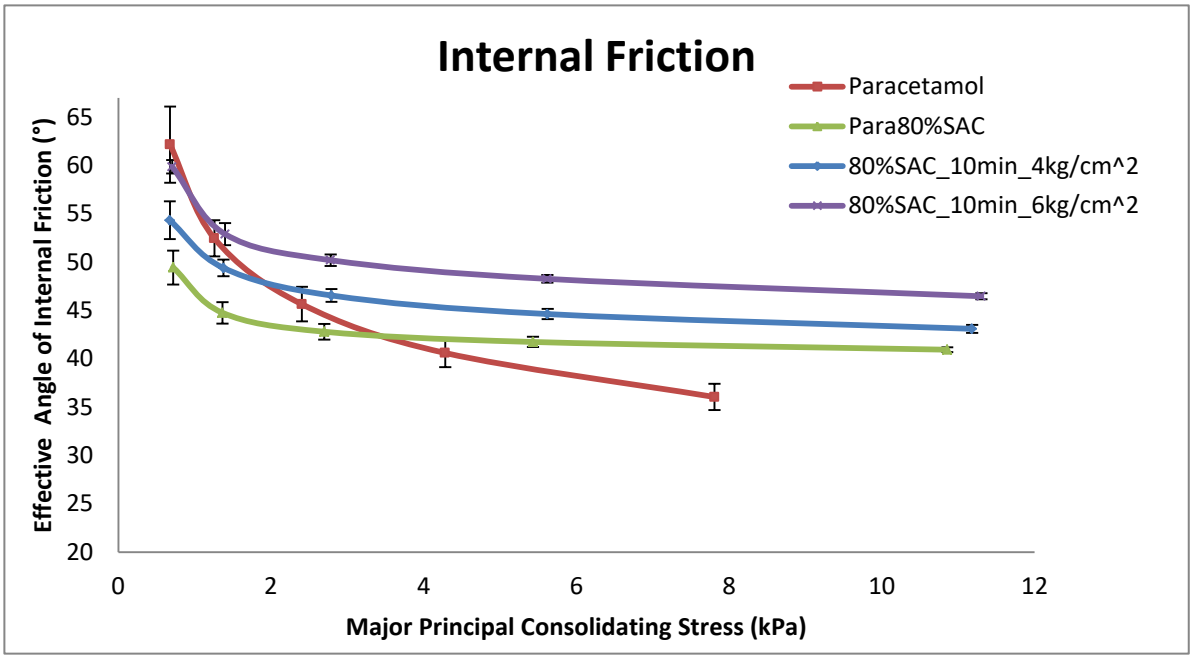

Figure 5.33. Internal friction curve of paracetamol dry coated with 80%SAC (1.98 wt./wt%. Aerosil R972 Pharma) at 4 kg/cm^2 and 6 kg/cm^2 pressure and 10 min processing time

As seen in Figure 5.32 the flowability of 4 kg/cm^2 10 minute processed sample was better than the flowability of 6 kg/cm^2 10 minute processed sample. The flowability of the 6 kg/cm^2 10 minute processed sample approached that of the pure paracetamol sample. The 4 kg/cm^2 minute processed sample had improved flowability but the flowability of 80%SAC hand blended sample was slightly better. The worsening of the flowability with increased

processing pressure can be attributed to possible particle attrition as at high pressure, the particles strike the wall surface with higher energy and usually attrition occurs.

Flowability results are well supported by the cohesion and effective angle of internal friction values tabulated in Table 5.7. Lower cohesion means greater flowability. It can be clearly seen that the cohesion values for the dry coated samples were greater than the hand blended sample but lesser than paracetamol, hence in agreement with the flowability results. The cohesion values of the 4 kg/cm^2 sample were not far off from the nano hand blended sample. Internal friction angle gives the friction between the powder particles, a greater variation in internal friction angle means greater compressibility of the powder sample. It is because at increasing stresses the powder particles are compacted and their interlocks are broken which are the primary source of friction. This is the reason the internal friction angle reduces with increasing stress. As can be seen the internal friction angle of nano blended sample was the least indicating poor compressibility but improved flowability as the angle was lower than paracetamol indicating reduced friction between particles. The nano blended and 4 kg/cm^2 sample had almost similar internal friction angles indicating almost comparable inter particle friction.

Table 5.7. Major principal consolidating stress, unconfined failure strength, effective angle of internal friction and cohesion values of paracetamol 80% SAC dry coated samples at 4 kg/cm^2 and 6 kg/cm^2 operating pressure and 10 minutes processing time

	Flow function			
Material	Major principal consolidating stress (kPa)	Unconfined failure strength (kPa)	Effective angle of internal friction (°)	Cohesion (kPa)
Paracetamol	0.6774	0.5578	62.15	0.1586
	1.2578	0.8718	52.45	0.2656
	2.4045	1.3372	45.64	0.415
	4.2808	2.1294	40.6	0.6986
	7.8068	3.3534	36.04	1.1332
Paracetamol 80%SAC	0.7186	0.3142	49.44	0.0776
	1.363	0.3844	44.76	0.0944
	2.6968	0.5696	42.8	0.1402
	5.43	0.9958	41.74	0.247
	10.8552	1.7752	40.94	0.4426
Paracetamol 80%SAC Dry coated 4 kg/cm^2 10min	0.6750	0.4408	54.33	0.1213
	1.3765	0.6365	49.40	0.1608
	2.7910	1.0293	46.55	0.2585
	5.6223	1.6613	44.63	0.4140
	11.1803	2.8258	43.10	0.7090
Paracetamol 80%SAC Dry coated 6 kg/cm^2 10min	0.7053	0.5323	59.87	0.1447
	1.3973	0.7950	52.90	0.2030
	2.7800	1.3377	50.20	0.3367
	5.6180	2.3040	48.27	0.5713
	11.3020	4.0130	46.47	0.9977

Chapter 6

Conclusions & Future Scope of Work

Conclusions

Blending paracetamol with Avicel PH-102 improved the flowability more than the blends of Avicel PH-101 but not by much. This is due to better flowability of Avicel PH-102 than Avicel PH-101. Both, Avicel PH-101 and Avicel PH-102 significantly improved the flowability in comparison to pure paracetamol. In blending with Avicel PH-101 and Avicel PH-102 maximum flowability in both cases was for 80% blends as pure Avicel PH-101 and Avicel PH-102 had better flowability than pure paracetamol. Linear increasing trend of flowability was observed with the increasing excipient percentage in the blends. Blending with nano-silica (less than 2% wt. / wt.) helped in improving the flow of paracetamol and transformed it into an easy flowing powder.

Wall friction of all paracetamol samples blended with Avicel PH-101 & Avicel PH-102 decreased barring one case. The decrease in wall friction angle helps in designing hoppers with lesser hopper angle in which powders can flow in mass flow regime. Blending with nano-silica saw a significant rise in wall friction angles. This can be attributed to the shape of the paracetamol particles coupled with the de-agglomeration of paracetamol particles. Rod shaped paracetamol particles offer a larger surface area to come in contact with the wall surface than sphere shaped particles. As paracetamol particles were de-agglomerated more particles could interact with the wall surface and hence, increasing wall friction.

Bulk density decreased for Avicel PH-101 and Avicel PH-102 as the bulk densities of both is lesser than pure paracetamol. Blending with nano-silica improved the bulk density significantly as nano-silica decreased the inter particle forces due to which packing improved and hence bulk density. Overall, compressibility of all samples including Avicel PH-101, Avicel PH-102 and nano-blended samples decreased due to better packing of particles.

Flowability of ibuprofen improved when blended with Avicel PH-101 and Avicel PH-102 but not to a great extent as the powder was already in the easy flowing region. The flowability improved dramatically when ibuprofen was nano-blended, with the powder shifting to the free flowing region and all the samples i.e. 20,40,60 & 80% SAC showed very little or zero unconfined yield strength at different consolidation stresses. The improvement can be attributed to the reduction in inter-particle forces of cohesion. Increasing the blending percentage of Avicel PH-101 and Avicel PH-102 did not change the flowability that much and up to certain stress value one blend had better improvement than the other.

Wall friction of the samples blended with Avicel PH-101 did not show a significant increment or decrement in the wall friction characteristics. Similarly samples blended with Avicel PH-102 did not show much variation with the 20, 40 and 80% blends having lesser

wall friction angles while 60% sample had a marginal increase. Avicel PH-101 blended samples had wall friction angles a little larger than pure ibuprofen. The wall friction angles of nano-blended ibuprofen increased significantly and can be attributed to the better de-agglomeration or improved packing of particles due to which more and more particles came into contact with the wall surface. 60% and 80% SAC samples showed no significant variation in wall friction angle with change in stress indicating the samples to be independent of normal stress applied.

Bulk density of all 8 samples blended with Avicel PH-101 and Avicel PH-102 decreased in comparison to pure ibuprofen and decreased with increasing blending percentage. Bulk density of nano-blended samples improved significantly at lower stress values and became comparable to pure ibuprofen after certain stress value. This again can be attributed to the packing as flowability of pure ibuprofen was already in easy flowing region, it can be said that its packing was already good and could only be improved by some factor. Compressibility of all 12 blended samples was lesser than pure ibuprofen with nano-blended samples showing little or no compressibility. This again can be attributed to the better packing after blending.

The study undertook shows that simple hand blending was sufficient in improving the flow of active pharmaceutical ingredient powders. Hand blending with excipients Avicel PH-101 and Avicel PH-102 improved the flow substantially but maximum improvement was seen in the nano blended samples. Similar reduction in cohesiveness of powders by hand mixing nano blending was seen in the study conducted by Yang *et al.* (2005)**.** Kojima and Elliott (2013) studied the effect of mixing silica nanoparticles in poly (styrene-co-di vinyl benzene) powder. The silica nanoparticles reduced the primary powder particle contacts and hence leading to reduced cohesion of powder. It was found that the nanoparticles only reduced cohesion up to a certain wt./wt.% because after that the nanoparticles produced continuous films on the particle surface which increases the cohesion. The results of this study match with the author's work with the maximum improvement in flowability coming at a particular wt./wt.%.

The dry coating machine gave the best flowability results for Para20%SAC at 3 kg/cm^2 operating pressure and 10 minute processing time but was lesser than the Para20%SAC hand blended sample. Increasing the operating pressure to 4 kg/cm^2 and 5 kg/cm^2 decreased the flowability. Increasing the processing time beyond 10 minutes deteriorated the flowability probably because of particle attrition. The initial results of Para80%SAC at 4 kg/cm^2 and 10 minute processing time gave promising results and should be tested at 3 and 5 kg/cm^2 pressure, and operating times of 10 and 20 minutes.

Future Scope of Work

Further studies can be conducted with different API and excipients and by varying excipient and API percentages to gauge the effect on flowability and other properties as different percentages of API and excipients are required in different manufacturing processes.

Testing of dry coating machine at the loop length of 4 sections and 8 sections for the Para20%SAC samples should be done. Testing of Para20%SAC has been currently completed at zero section length or only with bend at 3, 4 and 5 kg/cm^2 operating pressure and 10 and 20 minute processing times. Further testing of Para40%SAC, Para60%SAC, Para80%SAC at 3,4 and 5 kg/cm^2 operating pressure and 10 and 20 minute processing times should be carried out to gauge the optimum conditions for maximum improvement in flow properties. This testing should be done on all three loop lengths. Testing can be extended to various other cohesive API's and excipients and also to using the fabricated machine as a blending machine for two or more micrometer sized powders. Below is the image of the dry coating machine at conveying length of 8 sections.

Figure 6.1. Dry coating machine functioning with the maximum conveying length of 8 sections and a bend connecting the upper and lower sections together with the hopper assembly and bag filter connected to the upper hopper

References

Berry, R.J., Bradley, M.S.A. and McGregor, R.G., 2015. Brookfield powder flow tester–Results of round robin tests with CRM-116 limestone powder. *Proceedings of the Institution of Mechanical Engineers, Part E: Journal of Process Mechanical Engineering*, *229*(3), pp.215-230.

Cannavacciuolo, A., Barletta, D., Donsì, G., Ferrari, G. and Poletto, M., 2009. Arch-Free flow in aerated silo discharge of cohesive powders. *Powder Technology*, *191*(3), pp.272-279.

Capece, M., Ho, R., Strong, J. and Gao, P., 2015. Prediction of powder flow performance using a multi-component granular Bond number. *Powder Technology*, *286*, pp.561-571.

Chattoraj, S., Shi, L. and Sun, C.C., 2011. Profoundly improving flow properties of a cohesive cellulose powder by surface coating with nano-silica through comilling. *Journal of Pharmaceutical Sciences*, *100*(11), pp.4943-4952.

Chaudhuri, B., Mehrotra, A., Muzzio, F.J. and Tomassone, M.S., 2006. Cohesive effects in powder mixing in a tumbling blender. *Powder Technology*, *165*(2), pp.105-114.

Chen, Y., Jallo, L., Quintanilla, M.A. and Dave, R., 2010. Characterization of particle and bulk level cohesion reduction of surface modified fine aluminum powders. *Colloids and Surfaces A: Physicochemical and Engineering Aspects*, *361*(1), pp.66-80.

Deng, T., Paul, K.A., Bradley, M.S., Immins, L., Preston, C., Scott, J.F. and Welfare, E.H., 2010. Investigations on air induced segregation of pharmaceutical powders and effect of material flow functions. *Powder Technology*, *203*(2), pp.354-358.

Garg, V., 2017. An Experimental Investigation into the Flow Properties of Pharmaceutical and Detergent Powders (master's thesis). Thapar Institute of Engineering and Technology, Patiala.

Ghoroi, C., Gurumurthy, L., McDaniel, D.J., Jallo, L.J. and Davé, R.N., 2013.Multi-faceted characterization of pharmaceutical powders to discern the influence of surface modification. *Powder Technology*, *236*, pp.63-74.

Ghoroi, C., Han, X., To, D., Jallo, L., Gurumurthy, L. and Davé, R.N., 2013.Dispersion of fine and ultrafine powders through surface modification and rapid expansion. *Chemical Engineering Science*, *85*, pp.11-24.

Han, X., Ghoroi, C., To, D., Chen, Y. and Davé, R., 2011.Simultaneous micronization and surface modification for improvement of flow and dissolution of drug particles. *International Journal of Pharmaceutics*, *415*(1), pp.185-195.

Han, X., Jallo, L., To, D., Ghoroi, C. and Davé, R., 2013. Passivation of high-surface-energy sites of milled ibuprofen crystals via dry coating for reduced cohesion and improved flowability. *Journal of Pharmaceutical Sciences, 102*(7), pp.2282-2296.

Hann, D. and Stražišar, J., 2007. Influence of particle size distribution, moisture content, and particle shape on the flow properties of bulk solids. *Instrumentation Science and Technology, 35*(5), pp.571-584.

HOSOKAWA MICRON CORPORATION. *MECHANO FUSION System AMS | HOSOKAWAMICRON CORPORATION*. Accessed 22 June 2018. http://www.hosokawamicron.co.jp/en/machines/147.

Huang, Z., Scicolone, J.V., Han, X. and Davé, R.N., 2015. Improved blend and tablet properties of fine pharmaceutical powders via dry particle coating. *International Journal of Pharmaceutics*, *478*(2), pp.447-455.

Huang, Q., Zhang, H. and Zhu, J., 2010. Flow properties of fine powders in powder coating. *Particuology*,*8*(1), pp.19-27.

Iqbal, T. and Fitzpatrick, J.J., 2006. Effect of storage conditions on the wall friction characteristics of three food powders. *Journal of Food Engineering, 72*(3), pp.273-280.

Ittershagen, T., Zetzener, H., Schwedes, J. and Kwade, A., 2013. Anisotropic behaviour of bulk solids and its effect on silo design. *Powder Technology*, *247*, pp.260-264.

Jallo, L.J., Ghoroi, C., Gurumurthy, L., Patel, U. and Davé, R.N., 2012.Improvement of flow and bulk density of pharmaceutical powders using surface modification. *International Journal of Pharmaceutics*, *423*(2),pp.213-225.

Jallo, L.J., Schoenitz, M., Dreizin, E.L., Dave, R.N. and Johnson, C.E., 2010.The effect of surface modification of aluminum powder on its flowability, combustion and reactivity. *Powder Technology, 204*(1), pp.63-70.

Jenike, A.W., 1964. Storage and flow of solids. *Bulletin 123, Utah Eng. Exp. Sta., Univ. of Utah*.

Jonat, S., Hasenzahl, S., Gray, A. and Schmidt, P.C., 2004. Mechanism of glidants: Investigation of the effect of different colloidal silicon dioxide types on powder flow by atomic force and scanning electron microscopy. *Journal of Pharmaceutical Sciences*, *93*(10), pp.2635-2644.

Karde, V., Panda, S. and Ghoroi, C., 2015.Surface modification to improve powder bulk behavior under humid conditions. *Powder Technology, 278*, pp.181-188.

Kaerger, J.S., Edge, S. and Price, R., 2004. Influence of particle size and shape on flowability and compactibility of binary mixtures of paracetamol and microcrystalline cellulose. *European Journal of Pharmaceutical Sciences, 22*(2-3), pp.173-179.

Kendall, K., 1994. Adhesion: molecules and mechanics. *Science*, *263*(5154), pp.1720-1726.

Kendall, K. and Stainton, C., 2001.Adhesion and aggregation of fine particles. *Powder Technology*, *121*(2), pp.223-229.

Kojima, T. and Elliott, J.A., 2013. Effect of silica nanoparticles on the bulk flow properties of fine cohesive powders. *Chemical Engineering Science*, *101*, pp.315-328.

Lefebvre, G., Galet, L. and Chamayou, A., 2011. Dry coating of talc particles with fumed silica: Influence of the silica concentration on the wettability and dispersibility of the composite particles. *Powder Technology*, *208*(2), pp.372-377.

Mangal, S., Meiser, F., Tan, G., Gengenbach, T., Morton, D.A. and Larson, I., 2016. Applying surface energy derived cohesive–adhesive balance model in predicting the mixing, flow and compaction behaviour of interactive mixtures. *European Journal of Pharmaceutics and Biopharmaceutics*, *104*, pp.110-116.

Meyer, K. and Zimmermann, I., 2004.Effect of glidants in binary powder mixtures. *Powder Technology*,*139* (1), pp.40-54.

Mujumdar, A., Wei, D., Dave, R.N., Pfeffer, R. and Wu, C.Y., 2004.Improvement of humidity resistance of magnesium powder using dry particle coating. *Powder Technology*, *140*(1), pp.86-97.

Mullarney, M.P., Beach, L.E., Davé, R.N., Langdon, B.A., Polizzi, M. and Blackwood, D.O., 2011. Applying dry powder coatings to pharmaceutical powders using a comil for improving powder flow and bulk density. *Powder Technology*, *212*(3), pp.397-402.

Müller, A.K., Ruppel, J., Drexel, C.P. and Zimmermann, I., 2008. Precipitated silica as flow regulator. *European Journal of Pharmaceutical Sciences*, *34*(4-5), pp.303-308.

Osorio, J.G. and Muzzio, F.J., 2015.Evaluation of resonant acoustic mixing performance. *Powder Technology*, *278*, pp.46-56.

Ouabbas, Y., Chamayou, A., Galet, L., Baron, M., Thomas, G., Grosseau, P. and Guilhot, B., 2009.Surface modification of silica particles by dry coating: Characterization and powder ageing. *Powder Technology*, *190*(1), pp.200-209.

Pingali, K.C., Saranteas, K., Foroughi, R. and Muzzio, F.J., 2009.Practical methods for improving flow properties of active pharmaceutical ingredients. *Drug Development and Industrial Pharmacy*, *35*(12), pp.1460-1469.

Qian, Z., Wang, P. and Gogos, C.G., 2012. A novel method for preparing nanoparticle-coated additives used in polypropylene composites. *Polymer Engineering & Science*, *52*(6), pp.1195-1205.

Qu, L., Stewart, P.J., Hapgood, K.P., Lakio, S., Morton, D.A. and Zhou, Q.T., 2017.Single-step coprocessing of cohesive powder via mechanical dry coating for direct tablet compression. *Journal of Pharmaceutical Sciences*, *106*(1), pp.159-167.

Rabinovich, Y.I., Adler, J.J., Ata, A., Singh, R.K. and Moudgil, B.M., 2000 a. Adhesion between nanoscale rough surfaces: I. Role of asperity geometry. *Journal of Colloid and Interface Science*, *232*(1), pp.10-16.

Rabinovich, Y.I., Adler, J.J., Ata, A., Singh, R.K. and Moudgil, B.M., 2000 b. Adhesion between nanoscale rough surfaces: II.Measurement and comparison with theory. *Journal of Colloid and Interface Science*, *232*(1), pp.17-24.

Ramlakhan, M., Wu, C.Y., Watano, S., Dave, R.N. and Pfeffer, R., 2000. Dry particle coating using magnetically assisted impaction coating: modification of surface properties and optimization of system and operating parameters. *Powder Technology*, *112*(1), pp.137-148.

Rohilla, L., 2016. An Experimental Investigation on the Flow Properties of Bulk Solids (master's thesis). Thapar Institute of Engineering and Technology, Patiala.

Rohilla, L., Garg, V., Mallick, S.S. and Setia, G., 2018. An experimental investigation on the effect of particle size into the flowability of fly ash. *Powder Technology*, *330*, pp.164-173.

Rumpf, H., 2012.*Particle Technology* (Vol. 1). *Springer Science & Business Media.*

Ruzaidi, A.F.B., Mandal, U.K. and Chatterjee, B., 2017. Glidant effect of hydrophobic and hydrophilic nanosilica on a cohesive powder: Comparison of different flow characterization techniques. *Particuology*, *31*, pp.69-79.

Sato, A., Serris, E., Grosseau, P., Thomas, G., Galet, L., Chamayou, A. and Baron, M., 2013.Experiment and simulation of dry particle coating. *Chemical Engineering Science*, *86*, pp.164-172.

Sauer, D., Cerea, M., DiNunzio, J. and McGinity, J., 2013. Dry powder coating of pharmaceuticals: a review. *International Journal of Pharmaceutics*, *457*(2), pp.488-502.

Schulze, D., 2008.Powders and bulk solids. *Behaviour, Characterization, Storage and Flow. Springer*, pp.35-74.

Schwedes, J., 1996. Measurement of flow properties of bulk solids. *Powder Technology*, *88*(3), pp.285-290.

Teng, S., Wang, P., Zhu, L., Young, M.W. and Gogos, C.G., 2009.Experimental and numerical analysis of a lab-scale fluid energy mill. *Powder Technology*, *195*(1), pp.31-39.

Teunou, E. and Fitzpatrick, J.J., 2000. Effect of storage time and consolidation on food powder flowability. *Journal of Food Engineering*, *43*(2), pp.97-101.

Tomas, J. and Kleinschmidt, S., 2009.Improvement of flowability of fine cohesive powders by flow additives. *Chemical Engineering & Technology*, *32*(10), pp.1470-1483.

Wang, Y., Osorio, J.G., Li, T. and Muzzio, F.J., 2017. Controlled shear system and resonant acoustic mixing: Effects on lubrication and flow properties of pharmaceutical blends. *Powder Technology*, *322*, pp.332-339.

Wei, D., Dave, R. and Pfeffer, R., 2002. Mixing and characterization of nanosized powders: an assessment of different techniques. Journal of Nanoparticle Research, 4(1-2), pp.21-41.

Yang, J., Sliva, A., Banerjee, A., Dave, R.N. and Pfeffer, R., 2005.Dry particle coating for improving the flowability of cohesive powders. *Powder Technology*, *158*(1), pp.21-33.

Yuan, J., Shi, L., Sun, W.J., Chen, J., Zhou, Q. and Sun, C.C., 2013. Enabling direct compression of formulated Danshen powder by surface engineering. *Powder Technology*, *241*, pp.211-218.

Zhang, Q., Yang, J., Teng, S., Dave, R.N., Zhu, L., Wang, P., Young, M.W. and Gogos, C.G., 2009.In-situ, simultaneous milling and coating of particulates with nanoparticles. *Powder Technology*, *196*(3), pp.292-297.

Zhou, Q., Armstrong, B., Larson, I., Stewart, P.J. and Morton, D.A., 2010 a. Improving powder flow properties of a cohesive lactose monohydrate powder by intensive mechanical dry coating. *Journal of Pharmaceutical Sciences*, *99*(2), pp.969-981.

Zhou, Q., Armstrong, B., Larson, I., Stewart, P.J. and Morton, D.A., 2010 b. Effect of host particle size on the modification of powder flow behaviours for lactose monohydrate following dry coating. *Dairy Science & Technology*, *90*(2-3), pp.237-251.

Zhou, Q., Shi, L., Chattoraj, S. and Sun, C.C., 2012. Preparation and characterization of surface-engineered coarse microcrystalline cellulose through dry coating with silica nanoparticles. *Journal of Pharmaceutical Sciences*, *101*(11), pp.4258-4266.

Zhou, Q., Shi, L., Marinaro, W., Lu, Q. and Sun, C.C., 2013. Improving manufacturability of an ibuprofen powder blend by surface coating with silica nanoparticles. *Powder Technology*, *249*, pp.290-296.

Zhou, Q.T., Qu, L., Larson, I., Stewart, P.J. and Morton, D.A., 2011. Effect of mechanical dry particle coating on the improvement of powder flowability for lactose monohydrate: A model cohesive pharmaceutical powder. *Powder Technology, 207(1), pp.414-421.*

Zhu, X., Zhang, Q., Huang, C., Wang, Y., Yang, C. and Wei, F., 2017. Validation of surface coating with nanoparticles to improve the flowability of fine cohesive powders. *Particuology*, *30*, pp.53-61.

Appendix A

Results of two common food powders i.e. chilli & turmeric.

A scanning electron microscope (JEOL JSM-5510LV) was used to assess the morphology of particles.

(a)

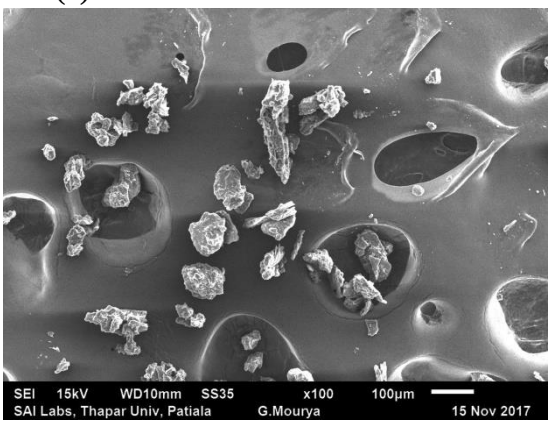

(b)

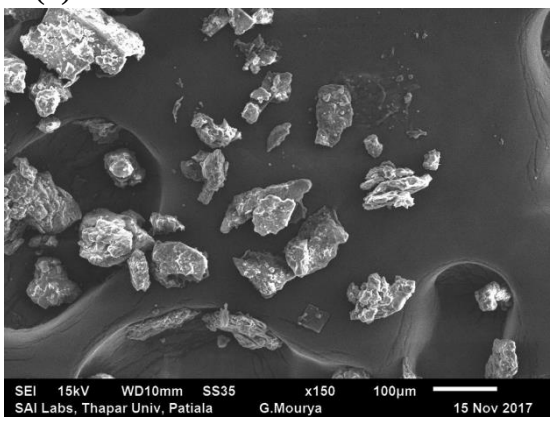

(c)

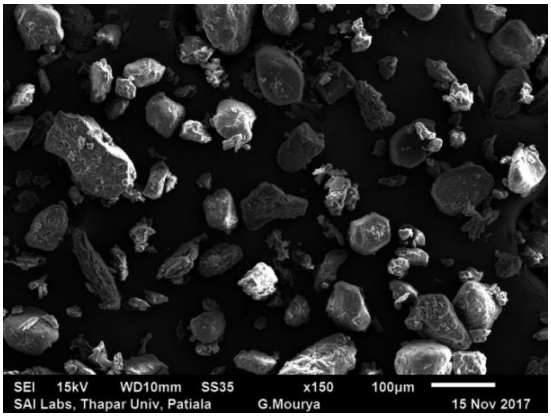

(d)

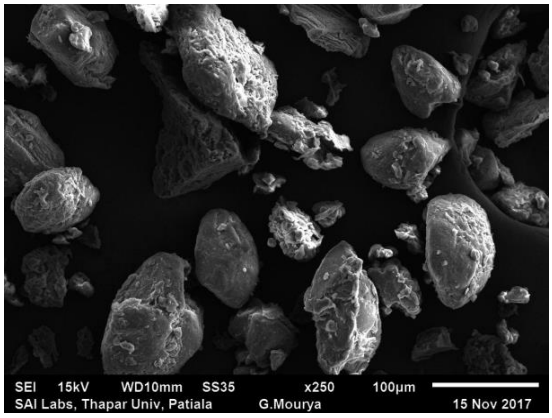

Figure A1. SEM images of (a) Chilli at magnification of 100x, (b) Chilli at magnification of 150x, (c) Turmeric at magnification of 150x, (d) Turmeric at magnification of 250x

Table A1: d_{10}, d_{50} , d_{90} and d_{32} diameters of chilli and turmeric

Material	d_{10} (µm)	d_{50}(µm)	d_{90}(µm)	d_{32}(µm)
Chilli	76.687	334.082	774.590	176.902
Turmeric	35.591	98.433	283.451	66.397

Note: d_{10}, d_{50}, d_{90} means 10%, 50% and 90% below this size; d_{32} = volume/surface mean

Energy-dispersive X-ray spectroscopy results of mean of three spectrums (all results in weight%)

Table A2. Chilli

Carbon	Oxygen	Magnesium	Potassium
53.05	43.61	0.46	2.88

Table A3. Turmeric

Carbon	Oxygen	Magnesium	Silicon	Potassium
46.07	50.55	0.29	0.60	2.49

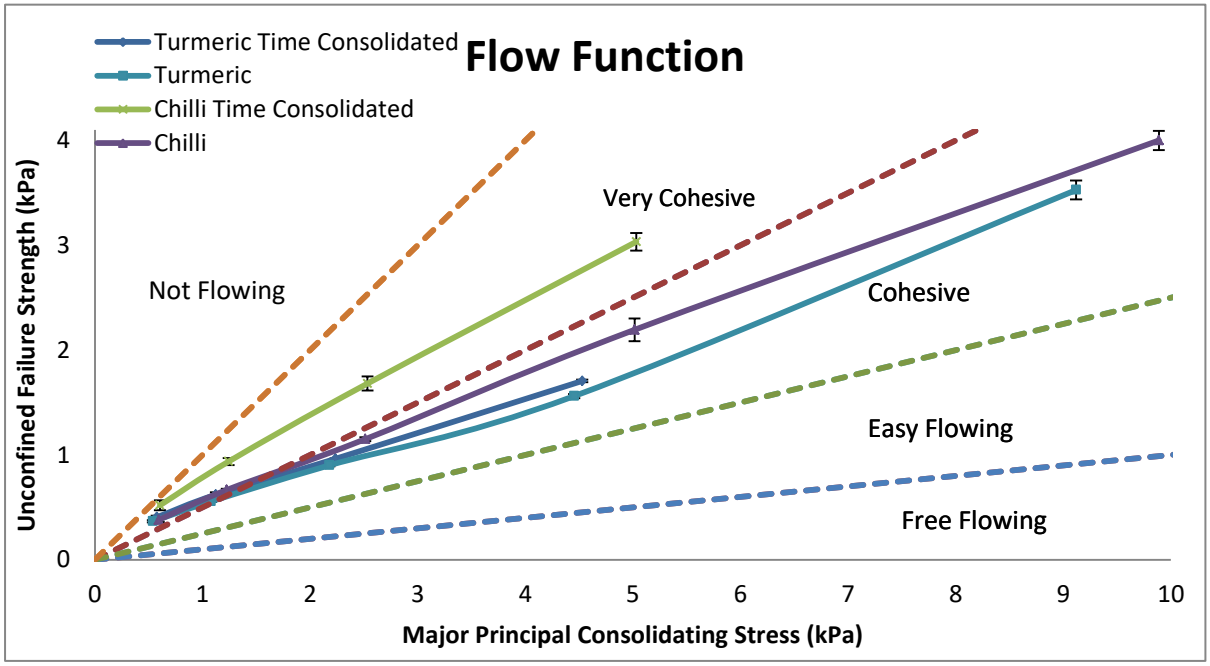

Figure A2. Flow function and time consolidated flow function curve of chilli and turmeric powder

As can be seen from Figure A2. chilli powder had lower flowability than turmeric powder. This can be attributed to the fact that chilli particles have severe attrition as seen in Figure A1, due to which they have lower flowability than turmeric particles which seem to have non attrition cylindrical particles. Particle attrition causes lower flowability. The worsening flowability of both time consolidated samples was on expected lines. The flowability results are well supported by the cohesion values.

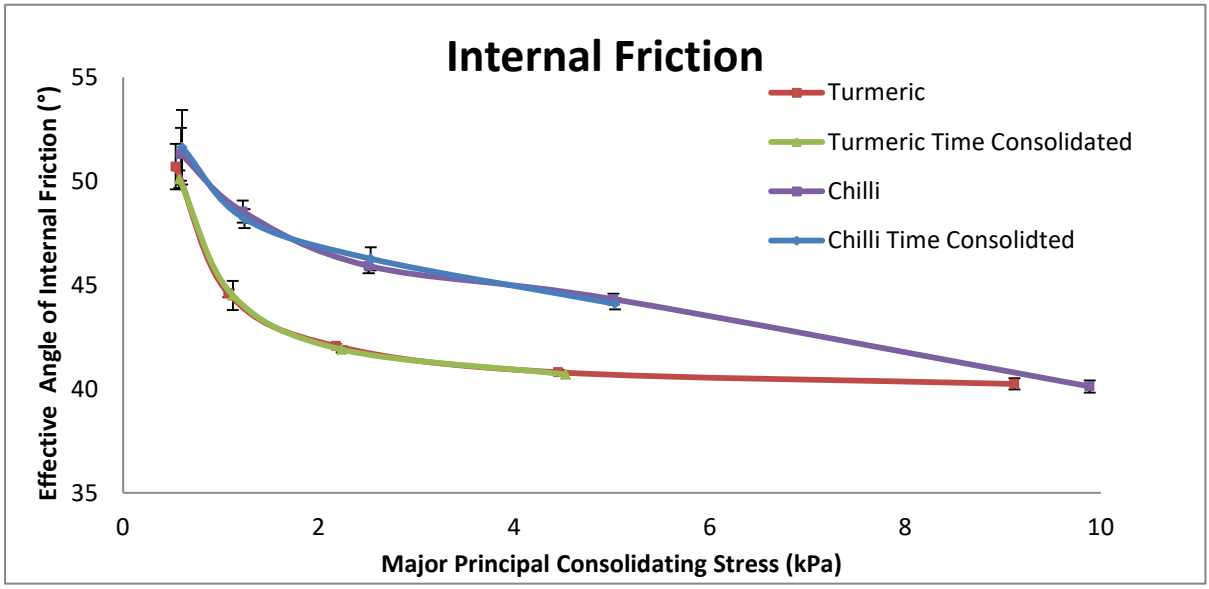

Figure A3. Internal friction curves of chilli and turmeric powder under flow function and time consolidated flow function curves

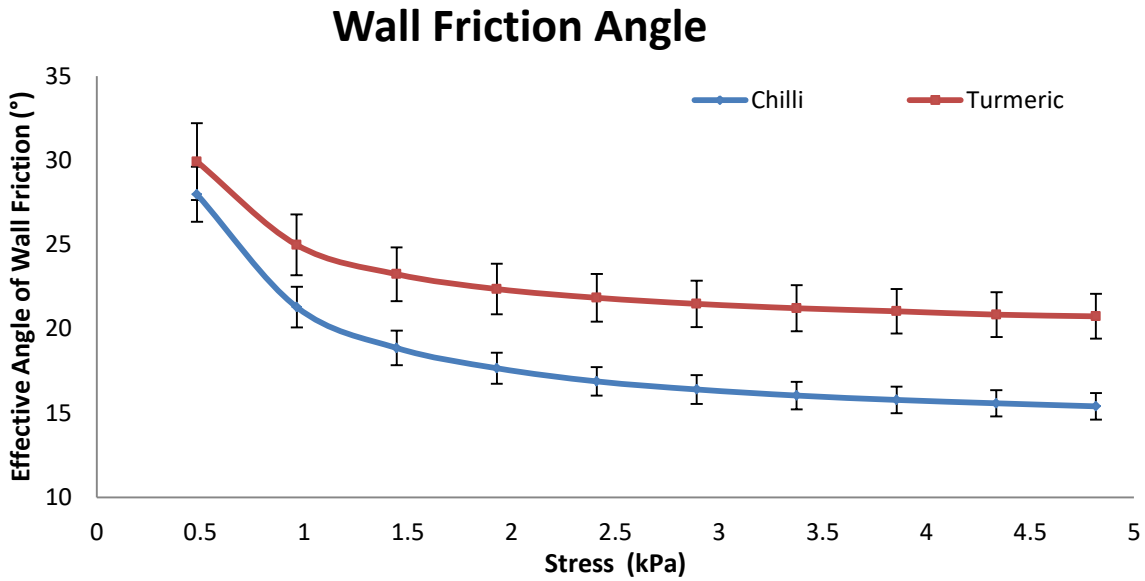

Figure A4. Wall friction curves of chilli and turmeric powder

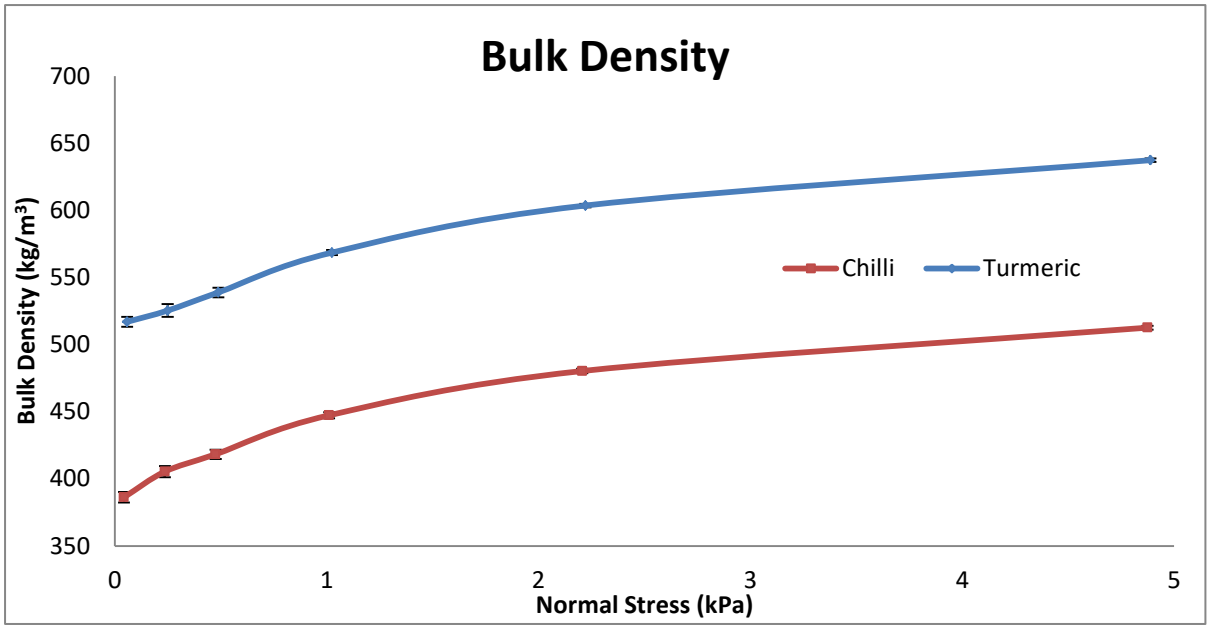

Figure A5. Bulk density curves of chilli and turmeric powder

Table A4. Major principal consolidating stress, unconfined failure strength, effective angle of internal friction and cohesion values of chilli and turmeric powder under flow function and time consolidation flow function tests

	Flow function			
Material	Major principal consolidating stress (kPa)	Unconfined failure strength (kPa)	Effective angle of internal friction (°)	Cohesion (kPa)
Chilli	0.5932	0.3808	51.3	0.1124
	1.2246	0.666	48.54	0.1864
	2.5136	1.1508	45.92	0.3164
	5.0158	2.1942	44.32	0.617
	9.8886	4.0004	40.12	1.2054
Turmeric	0.5394	0.3674	50.7	0.1162
	1.0792	0.5562	44.6	0.1672
	2.1796	0.9016	42.06	0.2618
	4.4544	1.5614	40.8	0.4434
	9.1192	3.5274	40.24	1.0446
Chilli time consolidated	0.6043	0.5197	51.63	0.1523
	1.2423	0.9370	48.20	0.2600
	2.5337	1.6817	46.27	0.4597
	5.0320	3.0340	44.10	0.8403
Turmeric time consolidated	0.5757	0.406	50.1	0.1285
	1.1237	0.6205	44.5	0.185
	2.2370	0.9635	41.9	0.279
	4.5293	1.706	40.7	0.482

Table A5. Wall friction and bulk densities values of chilli and turmeric

	Wall friction		Bulk density	
Material	Stress (kPa)	Effective angle of wall friction (°)	Stress (kPa)	Density (kg/m³)
Chilli	0.483	27.98	0.0428	386.28
	0.9646	21.28	0.2358	405.42
	1.4462	18.86	0.4752	418.32
	1.9288	17.66	1.0114	447.32
	2.41	16.88	2.206	480.3
	2.8922	16.4	4.8744	512.58
	3.374	16.04		
	3.8558	15.78		
	4.3362	15.58		
	4.817	15.4		
Turmeric	0.4828	29.92	0.0574	516.92
	0.9636	24.98	0.249	525.34
	1.4458	23.24	0.4886	538.86
	1.9286	22.36	1.025	568.5
	2.4104	21.84	2.2208	603.52
	2.892	21.48	4.8884	637.3
	3.374	21.22		
	3.8558	21.04		
	4.3376	20.84		
	4.817	20.74		

As can be seen from Figure A4. Turmeric had greater wall friction angle than chilli at comparable stress values meaning that turmeric particles faced greater wall friction.

As seen from Figure A5. bulk density of chilli was lower than turmeric at comparable stress values. This is in agreement with the flowability results as generally poor packing of particles leads to lower bulk density and lower flowability.

Publication

Sharma, R and Setia, G. Enhancing Flowability of Fine Cohesive Active Pharmaceutical Ingredients. Particuology. (Communicated)